Roberto Fernández Morán

Calibration of soil roughness and vegetation parameters in the SMOS retrieval algorithm and validation at local and global scale

Doctorado en Teledetección

Departament de Física de la Terra i Termodinàmica

Facultat de Física

VNIVERSITAT D VALÈNCIA Facultat de Física

PhD Thesis 2017

VNIVERSITAT D VALÈNCIA

PhD Thesis
September 2017
Roberto Fernández Morán

PhD advisors: Dr. Jean Pierre Wigneron
Dr. Yann Kerr
Dr. Ernesto López Baeza

UNIVERSITAT DE VALÈNCIA

Facultat de Física
Departament de Física de la Terra i Termodinàmica

Calibration of soil roughness and vegetation parameters in the SMOS retrieval algorithm and validation at local and global scale

Doctorado en Teledetección
PhD Thesis
September 2017
ROBERTO FERNÁNDEZ MORÁN

PhD advisors: Dr. Jean-Pierre Wigneron
Dr. Yann H. Kerr
Dr. Ernesto López Baeza

JEAN-PIERRE WIGNERON, Directeur de Recherche, Unité Interactions Sol Plante Atmosphère (ISPA) del Institut National de la Recherche Agronomique (INRA)-Bordeaux (Francia),

YANN H. KERR, SMOS (Soil Moisture and Ocean Salinity) Principal Investigator en el Centre d'Études Spatiales de la Biosphère (CESBIO), Toulouse (Francia), y

ERNESTO LÓPEZ BAEZA, Profesor Titular de Física Aplicada en el Departamento de Física de la Tierra y Termodinámica de la Facultad de Física, Universitat de València,

CERTIFICAN:

Que la presente memoria, titulada "Calibration of soil roughness and vegetation parameters in the SMOS retrieval algorithm and validation at local and global scale", corresponde al trabajo realizado bajo su dirección por D. Roberto Fernández Morán, para su presentación como Tesis Doctoral en el Programa de Doctorado en Teledetección de la Universitat de València.

Y para que conste, firman el presente certificado en Burdeos, Toulouse y Valencia, a 15 de septiembre de 2017.

Fdo.: Jean-Pierre Wigneron Fdo.: Yann H. Kerr Fdo.: Ernesto López Baeza

Este trabajo ha sido posible gracias a la financiación económica recibida por parte de:

El Proyecto MIDAS 7/UVEG "Productos y Aplicaciones Avanzadas de SMOS y Futuras Misiones (Parte UVEG)", financiado por el Ministerio de Economía y Competitividad del Gobierno de España.

El proyecto TOSCA (Terre Océan Surfaces Continentales et Atmosphère) financiado por el "Centre National d'Études Spatiales" (CNES).

A todos aquellos que me han
apoyado personal y profesionalmente…

À tous ceux qui m'ont donné
leur soutien personnel et professionnel…

Agradecimientos

Escribo estas líneas en agradecimiento a todas las personas que han hecho posible que hoy presente esta tesis doctoral. Ha sido un camino largo y emocionante en el que todas las dificultades se han ido convirtiendo en triunfos.

Mi primer contacto con la investigación no fue buscado; una oportunidad que llegó de la mano de Ernesto López Baeza, codirector de esta tesis en la Universidad de Valencia. A él debo agradecerle muy especialmente los comienzos, por permitirme involucrarme en el duro trabajo de campo (con todas las dificultades que conlleva el mantenimiento de las estaciones de medida), los congresos, las presentaciones orales… Todo esto me ha enriquecido personal y profesionalmente. Aprendí una metodología de trabajo diferente a la que me enseñaron como ingeniero, y comprendí la riqueza de trabajar con personas venidas de diferentes ámbitos académicos. En el grupo de Climatología desde satélite, para el cual trabajé desde 2012 a 2015, tuve la ocasión de colaborar con diferentes compañeros; muchos solo estuvieron unos meses allí, pero otros permanecieron en el tiempo y también lo harán en la memoria. En especial debo nombrar a Maura, Paula, Níobe y Amparo, con las que he compartido grandes momentos en la Valencia Anchor Station, en el despacho y fuera de él. Desde aquellos momentos bajo el abrasador sol de verano cuando medíamos la rugosidad del suelo a las cañas después del trabajo, todos son momentos para el recuerdo.

En diciembre de 2012 tuve la gran suerte de establecer mi primer contacto con INRA (Institut National de la Recherche Agronomique), en Burdeos, de la mano de Jean Pierre Wigneron. En mi primera etapa, trabajar con los datos de campo fue mi principal tarea, en especial con el radiómetro ELBARA-II. Jean Pierre coordinó desde la distancia mi trabajo y poco a poco fue involucrándose más en mi investigación. Cuando a finales de 2014 decidí comenzar la tesis doctoral, acordamos que también codirigiera este trabajo que hoy presento. A él le debo agradecer su gran aportación científica y el haberme guiado en todo momento de manera clara y precisa hacia los objetivos, sin dejar de lado mis propias ideas y aportaciones.

El tercer codirector de esta tesis, Yann Kerr, a él debo agradecerle aceptar codirigir este trabajo, pues ha sido sin duda un honor trabajar de primera mano con el líder de la misión SMOS. A él y a todo el equipo de CESBIO en Toulouse, debo agradecerles su gran apoyo científico y, al incluirme en su círculo, permitirme seguir todos los progresos dentro de la misión. Mis cortas estancias en CESBIO han sido siempre muy enriquecedoras. Debo dirigir mis agradecimientos en especial a Arnaud Mialon, Ali Mahmoodi, Marie Parrens, Philippe Richaume y Simone Bircher, por haber empleado parte de su tiempo en formarme; su contribución ha sido imprescindible para conseguir un buen resultado en todas mis publicaciones.

En enero de 2016 comencé a trabajar en INRA, donde me he establecido de forma permanente desde mayo de ese mismo año. En todo este tiempo, mi progreso ha sido enorme, no solo por el número de publicaciones científicas que he alcanzado en este tiempo, sino también por conseguir aprender una nueva lengua. Todo ha sido posible gracias a Jean Pierre Wigneron.

Debo hacer mención también a mis compañeros de trabajo más cercanos, Shu Wang, Amen Al-Yaari y Lei Fan, quienes han sido igualmente importantes en mi camino.

Por último, agradecer a mi entorno más cercano su gran apoyo, pues sin ellos nunca habría conseguido este logro. A mis amigos de siempre (aunque muchos estén lejos) y a mis nuevos amigos de Burdeos, que son una auténtica inyección de energía.

A todos vosotros,

¡Gracias!

Acknowledgments

I write these lines to express my gratitude to all the people who made this thesis possible. It has been a long and exciting way where all the troubles have turned into triumph.

My first contact with research came thanks to Ernesto López Baeza, co-director of this thesis at the University of Valencia. I must thank him for giving me the opportunity to be involved in the hard field work, conferences and oral presentations… All of that has enriched me not only academically but also personally. I have learnt a work methodology which is different from the one that I had learned as an engineer, and I have understood the richness of working with people from different backgrounds.

In the Climatology from Satellites' group, where I worked from 2012 to 2015, I had the chance to collaborate with different workmates. Concretely, I must mention Maura, Paula, Níobe and Amparo; I have shared great moments with them at the Valencia Anchor Station, at work and out of the office. From all those days measuring soil roughness under the burning summer sun of Valencia, to the beers after work, I will never forget these moments.

In December 2012, I had the chance of getting in contact with INRA (Institut National de la Recherche Agronomique), thanks to Jean Pierre Wigneron. In the first stage, I was in charge of the in situ stations and data, especially the ELBARA-II radiometer. Jean Pierre coordinated my work from the distance and he got more involved in my research little by little. When I decided to start this PhD, we have agreed with Jean Pierre that he co-directed it. I must thank him for his great scientific contribution and for leading me through clear and precise objectives, not forgetting my own ideas.

I must also thank my third thesis co-director, Yann Kerr, for accepting to co-direct this work; It has been an honour to work with the Lead-investigator of the SMOS mission. I want to express my gratitude to him and CESBIO team, where I received great scientific support and I could follow the progress of the mission. My short stays in CESBIO have been always very enriching. I must particularly thank Arnaud Mialon, Ali Mahmoodi, Marie Parrens, Philippe Richaume and Simone Bircher, for taking their time to teach me; their contribution has been essential to get such good results in my publications.

From January 2016 I work at INRA, in Bordeaux, where I moved in May 2016. In all this time, my progress has been enormous, not only for the number of scientific publications that I have reached, but also for learning a new language. This big opportunity has been only possible thanks to Jean Pierre Wigneron. I must mention too my closest workmates here, Shu Wang, Amen Al-Yaari and Lei Fan, who have become equally important in my way.

I also have to thank my old friends (even if they are far away) and the ones that I have met in Bordeaux (always so full of energy and plans). Finally, without the great support of my relatives I would never have got here.

Thanks to all of you!

Context

This PhD thesis is presented to obtain the Doctorate Degree in Remote Sensing from the Universitat de València (Spain), with International Doctorate Mention.

The study was developed between October 2014 and December 2015 at the Climatology from Satellites Group (Department of Earth Physics and Thermodynamics, Faculty of Physics, Universitat de València), and from January 2016 to September 2017 at the Interations Sol Plante Atmosphère (ISPA) unit (Institut National de la Recherche Agronomique, Bordeaux, France) with frequent short stays between both institutions and the Centre d'Études Spatiales de la Biosphère (Toulouse, France).

According to the regulations of the Universitat de València on deposit, evaluation and defense of the doctoral thesis (approved on June 28, 2016), the PhD thesis must be presented following one of the following cases:

1) Traditional thesis.
2) Compendium of publications.

The second option has been selected in this PhD thesis meeting the following requirements:

1) A minimum of three peer reviewed articles accepted or published in international journals with JCR (WoS) and/or SJR (Scopus) indexes, being the first author in all of them.
2) A global abstract explaining the main results and conclusions (minimum 4000 words).
3) A copy of all published articles in attach.

This PhD thesis is composed of the following publications:

1. **Fernandez-Moran, R.**; Wigneron, J.-P.; Lopez-Baeza, E.; Al-Yaari, A.; Coll-Pajaron, A.; Mialon, A.; Miernecki, M.; Parrens, M.; Salgado-Hernanz, P. M.; Schwank, M.; Wang, S.; Kerr, Y. H., 2015. Roughness and vegetation parameterizations at L-band for soil moisture retrievals over a vineyard field. Remote Sens. Environ. 170, 269–279.
2. **Fernandez-Moran, R.**; Wigneron, J.-P.; De Lannoy, G.; Lopez-Baeza, E.; Parrens, M.; Mialon, A.; Mahmoodi, A.; Al-Yaari, A.; Bircher, S.; Al Bitar, A.; Richaume, P.; Kerr, Y., 2017. A new calibration of the effective scattering albedo and soil roughness parameters in the SMOS SM retrieval algorithm. Int. J. Appl. Earth Obs. Geoinf. 62, 27–38.
3. **Fernandez-Moran, R.**; Al-Yaari, A.; Mialon, A.; Mahmoodi, A.; Al Bitar, A.; De Lannoy, G.; Rodriguez-Fernandez, N.; Lopez-Baeza, E.; Kerr, Y.; Wigneron, J.-P.,

2017. SMOS-IC: An Alternative SMOS Soil Moisture and Vegetation Optical Depth Product. Remote Sens. 9, 457.

CONTENT

RESUMEN EXTENSO

La humedad del suelo y SMOS

La humedad del suelo es un elemento clave que nos permite conocer los flujos de agua y energía entre el suelo y la atmósfera. Es además un parámetro de interés en aplicaciones hidrológicas y agricultura (Brocca et al., 2010), meteorología (de Rosnay et al., 2013), agricultura y predicción de riesgos naturales.

La humedad del suelo en superficie se define como la fracción de agua contenida en un volumen de suelo húmedo, considerando una capa superficial de suelo de unos pocos centímetros (WMO, https://www.wmo-sat.info/oscar/variables/view/149). Puede expresarse de forma gravimétrica o de forma volumétrica. En este estudio se utiliza la relación entre el volumen de agua y el volumen de suelo que la contiene ($m^3 \cdot m^{-3}$).

Dependiendo de su composición, todo suelo absorbe una cierta cantidad de agua hasta llegar a su punto de saturación. Existe por tanto una relación directa entre la humedad del suelo y su capacidad de infiltración, así como los flujos de calor sensible y humedad de la atmósfera, variables con una gran influencia en los modelos atmosféricos. La humedad del suelo es habitualmente una variable de iniciación de los modelos numéricos de predicción del tiempo (NWP) que permite mejorar su fiabilidad.

Una aplicación significativa de la humedad del suelo a escala global es la monitorización de sequías y déficit hídrico en las plantas. El crecimiento y buen estado de la vegetación se relaciona con la cantidad de agua disponible en las raíces de la planta (hasta 1-2 m de profundidad), y esta a su vez, con la humedad superficial del suelo. La productividad de una planta dependerá por tanto de su nivel de estrés hídrico, humedad del suelo y el riesgo de hielo.

La medida de la humedad del suelo desde satélite es posible gracias a la sensibilidad de la temperatura de brillo emitida en banda L a la humedad presente en la capa más superficial del suelo (~ 0-3 cm) (Escorihuela et al., 2010; Njoku and Kong, 1977). Esta relación se debe a que la emisividad del suelo en microondas está relacionada con su constante dieléctrica, y esta a su vez con la humedad del suelo.

El satélite SMOS (Soil Moisture Ocean Salinity) forma parte de la primera misión cuyo objetivo es la estimación de la humedad del suelo (Kerr et al., 2012) y salinidad del agua en la Tierra (Reul et al., 2014). Su lanzamiento se produjo en Noviembre de 2009 por parte de la Agencia Espacial Europea (ESA) y fue seguido por el lanzamiento en Enero de 2015 de la misión SMAP (Soil Moisture Active Passive) por parte de NASA (Administración Nacional de la Aeronáutica y del Espacio) (Entekhabi et al., 2010), cuyo objetivo principal es la estimación de la humedad del suelo a escala global.

La misión SMOS fue un proyecto ideado por la ESA en colaboración con el CDTI (Centro para el Desarrollo Tecnológico Industrial) en España, y el CNES (Centre National d'Études

Spatiales) en Francia. El satélite SMOS posee un radiómetro interferométrico en banda L (1400 - 1427 MHz) de doble polarización (Kerr et al., 2001) con una resolución espacial de aproximadamente 43 km. Este radiómetro proporciona medidas multi-angulares y en polarización completa de temperatura de brillo de la Tierra con un periodo de revisita de 3 días.

SMOS proporciona no solo medidas de humedad de suelo, sino también de espesor óptico de la vegetación. Este último parámetro se relaciona con ciertas características tales como el contenido en agua de la vegetación o la estructura de la misma (Grant et al., 2016).

El modelo L-MEB (L-band Emission of the Biosphere) es la base de los algoritmos de nivel 2 (L2) y 3 (L3) de SMOS (Kerr et al., 2012). En ambos algoritmos, los parámetros del modelo de transferencia radiativa (Mo et al., 1982) relativos a la rugosidad del suelo y la vegetación, se consideran invariables en el tiempo y su valor viene dado por el tipo de cobertura vegetal siguiendo la clasificación de ECOCLIMAP (Masson et al., 2003).

Los productos de SMOS se dividen en varios niveles (del 1 al 4). El nivel 1 es el producto primario que corresponde a las medidas de temperatura de brillo realizadas por el radiómetro. Los niveles 2 y 3 ofrecen además del producto de temperatura de brillo, la humedad de suelo y espesor óptico de la vegetación, así como todos los datos auxiliares utilizados en el modelo. Los productos de nivel 2 y 3 están geo-referenciados y usan, respectivamente, la malla ISEA (Icosahedral Synder Equal Area), 4H9 (Talone et al., 2015) y EASE (Equal-Area Scalable Earth) 2.0 (Armstrong et al., 1997).

El modelo L-MEB

El modelo L-MEB (Wigneron et al., 2007) es la base de los algoritmos L2 y L3 de SMOS, en los cuales se estima la humedad del suelo y el espesor óptico de la vegetación a partir de las observaciones de satélite. L-MEB emplea datos multi-angulares de temperatura de brillo en polarización horizontal (H) y vertical (V) y un modelo iterativo que consiste en la minimización de una función de coste basada en la diferencia entre la temperatura de brillo observada y la simulada, para todos los ángulos disponibles. Esta función tiene también en cuenta la incertidumbre de los parámetros elegidos para su estimación (humedad del suelo y espesor óptico de la vegetación, en el caso de los algoritmos L2 y L3 de SMOS).

L-MEB modela la emisión de la capa de suelo cubierta por vegetación, teniendo en cuenta las contribuciones del suelo, la vegetación y la radiación del cielo. El suelo se presenta como una superficie rugosa cubierta de vegetación. La temperatura de brillo simulada para un suelo cubierto de vegetación se expresa como suma de la emisión directa de la vegetación, la emisión del suelo atenuada por la capa vegetal y la emisión de la vegetación que es reflejada por el suelo y atenuada por la vegetación.

La relación entre la humedad del suelo y la emisión del suelo vienen dadas por el modelo dieléctrico de Mironov et al. (2012) y las ecuaciones de Fresnel, donde la humedad del suelo y la constante dieléctrica del suelo están relacionadas con la reflectividad de una superficie plana. Los efectos de rugosidad del suelo se consideran mediante una aproximación semi-empírica, mientras que para la modelización de la vegetación se considera el modelo de

transferencia radiativa τ-ω (Mo et al., 1982), donde τ es el espesor óptico de la vegetación y ω el albedo de dispersión simple de la vegetación.

Parámetros de rugosidad del suelo y vegetación en L-MEB

En banda L, la temperatura de brillo es muy sensible a la humedad del suelo, pero existen otros factores que perturban la señal y que deben tenerse en cuenta, tales como la temperatura del suelo y la vegetación (Wigneron et al., 2007), la textura, rugosidad del suelo (Wigneron et al., 2008) y la cubierta vegetal (Grant et al., 2007).

El valor efectivo del albedo de dispersión simple ω tiene en cuenta los efectos de absorción y dispersión debidos a la cubierta vegetal (Kurum, 2013). En los algoritmos L2 y L3 de SMOS, el valor de ω es 0.06 ó 0.08 en bosques (Kerr et al., 2012) y cero en cubiertas vegetales de escasa vegetación. Este último valor está basado en el análisis de campañas de medidas en banda L (Wigneron et al., 2007) sobre ciertas áreas agrícolas y por lo tanto no es aplicable a todas las clases de vegetación. El estudio de ω a escala global es reducido y no existe un gran número de referencias al respecto. En el algoritmo de nivel 2 de SMAP, los valores de ω dependen del tipo de cobertura vegetal, variando de 0 a 0.08 (O'Neill et al., 2012), mientras que el producto de nivel 4 de SMAP proporciona, entre otros parámetros, estimaciones de ω a escala global (De Lannoy et al., 2014). Otro estudio que trata el parámetro ω a escala global es Konings et al. (2016), donde se muestra un mapa de valores de ω, con valores entre 0.02 y 0.04 para coberturas vegetales de escasa vegetación y $\omega = 0.03 – 0.06$ en bosques. Por su parte, el estudio de Van Der Schalie et al. (2016) establece $\omega = 0.12$ como el valor más representativo a escala global tras aplicar el algoritmo LPRM (Land Parameter Retrieval Model) sobre las observaciones de SMOS y comparando el resultado de humedad del suelo con diferentes modelos.

Otros parámetros que caracterizan la vegetación en el algoritmo L-MEB son tt_V and tt_H. Estos parámetros cuantifican la influencia del ángulo de incidencia θ en el espesor óptico de la vegetación. Un estudio detallado de estos parámetros fue llevado a cabo por Schwank et al. (2012) en la Valencia Anchor Station demostrando que existen variaciones importantes en los valores de tt_P (p = H, V) entre verano e invierno y también entre las polarizaciones vertical y horizontal. Sin embargo, a escala global estos parámetros son difíciles de estimar debido a la complejidad de los efectos del tronco de la planta, tallos, hojas y ramas, cuya orientación es altamente aleatoria. El valor de tt_P en los algoritmos L2 y L3 de SMOS es invariable e igual a 1, suponiendo que la vegetación es isotrópica. Un valor de $tt_P > 1$ o $tt_P < 1$ supone asumir una distribución anisotrópica de la vegetación y conlleva, respectivamente, un incremento o un decremento de τ_P en función de θ.

Para tener en cuenta los efectos de la rugosidad del suelo, los algoritmos L2 y L3 de SMOS incluyen cuatro parámetros (H_R, Q_R, N_{RH} and N_{RV}) (Wigneron et al., 2007). El parámetro H_R tiene en cuenta la disminución en la reflectividad del suelo debida a los efectos de rugosidad; Q_R parametriza los efectos de la polarización (mayor o menor influencia) y N_{Rp} (p = H, V) la dependencia de la reflectividad con el ángulo de incidencia. En ambos algoritmos (L2 and L3 de SMOS), el valor de Q_R se supone igual a cero de manera global, mientras que a N_{RH} y N_{RV} se les asignan los valores 2 y 0, respectivamente. Por su parte, los valores de H_R vienen

definidos en función de la clasificación de usos del suelo ECOCLIMAP, siendo H_R = 0.3 en bosque y H_R = 0.1 en el resto de suelos (Kerr et al., 2012). En el algoritmo de humedad del suelo de SMAP L2, el valor de H_R es diferente según la clasificación IGBP (International Geosphere-Biosphere), mientras que N_{Rp} = 2 (p = H, V). A escala local, existen algunas referencias sobre el valor de los parámetros de rugosidad. Como ejemplo, el estudio de Wigneron et al. (2007) arroja valores de H_R = 0.1 - 0.2 para cultivos de soja y trigo y ~ 0.7 para campos de maíz. En España, el estudio de Cano et al. (2010) estima el valor de H_R ~ 0.35 sobre la vegetación de matorral mediterráneo, mientras que el parámetro Q_R se analiza en Lawrence et al. (2013), concluyendo que Q_R = 0 es un valor generalizable en ausencia de condiciones de rugosidad extremas. En lo que respecta a los parámetros N_{RH} y N_{RV}, Escorihuela et al. (2007) y Lawrence et al. (2013) proponen una diferencia de $N_{RH} - N_{RV}$ ~ 2 para superficies de poco relieve y (~ 1 – 1.5) para suelos rugosos.

Objetivos y organización

Esta tesis doctoral se enmarca dentro de los estudios de calibración y validación de los algoritmos L2 y L3 de SMOS, elementos clave para la ESA. En estos, el impacto de los parámetros de rugosidad del suelo y vegetación sobre las estimaciones de humedad del suelo es de gran importancia. La falta de estudios suficientes que traten la calibración de dichos parámetros a escala global es la principal motivación de esta tesis.

El principal objetivo es la calibración de los parámetros de rugosidad del suelo y vegetación, creando un nuevo modelo. En primer lugar, dichos parámetros se calibran y el modelo se evalúa a escala local, en la Valencia Anchor Station; ésta es una estación completamente equipada para llevar a cabo experimentos en banda L, incluyendo el radiómetro ELBARA-II proporcionado por ESA para asistir en la validación de SMOS. En segundo lugar, el objetivo es trasladar la calibración de los mismos parámetros a escala global, creando un nuevo producto de SMOS.

Los objetivos específicos de esta tesis se detallan a continuación:

- Procesar los datos primarios del radiómetro ELBARA-II, así como medidas *in situ* de humedad y temperatura del suelo en la Valencia Anchor Station, incluyendo medidas detalladas de rugosidad del suelo.
- Encontrar la combinación de parámetros de rugosidad del suelo y vegetación que optimizan las estimaciones de humedad del suelo en la Valencia Anchor Station aplicando el modelo L-MEB a series temporales extensas de datos de ELBARA-II.
- Simplificar el algoritmo de SMOS considerando píxeles homogéneos.
- Calibrar los parámetros de vegetación y rugosidad del suelo en el modelo L-MEB a escala global con los datos de temperatura de brillo de SMOS y las medidas de humedad del suelo de la red de estaciones de medida ISMN (International Soil Moisture Network), usadas como referencia.
- Crear un nuevo producto de humedad del suelo y espesor óptico de la vegetación, basado en la calibración previa.

- Evaluar el nuevo producto de SMOS con datos *in situ*, estimaciones de modelos y datos de satélite.

Resultados y conclusiones

Los resultados y conclusiones de esta tesis se refieren a los tres artículos de los que está compuesta, anexos al final de este documento. El primero, es el Artículo 1 (Fernandez-Moran et al., 2015), basado en resultados de la Valencia Anchor Station, al que le siguen las dos publicaciones de calibración y evaluación a escala global, el Artículo 2 (Fernandez-Moran et al., 2017b) y Artículo 3 (Fernandez-Moran et al., 2017a). La metodología y resultados completos pueden consultarse en los artículos señalados.

- ***Artículo 1: "Parametrizaciones de rugosidad del suelo y vegetación en banda L para la estimación de la humedad del suelo en un campo de viñas"***

La primera publicación de esta tesis trata sobre el impacto a escala local de diversas parametrizaciones de la rugosidad del suelo y vegetación en las estimaciones de humedad del suelo (Fernandez-Moran et al., 2015). Con este objetivo, se utilizaron diferentes datos procedentes de la Valencia Anchor Station; por un lado, las observaciones en banda L del radiómetro ELBARA-II y la medición automatizada de la humedad del suelo efectuada con los sensores Delta-T ML2x, así como una campaña de medidas de rugosidad del suelo realizadas con un rugosímetro, o perfilador de la rugosidad del suelo.

En este estudio se emplearon diferentes valores de los parámetros de rugosidad (H_R, Q_R, N_{RV}, N_{RH}) como entradas en el modelo L-MEB. En una primera etapa, se procedió a la estimación (recuperación) de dos parámetros resultantes (2-P), concretamente la humedad del suelo y el espesor óptico de la vegetación en nadir (τ_{NAD}). En una segunda fase, se realizó una estimación (recuperación) de tres parámetros (3-P), añadiendo a los anteriores el parámetro de vegetación tt_V.

Se demostró que al fijar el parámetro $N_{Rp} = -1$ (p = H, V) en las estimaciones 2-P (suponiendo $\omega = 0$), la ecuación para el cálculo de la temperatura de brillo se simplificaba. Este nuevo método se denominó SRP (Simplified Roughness Parameterizacion). Con dicho método, los parámetros de rugosidad del suelo H_R y vegetación τ_{NAD} se simplifican en un solo parámetro (TR) de salida en el modelo L-MEB. Esta combinación implica la necesidad de calibrar el parámetro H_R, ya estando implícita su contribución en el parámetro de salida TR, que se extrae conjuntamente con la humedad del suelo.

Con el método SRP se obtuvieron las mejores estimaciones de humedad del suelo al maximizar la correlación (R) y minimizar el error cuadrático medio sin sesgo (ECM), obtenido al comparar dichas estimaciones con las medidas *in situ* de humedad del suelo de los sensores Delta-T ML2x, considerados como referencia en la Valencia Anchor Station. No se obtuvo, sin embargo, el menor sesgo absoluto con el método SRP. Una de las posibles causas de los valores de sesgo negativos que se encontraron es la diferencia en la profundidad de muestreo de las estimaciones del radiómetro frente a las medidas *in situ* (≈ 0–6 cm).

En cuanto a las estimaciones 3-P, se encontraron correlaciones más altas y un descenso del ECM frente a las estimaciones 2-P, mientras que el sesgo absoluto obtenido fue notablemente más alto. La ventaja del método 3-P frente al 2-P puede deberse al hecho de que el primero tiene en cuenta las características propias de las viñas, con una orientación de sus ramas fundamentalmente vertical. En el método 3-P, tt_V tiene en cuenta el efecto del ángulo de incidencia sobre el espesor óptico de la vegetación en polarización vertical. Sin embargo, en las estimaciones 2-P, tt_V y tt_H son considerados iguales ($tt_V = tt_H = 1$) y por tanto la vegetación se supone isotrópica, lo que significa que no se tienen en cuenta los cambios en la estructura de la vegetación en relación con su ciclo de crecimiento y senescencia, o las prácticas agrícolas.

Aunque los valores estadísticos de este estudio indicaron que el método 3-P fue el más adecuado, la desventaja de este método reside en su dependencia del parámetro H_R. Dicha dependencia, sin embargo, fue menos pronunciada en el caso $N_{RV} = N_{RH} = -1$. Esta última suposición, por lo tanto, resultó ser la más conveniente para los modelos 2-P y 3-P. Para el resto de combinaciones de H_R, Q_R, N_{RV} y N_{RH} donde $N_{Rp} \neq -1$, se encontró una correlación decreciente y ECM creciente, al aumentar los valores de H_R.

Por otro lado, el uso de las estimaciones de rugosidad del suelo a partir de una campaña de medidas *in situ*, no demostró una mejora en las estimaciones de la humedad del suelo respecto al método SRP. Sin embargo, su estudio fue de gran utilidad para confirmar que la señal de τ_{NAD} en el modelo 2-P está afectada por los cambios de rugosidad en el terreno; estos cambios son principalmente debidos a las lluvias y prácticas agrícolas.

En conclusión, este estudio presenta el método SRP como una interesante alternativa que permite tener en cuenta los efectos de rugosidad del suelo en la estimación de la humedad del suelo, sin necesidad de calibrar el parámetro H_R.

- ***Artículo 2: "Una nueva calibración de los parámetros de rugosidad del suelo y albedo de dispersión simple en el algoritmo de humedad del suelo de SMOS"***

Con el objetivo de confirmar los hallazgos del estudio anterior (Fernandez-Moran et al., 2015), se desarrolló un nuevo estudio a escala global usando los datos de temperatura de brillo de SMOS (Fernandez-Moran et al., 2017b) (en el estudio anterior los datos de temperatura de brillo provenían del radiómetro ELBARA-II situado en la Valencia Anchor Station). Este estudio se centró en la calibración de los parámetros de rugosidad del suelo (H_R, N_{RH} y N_{RV}) y vegetación (mediante el parámetro ω). Para ello, se utilizó un amplio rango de valores de los citados parámetros, obteniendo humedad del suelo y τ_{NAD} en un número significativo de estaciones donde existen medidas *in situ* de humedad del suelo. Dichas estaciones están situadas en diversas zonas geográficas con coberturas vegetales variables.

Los algoritmos L2 y L3 de SMOS tienen en cuenta diferentes fracciones de suelo (suelo desnudo o con escasa vegetación, bosque, agua, ciudad, etc.) dentro de cada *footprint* de SMOS. Sin embargo, la estimación de parámetros (es decir, humedad del suelo y τ_{NAD}), solo se realiza sobre una fracción: o bien la nominal (área de vegetación escasa) en la mayor parte de los casos, o sobre bosque. Se estiman también los valores de temperatura de brillo de las fracciones de pixel que no se consideran para la obtención de la humedad del suelo y τ_{NAD}.

En el caso de la fracción de bosque, esta estimación se realiza en base a datos auxiliares de humedad del suelo del modelo proporcionados por ECMWF (Centro Europeo de Previsiones Meteorológicas a Medio Plazo). Según el estudio de Wigneron et al. (2012), el sesgo introducido en el modelo debido a estos datos auxiliares, produce una subestimación de la humedad del suelo en regiones boscosas. Con el fin de evitar dicha subestimación y simplificar el algoritmo, en este estudio (Artículo 2) se usó la temperatura de brillo de nivel 3 de SMOS como entrada en el modelo, suponiendo una distribución homogénea del pixel. A este procedimiento se le denominó *algoritmo simplificado*.

Las estimaciones de humedad del suelo se compararon con las correspondientes medidas *in situ* procedentes de la red de estaciones de medida ISMN (International Soil Moisture Network) en el periodo 2011 – 2013 y se evaluaron mediante diferentes estadísticos (R, sesgo y ECM). En el estudio, solo se consideraron aquellas estaciones contenidas en píxeles suficientemente homogéneos. Para calibrar los parámetros de vegetación y rugosidad del suelo en el algoritmo, se buscó un compromiso entre los valores óptimos de los estadísticos analizados; el sesgo se consideró como el criterio menos importante, debido a la diferencia entre la profundidad de muestreo de las medidas *in situ* (0-5 cm) y las estimaciones de SMOS en banda L (~ 0–3 cm).

Las estimaciones de humedad del suelo evaluadas mediante los estadísticos anteriormente expuestos, mostraron una gran sensibilidad de la humedad del suelo a los valores de ω; siendo $\omega \sim 0.10$ el valor óptimo para todos los estadísticos. Por el contrario, se demostró que la calibración del parámetro H_R requiere el compromiso entre los valores de sesgo absoluto (menores cuanto mayor es H_R) y el ECM (menor cuanto menor es H_R). Los resultados también mostraron que el aumento de ω y la disminución de H_R conllevan una subestimación de la humedad del suelo.

El estudio estableció los valores $\omega = 0.10$, $H_R = 0.4$ y $N_{Rp} = -1$ (p = H, V) como óptimos a escala global. Estos resultados concuerdan con las conclusiones extraídas del anterior estudio en la Valencia Anchor Station (Fernandez-Moran et al., 2015), donde se proponía el método SRP, siendo $N_{Rp} = -1$. Sin embargo, en el método SRP, el valor de ω no se calibró y se fijó a 0 (siguiendo los algoritmos L2 y L3 de SMOS). Esta nueva calibración del parámetro ω es consistente con los mapas de ω de nivel 4 de SMAP ($\omega = 0.09 \pm 0.07$) y el estudio de Van der Schalie et al. (2016), que obtuvo un valor de ω igual a 0.12 después de aplicar el modelo LPRM (Land Parameter Retrieval Model) y evaluar las estimaciones de humedad del suelo resultantes frente a las estimaciones de ERA-Interim/Land y MERRA-Land. Este estudio también mostró que el impacto de la rugosidad del suelo sobre la correlación entre las estimaciones y los modelos es despreciable cuando se supone $\omega = 0.12$. Por otro lado, el estudio de Konings et al. (2016) muestra valores de ω entre 0.02 y 0.06, mientras que tanto en el algoritmo de nivel 2 como en el de nivel 3 de SMOS, el valor de ω es 0.06 – 0.08 para bosques y 0 para el resto de coberturas vegetales.

Para realizar la clasificación de las estaciones *in situ*, se usó el esquema IGBP (International Geosphere-Biosphere) y se propusieron diferentes valores de H_R, N_{Rp} (p = H, V) y ω para cada clase. Los valores de H_R variaban entre la vegetación poco densa ($H_R \sim 0.1$) y el resto de coberturas (entre 0.4 y 0.5) y se estableció $N_{Rp} = -1$ a escala global. Los resultados son consecuentes con los de Parrens et al. (2017), estudio en el que se calibró el parámetro H_R usando estimaciones de SMOS y LAI (Leaf Area Index) de MODIS (Moderate-Resolution

Imaging Spectroradiometer). Por otro lado, se propusieron valores de ω entre 0.06 y 0.08.

El algoritmo simplificado con las calibraciones propuestas en este estudio, se evaluó con los datos *in situ* de humedad del suelo de las estaciones ISMN (incluyendo y excluyendo aquellas estaciones empleadas en el proceso de calibración). Las estadísticas mostraron que tanto usando los parámetros calibrados globalmente como los dependientes de la clasificación IGBP, se obtuvieron valores óptimos de humedad del suelo respecto a aquellos obtenidos con el producto oficial de nivel 3 de SMOS (versión 300): siendo R = 0.61, sesgo = -0.01 $m^3 \cdot m^3$ y ECM = 0.062 $m^3 \cdot m^{-3}$ para el algoritmo simplificado (con la calibración dependiente de IGBP) y R = 0.54, sesgo = -0.034 $m^3 \cdot m^{-3}$ y ECM = 0.070 $m^3 \cdot m^{-3}$ para el producto oficial de nivel 3 de SMOS. Esta mejora no se pudo demostrar como una consecuencia del uso de píxeles homogéneos. No obstante, el algoritmo de nivel 3 de SMOS mostró un efecto de subestimación de la humedad del suelo asociado al uso de píxeles heterogéneos. Esto se demostró ya que al emplear el algoritmo simplificado (píxeles homogéneos) con una configuración de parámetros de entrada en el modelo L-MEB similares a los del algoritmo L3 de SMOS, se obtuvo un sesgo de 0.028 $m^3 \cdot m^{-3}$, frente a -0.034 $m^3 \cdot m^{-3}$ obtenido con el producto oficial L3 de SMOS (píxeles heterogéneos).

Los resultados de este estudio tendrán consecuencias directas en la calibración de los parámetros de rugosidad del suelo y vegetación en las versiones oficiales futuras de los algoritmos L2 y L3 de SMOS. Sus resultados son la base de un nuevo producto desarrollado entre INRA (Institute National de la Recherche Agronomique) y CESBIO (Centre d'Études Spatiales de la BIOsphère), denominado SMOS-IC (SMOS-INRA-CESBIO). La simplicidad de este algoritmo supone en la práctica la implementación de un procesador eficiente y rápido, capaz de generar varios años de datos en unas cuantas horas mediante el uso de una supercomputadora.

- ***Artículo 3: "SMOS-IC: Un producto alternativo de humedad del suelo y espesor óptico de la vegetación de SMOS"***

El producto SMOS-IC (Fernandez-Moran et al., 2017a) proporciona diariamente la humedad del suelo y τ_{NAD} a escala global. En esta tesis se empleó una versión de prueba (v102) de dicho producto, el cual se presenta en formato NetCDF con una malla EASE 2.0 (Equal-Area Scalable Earth) de 25 x 25 km^2 (Armstrong et al., 1997), al igual que los productos de nivel 3 de SMOS.

El algoritmo de SMOS-IC simplifica el de nivel 3 de SMOS y no tiene en cuenta ciertas correcciones relativas al patrón de radiación de la antena y el ángulo de visión. El principal dato de entrada en el algoritmo de SMOS-IC para el proceso de inversión de L-MEB es el producto multi-angular y en doble polarización de TB de nivel 3 de SMOS. En el algoritmo se consideran los píxeles como homogéneos para evitar posibles errores en los datos que se emplean para la caracterización de la heterogeneidad del píxel. En concreto, SMOS-IC no se basa en datos LAI de MODIS ni de humedad del suelo de ECMWF; de estos últimos, además, se conoce su subestimación de la humedad del suelo (Albergel et al., 2012).

En SMOS-IC, los parámetros de entrada del modelo L-MEB relativos a rugosidad del suelo

(H_R) y ω se estiman en función de su categoría en la clasificación IGBP. Estos valores se derivaron de la calibración del Artículo 2 mostrado anteriormente (Fernandez-Moran et al., 2017b) y los mapas de rugosidad H_R estimados por Parrens et al. (2016).

En el Artículo 3 (Fernandez-Moran et al.; 2017a), se presenta SMOS-IC y se muestra una evaluación a escala global. Para ello, la humedad del suelo del producto oficial de SMOS de nivel 3 (versión 300) y de SMOS-IC se compararon globalmente con la humedad del suelo del modelo ECMWF en el periodo 2010 – 2015. Este análisis es una extensión de la evaluación mostrada en el Artículo 2 (Fernandez-Moran et al., 2017b), donde se utilizaron como referencia un gran número de estaciones de la red internacional ISMN.

Se demostró que, a escala global, tanto SMOS-IC como el producto de nivel 3 de SMOS subestimaron la humedad del suelo con respecto a las estimaciones del modelo ECMWF. Este resultado puede explicarse en parte por la diferencia en la profundidad de muestreo del modelo ECMWF (los primeros 7 cm superficiales) frente a SMOS (~ 0 - 3 cm). Por regla general, se encontró una correlación más elevada y menor ECM (error cuadrático medio) para SMOS-IC que para el producto de nivel 3 de SMOS.

En cuanto a la evaluación del espesor óptico de la vegetación τ_{NAD}, se empleó el índice *NDVI* como referencia. Este índice es un estimador habitual del parámetro τ_{NAD} en banda L para coberturas de poca densidad vegetal durante el periodo de crecimiento de la vegetación (O'Neill et al., 2012; Wigneron et al., 2007; Lawrence et al., 2014; Grant et al., 2016). Sin embargo, deben señalarse algunas diferencias entre ambos productos. En primer lugar, el índice *NDVI* se obtiene mediante sensores ópticos (y no de microondas). En segundo lugar, el índice *NDVI* permite monitorizar el verdor de la vegetación, mientras que el índice τ_{NAD} se relaciona con el contenido en agua de la vegetación (incluyendo fundamentalmente tallos, ramas y troncos). Los valores de τ_{NAD} de SMOS-IC presentaron un menor rango de valores (~ 0-1.3) respecto al correspondiente producto de nivel 3 de SMOS (~ 0-1.5) y, en general, se encontraron correlaciones más altas entre el índice τ_{NAD}de SMOS-IC y el índice NDVI de MODIS, que entre el índice τ_{NAD}de nivel 3 de SMOS y el NDVI.

Los buenos resultados hallados en este estudio, demuestran la utilidad e impacto de SMOS-IC en la evaluación y futura mejora de los productos oficiales de nivel 2 y 3 de SMOS. Además, al asumir la homogeneidad de los píxeles, SMOS-IC se alinea con otros algoritmos como el de SMAP o el de AMSR-E (Advanced Microwave Scanning Radiometer); este último ofreciendo estimaciones de humedad del suelo en banda C.

Nuevos estudios que incluyan la validación de SMOS-IC a escala global serán de gran utilidad. Los resultados de esta tesis abren futuras vías de estudio; entre ellas se encuentra la inter-comparación de los productos de humedad del suelo y τ_{NAD} con datos de satélite tales como la humedad del suelo de SMAP y AMSR-E, el índice LAI de MODIS, medidas de biomasa de los bosques o estimaciones de humedad del suelo de modelos como MERRA (Modern-Era Retrospective analysis for Research and Applications) (Reichle et al., 2011).

La simplicidad del algoritmo de SMOS-IC permite implementar mejoras en el algoritmo con mayor rapidez. Una propuesta de futuro es la utilización de temperaturas de suelo y vegetación de otros modelos diferentes a ECMWF, o incluso datos de satélite, como entradas en el modelo L-MEB. Otra opción de interés es la estimación de tres parámetros (3-P), donde la humedad del suelo y τ_{NAD} se estiman junto a la temperatura efectiva del suelo/vegetación.

ABSTRACT

The capability of L-band radiometry to monitor surface soil moisture (SM) at global scale has been analyzed in numerous studies, mostly in the framework of the Soil Moisture Ocean Salinity (SMOS) and near future SMAP (Soil Moisture Active Passive) space borne missions. While the soil moisture of the first centimeters of the soil surface (~3 cm) is strongly related to the Brightness Temperature (TB) measurements, other parameters must be accounted for in order to produce accurate estimations of SM. To retrieve SM from L-band radiometric observations, two significant effects have to be accounted for: soil roughness and vegetation. In the first part of this thesis, the effects of soil roughness on retrieved SM values were evaluated using in-situ observations acquired by the L-band ELBARA-II radiometer, over a vineyard field at the Valencia Anchor Station (VAS) site during the year 2013. In the SMOS algorithm, L-MEB (L-band Microwave Emission of the Biosphere) is the forward model. Different combinations of the values of the model parameters used to account for soil roughness effects (H_R, Q_R, N_{RH} and N_{RV}) were evaluated. The evaluations were made by comparing in-situ measurements of SM (used here as a reference) against SM retrievals derived from tower-based ELBARA-II brightness temperatures. The general retrieval approach consists of the inversion of L-MEB. Two specific configurations were tested: the classical 2-Parameter (2-P) retrieval configuration [where *SM* and τ_{NAD} (vegetation optical depth at nadir) were retrieved] and a 3-Parameter (3-P) configuration, accounting for the additional effects of the vineyard vegetation structure.

Using the 2-P configuration, it was found that setting N_{RP} (P = H or V) equal to -1 produced the best SM estimations in terms of correlation and unbiased Root Mean Square Error (ubRMSE). The assumption $N_{RV} = N_{RH} = -1$ leads to a simplification in L-MEB, since the two parameters τ_{NAD} and H_R can be grouped and retrieved as a single parameter (method defined here as the Simplified Retrieval Method (SRP)). A main advantage of the SRP method is that it is not necessary to calibrate the value of H_R before performing SM retrievals. Using the 3-P configuration, improved results were obtained in the SM retrievals in terms of correlation and ubRMSE. Finally, it was found that the use of in-situ roughness measurements to calibrate the values of the roughness model parameters did not provide significant improvements in the SM retrievals in comparison with the SRP method.

The second part of the thesis focuses on the calibration of the effective vegetation scattering albedo (ω) and surface soil roughness parameters in the SM retrieval at global scale. In the current SMOS Level 2 (L2) and Level 3 (L3) retrieval algorithms, low vegetated areas are parameterized by $\omega = 0$ and $H_R = 0.1$, whereas values of $\omega = 0.06$ - 0.08 and $H_R = 0.3$ are used

for forests. Several parameterizations of the vegetation and soil roughness parameters (ω, H_R and N_{Rp}, p = H, V) were tested. In addition, the inversion approach was simplified by considering the SMOS pixels as homogeneous instead of retrieving SM only over a fraction of the pixel (excluding forested areas), as implemented in the operational SMOS L2 and L3 algorithms. Globally-constant values of $\omega = 0.10$, $H_R = 0.4$ and $N_{Rp} = -1$ (p = H, V) were found to yield SM retrievals that compared best with *in situ* SM data measured at many sites worldwide from the International Soil Moisture Network (ISMN). The calibration was repeated for collections of *in situ* sites classified in different land cover categories based on the International Geosphere-Biosphere Programme (IGBP) scheme. Depending on the IGBP land cover class, values of ω and H_R varied, respectively, in the range 0.08 - 0.12 and 0.1 - 0.5. A validation exercise based on in situ measurements confirmed that using either a global or an IGBP-based calibration, there was an improvement in the accuracy of the SM retrievals compared to the SMOS L3 SM product considering all statistical metrics. This result is a key step in the calibration of the roughness and vegetation parameters of future versions of the operational SMOS retrieval algorithm. This result was also at the base of the development of the so-called SMOS-INRA-CESBIO (SMOS-IC) product.

The SMOS-IC product provides daily values of the SM and τ_{NAD} parameters at the global scale and differs from the operational SMOS Level 3 (SMOSL3) product in the treatment of retrievals over heterogeneous pixels. SMOS-IC is much simpler and does not account for corrections associated to the antenna pattern and the complex SMOS viewing angle geometry. It considers pixels as homogeneous to avoid uncertainties and errors linked to inconsistent auxiliary data sets which are used to characterize the pixel heterogeneity in the SMOS L3 algorithm. SMOS-IC also differs from the current SMOSL3 product (Version 300, V300) in the values of the effective vegetation scattering albedo (ω) and soil roughness parameters. An inter-comparison of the SMOS-IC and SMO3L3 products (V300) is presented in this thesis based on the use of ECMWF (European Center for Medium range Weather Forecasting) SM and NDVI (Normalized Difference Vegetation Index) from MODIS (Moderate-Resolution Imaging Spectroradiometer). A 6 year (2010-2015) inter-comparison of the two SMOS products (SMOS-IC and SMOSL3 SM (V300)) with ECMWF SM yielded higher correlations and lower ubRMSD (unbiased root mean square difference) for SMOS-IC over most of the pixels. In terms of τ_{NAD}, SMOS-IC was found to be better correlated to MODIS NDVI in most regions of the globe, with the exception of the Amazonian basin and of the northern mid-latitudes. The SMOS-IC VOD product is now extensively used in applications analyzing the impact of droughts on vegetation carbon budgets/biomass at continental scales.

1 INTRODUCTION

The references to Article 1, 2 and 3 correspond to the articles annexed at the end of this PhD thesis

This chapter intends to introduce the significance of soil moisture at global scale in the context of the Soil Moisture and Ocean Salinity (SMOS) mission. It defines briefly the main concepts and presents the data used in the three papers annexed at the end of this document, where an extensive methodology for each study can be found. It also shows the motivation of this PhD study and the thesis outline.

1.1 Background

1.1.1 Soil moisture

Soil moisture is a key element of the global water cycle which allows us to determine the water and energy fluxes at the surface-atmosphere interface. Direct observations of soil moisture from the space allow improved estimates of water, energy and carbon transfers between the land and the atmosphere. Soil moisture is a physical parameter of interest for many hydrological and agricultural applications (Brocca et al., 2010), weather and climate predictions (de Rosnay et al., 2013) and early warning of natural hazards.

Before being saturated, any soil absorbs a given amount of water depending of its composition. Soil moisture interacts directly with the atmosphere through evapotranspiration and it is related with soil infiltration. The fluxes of sensible heat and moisture at the base of the atmosphere influence the evolution of weather, then soil moisture is often a significant factor in the performance of atmospheric models. For numerical weather prediction (NWP) models, soil moisture is used in forecast initialization. Accurate soil moisture information enhances their prediction skills.

The availability of soil moisture data set at global scale permits drought monitoring and plant water stress. Moreover, natural hazards including floods and landslides can be detected, allowing disaster preparation and response. Flood prediction models require soil moisture information to understand the partitioning of precipitation into infiltration and runoff. Similarly, soil moisture plays an important role in the landslides over mountainous areas.

Another application of soil moisture information is on agriculture for crop management and forecasting extreme events. Vegetation health and growth is linked directly to the amount of water available in the root zone (up to 1-2 m), and this zone is related to the soil moisture measured in the first centimetres of the soil surface. Particularly, the estimation of plant productivity requires information of the plant water stress, soil moisture status and potential frost damage.

The measurement of soil moisture from satellite data is possible due to the strong dependence of surface soil moisture (first centimetres of soil) to the emitted brightness temperature (*TB*) at L-band. The sensitivity of the measured *TB* with respect to soil moisture is due to the fact that soil emissivity in the microwave domain is highly related to the soil dielectric constant which is mainly determined by soil moisture.

Surface soil moisture is defined as the fraction of water contained in a volume of humid soil, considering a superficial soil layer of a few centimeters (WMO, https://www.wmo-sat.info/oscar/variables/view/149). It can be expressed gravimetrically or volumetrically. In this study, the ratio of water volume to the volume of the soil containing is used ($m^3 \cdot m^{-3}$).

1.1.2 SMOS

SMOS (Soil Moisture Ocean and Salinity) is the first mission dedicated to the measurement of moisture (Kerr et al., 2012) and salinity at the surface water of the oceans (Reul et al., 2014). It was launched in November 2009 by the European Space Agency (ESA) and followed by the Soil Moisture Active Passive (SMAP) mission from National Aeronautics and Space Administration (NASA), launched in January 2015 (Entekhabi et al., 2010). The development of the SMOS mission was led by the European Space Agency (ESA) in collaboration with the *Centro para el Desarrollo Tecnológico Industrial* (CDTI) in Spain and the *Centre National d'Études Spatiales* (CNES) in France. SMOS carries a full polarization L-band 2-D interferometric radiometer operating in the 1400 – 1427 MHz protected band (Kerr et al., 2001) and achieves a spatial resolution of around 50 km (43 km on average over the field of view). Moreover, it provides multi-angular dual polarized *TB* over the globe with a revisit time of less than 3 days.

Soil moisture in the first centimetres of the soil surface (~ 0 - 3 cm) is strongly related to the measurements of the emitted *TB* at L-band (Escorihuela et al., 2010; Njoku and Kong, 1977). Currently, SMOS and SMAP missions provide global maps of soil moisture and vegetation optical depth (only operational in the case of SMOS for the latter). The vegetation optical depth is related to vegetation characteristics such as water content and vegetation structure (Grant et al., 2016).

The L-band Microwave Emission of the Biosphere (L-MEB) model is the core of the SMOS level 2 (L2) and 3 (L3) retrieval algorithms (Kerr et al., 2012). In these algorithms, the radiative transfer model (Mo et al., 1982) parameters related to soil roughness and some vegetation parameters (Wigneron et al., 2007) are considered to be time independent and their values are computed based on a land cover map (ECOCLIMAP, Masson et al., 2003).

The SMOS data products are delivered up to level 4 inclusive. The L1 product is the primary

measurement of the SMOS radiometer, i.e. brightness temperature. The L2 and L3 products offer the retrieved soil moisture and vegetation optical depth and all the ancillary data involved in the processing; these products are geo-located, respectively, on the Icosahedral Snyder Equal Area (ISEA) 4H9 grid (Talone et al., 2015) and Equal-Area Scalable Earth (EASE) grid 2.0 (Armstrong et al., 1997).

1.1.3 L-MEB model: Soil moisture and vegetation optical depth retrieval

The L-MEB model (Wigneron et al., 2007) is the forward model used in the SMOS L2 and L3 soil moisture algorithms, and the basis of all soil moisture and vegetation optical depth retrievals showed in this study. This model uses multi-angular *TB* data in horizontal (H) and vertical (V) polarization and an iterative approach which consists on minimizing a Bayesian cost function based on the differences between the observed and the simulated brightness temperature, for all observation angles. This function accounts for the observation uncertainty, and also contains a prior parameter constraint for the parameters to be retrieved (soil moisture and vegetation optical depth in the L2 and L3 SMOS algorithms).

L-MEB models the emission of a vegetation-covered soil, taking into account the contributions of soil, vegetation and sky radiation contributions. The model represents the soil as a rough surface with a vegetation layer. The simulated *TB* from the soil vegetation medium is calculated as the sum of the direct vegetation emission, the soil emission attenuated by the canopy and the vegetation emission reflected by the soil and attenuated by the canopy.

Soil moisture and soil emission are linked through the use of the Mironov et al. (2012) dielectric model and the Fresnel equations, which relate soil moisture to soil dielectric constant, and the latter to the soil reflectivity of a smooth surface. The soil roughness effects are considered through a semi-empirical approach. Besides, vegetation is accounted through the zero-order τ-ω radiative transfer model (Mo et al., 1982), where τ denotes the vegetation optical depth and ω the single scattering albedo.

1.1.4 Soil roughness and vegetation parameters in L-MEB

At L-band, the measured *TB* is highly sensitive to soil moisture, but it is important to account for other factors such as soil and vegetation temperatures (Wigneron et al., 2007), soil texture and roughness (Wigneron et al., 2008) and vegetation cover and litter (Grant et al., 2007).

The effective vegetation scattering albedo ω accounts for absorption and scattering effects within the vegetation canopy (Kurum, 2013). In the current L2 and L3 SMOS algorithms, the value of ω is assumed to be 0.06 – 0.08 over forests (Kerr et al., 2012), and zero over low vegetation canopies (non-forested biomes). The value of ω assigned to low vegetation is based on the analysis of tower-based L-band radiometric measurements (Wigneron et al., 2007) but it may not be accurate for all canopy types as it was studied over few specific agricultural sites. Few studies can be found in the literature investigating ω at a global scale. In the SMAP L2 algorithm, the values of ω are based on the vegetation type (O'Neill et al.,

2012) varying from 0 to 0.08. Additionally, the SMAP L4 product globally provides variable estimates of the effective scattering albedo (and all other parameters) (De Lannoy et al., 2014). The study of Konings et al. (2016) gives values of ω = 0.02 – 0.04 over low vegetation and 0.03 – 0.06 over forested areas. On the other hand, the study of Van Der Schalie et al. (2016) found globally an optimal value of ω = 0.12 after applying the Land Parameter Retrieval Model (LPRM) on SMOS observations against different modelled soil moisture data.

Other parameters that account for vegetation effects in the L-MEB algorithm are tt_V and tt_H. These parameters are used to quantify the dependence of vegetation optical depth (τ_P) on the incidence angle θ. The study of Schwank et al. (2012) focused on the calibration of those parameters after carrying out an experiment at the Valencia Anchor Station (VAS). This study found significant variations of tt_P (p = H, V) between summer and winter and also for horizontal and vertical polarization. However, accounting for these effects at global scale is a difficult task due to the complex effects of trunks, stems, branches and leaves, with irregular and random orientation. For that reason, in the SMOS L2 and L3 algorithms a value of $tt_P = 1$ is assumed. This value corresponds to the isotropic case in which τ_P is polarization independent ($\tau_H(\theta) = \tau_V(\theta) = \tau_{NAD}$). A value of $tt_P > 1$ or $tt_P < 1$ leads to an increase or decrease of τ_P as function of θ corresponding to anisotropic vegetation.

In terms of soil roughness, the SMOS L2 and L3 retrieval algorithms include four parameters (H_R, Q_R, N_{RH} and N_{RV}) (Wigneron et al., 2007). The parameter H_R accounts for the decrease in the soil reflectivity due to soil roughness effects, Q_R for polarization mixing effects, and N_{Rp} (p = H, V) for the angular dependence of reflectivity. In the SMOS L2 and L3 soil moisture retrieval algorithms, Q_R is fixed globally to 0, while N_{RH} and N_{RV} are set to 2 and 0 respectively. The value of H_R is defined based on the ECOCLIMAP classification schema, with H_R = 0.3 for forests and H_R = 0.1 for the rest of the cover types (Kerr et al., 2012). In the SMAP L2 soil moisture algorithm, N_{Rp} = 2 (p = H, V) and the value of H_R differs from the International Geosphere-Biosphere (IGBP) classes. Some studies have been done over specific vegetation types. For instance, Wigneron et al. (2007) found values of H_R = 0.1 - 0.2 for soybean and wheat crops and ~ 0.7 for corn fields. Over Spain, Cano et al. (2010) estimated that H_R ~ 0.35 over Mediterranean vegetation. Regarding the Q_R parameter, Lawrence et al. (2013) found that Q_R = 0 is a reasonable value for non-extreme roughness conditions. As for the parameters N_{RH} and N_{RV}, Escorihuela et al. (2007) and Lawrence et al. (2013) proposed a difference of N_{RH} – N_{RV} ~ 2 for smooth surfaces and (~ 1 – 1.5) for rough soils.

1.2 Research objectives

This PhD research is part of the studies developed in the frame of the SMOS mission. The calibration of the SMOS L2 and L3 algorithms and the validation of SMOS soil moisture are key elements for ESA. In these algorithms, soil roughness and vegetation parameters have an important impact on the retrieved soil moisture. The lack of sufficient studies about the calibration of these parameters at global scale is the main motivation of this PhD thesis.

The first main objective is the calibration of the soil roughness and vegetation parameters, creating a new model. Firstly, these parameters are calibrated and the model is evaluated at

local scale, specifically at the VAS, a fully-equipped station where very specific *in situ* experiments can be carried out. In a second step, a similar calibration and evaluation is done at global scale and a new SMOS product is developed.

The particular objectives are listed in the following:

1. Process the ELBARA-II raw data, soil moisture and soil temperature measurements at the VAS. Perform regular *in situ* soil roughness measurements.
2. Find the optimal combination of soil roughness and vegetation parameters that produce the best soil moisture retrievals at the VAS applying the L-MEB model to long temporal series of ELBARA-II data.
3. Simplify the SMOS retrieval algorithm using an approach based on homogeneous pixels.
4. Calibrate the soil roughness and vegetation parameters in the L-MEB model at global scale using SMOS *TB* data where the soil moisture measurements from the ISMN are used as reference.
5. Create a new product of soil moisture and vegetation optical depth based on the previous calibration
6. Evaluate the new product with *in situ*, modelled and satellite data.

1.3 Thesis outline

The thesis Chapter 1 intends to introduce the objectives of this thesis and also provide background information on soil moisture estimation at L-band. Chapter 2 shows a summary of the main results and conclusions from the three articles that make up this thesis, in answer to the research objectives previously addressed. Chapter "References" lists the main and basic bibliography for the contents presented in here and additionally a "List of publications" is given, where all articles (national and international) and conference proceedings, poster and oral presentations are listed. The previous Chapters are followed by an original copy of the three papers, where their particular methodology, data and results are well detailed.

Article 1 (Fernandez-Moran et al., 2015) is a local experiment taken at the Valencia Anchor Station where fieldwork was combined with data analysis, modelling, calibration and validation. Its aim was the calibration of the soil roughness and vegetation parameters in the L-MEB model in a vineyard field within the VAS. This paper proposed a method in which soil moisture could be retrieved jointly with a combination of both vegetation optical depth and H_R, as both parameters were demonstrated to be strongly linked and not easily decoupled. The method did not require H_R and it was found that the use of *in situ* soil roughness measurements did not improve the soil moisture retrieval.

Article 2 (Fernandez-Moran et al., 2017b) is a global scale calibration of soil roughness and vegetation parameters in the L-MEB model. The methodology extended the one presented in Article 1 and included the calibration of the vegetation scattering albedo parameter. A number of soil roughness and vegetation scattering albedo parameterizations were used in the retrieval of soil moisture through a simple algorithm where homogeneous pixels were

assumed. Then, the soil moisture retrieved from these different parameterizations was compared to long term *in situ* soil moisture series coming from the International Soil Moisture Network. A new SMOS product, called SMOS-IC, was developed based on this new calibration.

Article 3 (Fernandez-Moran et al., 2017a) is a comparison exercise between the SMOS-IC soil moisture and τ_{NAD} against, respectively, the soil moisture modelled by ECMWF and the *NDVI* from MODIS. The results were analysed against the SMOS L3 *SM* and τ_{NAD} and showed an improved performance of SMOS-IC in comparison to SMOS L3.

2 SUMMARY AND CONCLUSIONS

This chapter intends to show the main results and conclusions from Article 1 (Fernandez-Moran et al., 2015), Article 2 (Fernandez-Moran et al., 2017b) and Article 3 (Fernandez-Moran et al., 2017a). An original copy of the three papers is annexed at the end of this thesis.

2.1 Roughness and vegetation parameterizations at L-band for soil moisture retrievals over a vineyard field

The first study contained in this thesis aims at analysing the impact of several roughness and vegetation parameterizations on soil moisture retrievals (Fernandez-Moran et al., 2015). To this aim, different *in situ* data measured at the Valencia Anchor Station (VAS) were used, namely the brightness temperature (*TB*) observations from the L-band ELBARA-II radiometer, the soil moisture (*SM*) measured with two Delta-T ML2x soil moisture probes and the *in situ* roughness measurements performed with a profiling needle board.

Several values of the roughness parameters (H_R, Q_R, N_{RV}, N_{RH}) were set as inputs for the L-MEB model. In a first step, two parameters were retrieved (2-P retrieval), namely soil moisture and vegetation optical depth at nadir (τ_{NAD}). Secondly, a 3-P retrieval was achieved, adding the retrieval of the vegetation parameter (tt_V) to the 2-P retrieval.

It was found that the original formulation of the soil roughness approach used to compute *TB* could be simplified when setting $N_{Rp} = -1$ (p = H, V) in the 2-P retrievals (where $\omega = 0$). We called this the Simplified Roughness Parameterization (SRP) method. In this method, soil roughness (H_R) and vegetation (in terms of τ_{NAD}) parameters can be accounted for through a single parameter (*TR*) that is retrieved (instead of τ_{NAD}). Consequently, H_R does not need to be calibrated, as its contribution is already accounted for in the *TR* parameter which is simultaneously retrieved with *SM*.

According to the tests done at the VAS in 2013, it was found that the SRP method led to the best retrievals of *SM* values in terms of correlation coefficient (R) and unbiased Root Mean Square Error (ubRMSE) when compared with synchronous *in situ SM* measurements, considered as the reference. Conversely, the lowest bias was found with other combinations of the roughness parameters. Using the SRP configuration, the retrieved *SM* values underestimated the measured ones for all tested configurations. However, this result could be partly explained by the different sampling depths of the retrieved *SM* data (≈ 0–3 cm) (Escorihuela et al., 2010) and of the *in situ* measurements (≈ 0 – 6 cm), which may affect the analyses in a way or another.

The 3-P retrieval at the VAS generally led to improved results in terms of correlation R and

ubRMSE against the 2-P retrieval, but the bias between the measured and retrieved *SM* data was generally larger. This improvement could be due to the fact that the specific structural characteristics of the vineyards, with a preferential vertical orientation of the vine stems and stocks, could be accounted for in the 3-P retrievals, where the free parameter tt_V parameterizes the dependence of the optical depth at V-polarization (τ_V) on the incidence angle. Conversely, in 2-P retrievals, both tt_V and tt_H were set equal to $tt_V = tt_H = 1$, corresponding to isotropic conditions which could not account for the changes in the vegetation structure in relation to the vegetation phenological cycle (growth and senescence) and the agricultural practices.

Although the 3-P retrieval was found to be the most efficient approach in terms of correlation R and ubRMSE, over the vineyard field at the VAS, this configuration presents the disadvantage of being dependent on the H_R parameter. This dependency was less pronounced for $N_{RV} = N_{RH} = -1$.

For both 2-P and 3-P retrievals, the approaches showing the highest performance in terms of correlation coefficient R and ubRMSE were those corresponding to the case $N_{RV} = N_{RH} = -1$ (i.e. the SRP method in the case of 2-P retrievals). For all the other roughness configurations (H_R, Q_R, N_{RV}, N_{RH}), it was found that the correlation coefficient decreased and the ubRMSE increased for increasing values of H_R.

The use of soil roughness *in situ* measurements to calibrate the model following the method described in Lawrence et al., (2013) did not lead to any improvement in the *SM* retrieval over the SRP method. However, the estimation of H_R from *in situ* data showed how the τ_{NAD} signal can be polluted from soil roughness changes in the field, mainly due to agricultural practices and rainfall events.

In conclusion, the SRP method was found to be an efficient approach to account for surface roughness effects in *SM* retrievals, where the soil roughness parameter H_R does no longer need to be calibrated.

2.2 A new calibration of the effective scattering albedo and soil roughness parameters in the SMOS soil moisture retrieval algorithm

In order to confirm the findings of Fernandez-Moran et al. (2015), a second study was carried out at global scale using SMOS *TB* data (at the VAS the ELBARA-II *TBs* were used). The main objective of this study was to calibrate the parameters which account for soil roughness (in terms of H_R, N_{RH} and N_{RV} values) and vegetation (in terms of effective scattering albedo, ω). For that purpose, a large range of values of the latter parameters were used in order to retrieve soil moisture (*SM*) and vegetation optical depth (τ_{NAD}) over a large number of sites worldwide.

The SMOS level 2 (L2) and level 3 (L3) *SM* retrieval algorithms account for the surface fraction of the main cover types (bare soil and low vegetation, forest, water, urban, etc.) within each

SMOS footprint. The retrieval is only made over one specific fraction: either the nominal low vegetation, in most cases, or the forest fraction. Then, the *TB* value of the pixel fraction which is not considered in the retrieval is estimated. If that is the case of the forest fraction, this is estimated based on auxiliary *SM* data from the European Centre for Medium-range Weather Forecasting (ECMWF). This specific approach may lead to dry *SM* bias in forested regions, as noted by Wigneron et al. (2012). In the simplified retrieval algorithm used in this study, the SMOS L3 *TB* was used as input and pixels were assumed to be homogeneous.

Long term *SM* retrievals were compared to *in situ* measurements obtained from the International Soil Moisture Network (ISMN) over the period 2011 – 2013, and were evaluated using different metrics (R, bias and ubRMSE). Only stations contained in rather homogeneous pixels were considered. A compromise between the optimal values of all these metrics was the basis to find the best values of the vegetation and soil roughness parameters in the *SM* retrieval. Bias was considered as a second-order criterion in the assessment of the results due to the different sampling depths of the *in situ* measurements (0 - 5 cm) and of the SMOS L-band observations (~ 0 – 3 cm).

Performances of the *SM* retrievals, evaluated in terms of R, bias and ubRMSE, showed a high sensitivity of *SM* to ω and were found optimum for high ω values (ω ~ 0.10). On the contrary, the calibration of H_R required to find a compromise between the performances obtained in terms of ubRMSE (lower for low H_R values) and |bias| (lower for larger H_R values). It was found that both, increasing ω and decreasing H_R values, led to drier *SM* retrievals.

Values of ω = 0.10, H_R = 0.4 and N_{Rp} = -1 (p = H, V) were found optimum at global scale. This finding is consistent with the previous study carried out at the VAS area (Fernandez-Moran et al., 2015), where N_{Rp} = -1 was the main basis of the SRP method. However, in that study ω was set to 0, following the calibration of SMOS L2 and L3 algorithms in non-forest areas. The new calibration is consistent with the global map of the effective scattering albedo provided by the SMAP L4 product (ω = 0.09 ± 0.07) and with the work of Van der Schalie et al. (2016), who globally obtained ω equal to 0.12 after applying the Land Parameter Retrieval Model (LPRM) and evaluating *SM* retrievals against model datasets as ERA-Interim/Land and MERRA-Land. The latter study also showed the low impact of soil roughness on the correlation statistics in the *SM* retrieval when ω = 0.12. On the contrary, studies by Konings et al. (2016) found lower values (ω = 0.02 – 0.06) whereas the current set of effective scattering albedo in the SMOSL3 *SM* product is ω = 0.06 – 0.08 for forest and ω = 0 for the rest of the cover types.

The *in situ* sites used in the study were classified using the International Geosphere-Biosphere (IGBP) land cover classification scheme. Then, specific values of H_R, N_{Rp} (p = H, V) and ω were proposed for each class. In low vegetation cover types (open scrublands and barren or sparsely vegetated covers), low values of H_R (~ 0.1) were found, whereas higher values, from 0.4 to 0.5, were found for the rest of the IGBP classes. These results are in good agreement with the global map of H_R obtained by Parrens et al. (2017), who calibrated this parameter using SMOS retrievals and Leaf Area Index (*LAI*) data from Moderate-Resolution Imaging Spectroradiometer (MODIS) as auxiliary data. The values of ω ranged from 0.08 to 0.12.

The performance of the simplified soil moisture retrieval algorithm using the calibrated soil roughness and ω values was evaluated against the *SM* data measured at the *in situ* sites

(including and excluding the ones used for calibration purposes). The metrics showed that using either globally-constant or IGBP dependent parameters, there was improvement over SMOSL3 V300 (R = 0.61, bias = -0.019 $m^3 \cdot m^{-3}$ and ubRMSE = 0.062 $m^3 \cdot m^{-3}$ for the IGBP-based calibration; R = 0.54, bias = -0.034 $m^3 \cdot m^{-3}$ and ubRMSE = 0.070 $m^3 \cdot m^{-3}$ for SMOSL3 V300), but this improvement could not be demonstrated only by the use of the homogeneous retrieval algorithm. Nonetheless, we noted a drying effect of the SMOSL3 *SM* algorithm retrieval caused by the use of the "heterogeneity" approach: considering the same model parameter calibration, the bias varied from -0.034 $m^3 \cdot m^{-3}$, when using the SMOSL3 *SM* algorithm (heterogeneous pixels), to 0.028 $m^3 \cdot m^{-3}$ with the homogeneous approach.

The findings presented in this study will have implications for the calibration of soil roughness and vegetation in the future official versions of the SMOS L2 and L3 algorithms. Due to the good performance of the product developed in this study, the *Institute National de la Recherche Agronomique* (INRA) and the *Centre d'Études Spatiales de la BIOsphère* (CESBIO) decided to develop a new and alternative SMOS product (referred to as SMOS-INRA-CESBIO, or SMOS-IC for short) based on the calibration found in this study and the simplified retrieval algorithm. This simple approach leads to an efficient processor capable of processing one year of data over a few hours.

2.3 SMOS-IC: An alternative SMOS soil moisture and vegetation optical depth product

The SMOS-IC product (Fernandez-Moran et al., 2017a) provides daily *SM* and τ_{NAD} at the global scale and, as explained previously, differs from the operational SMOS L3 (SMOSL3 V300) product in the treatment of the retrieval over heterogeneous pixels. The version developed and used in this PhD thesis is a beta version (v102) provided in a NetCDF format on the Equal-Area Scalable Earth (EASE) 2.0 grid (Armstrong et al., 1997), the same as all SMOS L3 products.

SMOS-IC is much simpler than the SMOSL3 algorithm and does not account for corrections associated to the complex antenna pattern and SMOS viewing angle geometry. It uses the multi-angular and dual-polarization SMOSL3 *TB* product as the main input for the L-MEB model inversion. It also considers pixels as homogeneous to avoid uncertainties linked to inconsistent auxiliary data sets which are used to characterize the pixel heterogeneity in the SMOS L3 algorithm. Specifically, SMOS-IC does not use MODIS *LAI* and ECMWF *SM* data, whose tendency to *SM* overestimation is well-known (Albergel et al., 2012).

In SMOS-IC, the L-MEB model input parameters (effective vegetation scattering albedo ω and the roughness parameter H_R) were estimated as a function of IGBP land category classes which compose the pixel. These parameter values were derived from previous analyses (Fernandez-Moran et al., 2017b) and global maps of the roughness H_R parameter estimated by Parrens et al., 2016.

In Fernandez-Moran et al. (2017a), SMOS-IC was presented and evaluated at global scale. The SMOSL3 V300 and SMOS-IC soil moisture retrievals were compared globally against

ECMWF *SM* data for the period 2010 - 2015. This analysis extends the previous evaluation shown in (Fernandez-Moran et al., 2017b) where numerous *in situ SM* stations from ISMN were used as reference.

At global scale, it was found that both the SMOS-IC and SMOSL3 *SM* products were generally drier than the ECMWF *SM* product. However, this result was expected as the soil layer considered in the modelled ECMWF *SM* (top 0-7 cm) differs from the (~ top 0-3 cm) soil layer measured by SMOS. For this reason, it is a difficult task to truly assess the performance of the SMOS products in terms of bias at global scale. In terms of temporal variations, higher correlation values and lower unbiased Root Mean Square Deviation (ubRMSD) values were generally found between SMOS-IC *SM* and ECMWF *SM*, than between SMOSL3 *SM* and ECMWF *SM*.

For the τ_{NAD} evaluation, the *NDVI* index was taken as reference. This index is frequently used in literature to provide an estimate of τ_{NAD} at L-band over rather low vegetation covers during the vegetation growth (O'Neill et al., 2012; Wigneron et al., 2007; Lawrence et al., 2014; Grant et al., 2016). However, some differences between both products must be remarked. Firstly, the *NDVI* index is derived from optical sensors while the τ_{NAD} index is derived from L-band microwave measurements, meaning that it can sense deeper through the vegetation canopy. Secondly, the *NDVI* index is used to monitor the green vegetation, while the τ_{NAD} index is related to the whole vegetation water content (including stems, trunks, branches and senescent vegetation elements). It was found that the SMOS-IC τ_{NAD} product presented a slightly lower range of values (~ 0-1.3) than the one obtained with the SMOSL3 τ_{NAD} product (~ 0-1.5). In general terms, higher correlation values were obtained between SMOS-IC τ_{NAD} and MODIS *NDVI*, than between SMOSL3 τ_{NAD} and MODIS *NDVI*.

SMOS-IC is an alternative and complementary *SM* and τ_{NAD} product which will be key in the assessment and development of new versions of the current L2 and L3 SMOS algorithms. The fact that the SMOS-IC approach is based on homogeneous pixels makes it more aligned to *SM* products derived from other space-borne sensors where the retrieval is done under the homogeneity assumption, such as SMAP and the Advanced Microwave Scanning Radiometer (AMSR-E); the latter offering a C-band soil moisture product.

Future studies focusing on the global-scale validation would be helpful to assess the performance of the SMOS-IC product, for instance remotely sensed products such as SMAP and AMSR-E *SM*, MODIS *LAI*, forest biomass or modelled data as MERRA (Modern-Era Retrospective analysis for Research and Applications) (Reichle et al., 2011).

The simplicity of the SMOS-IC algorithm will also facilitate to implement and test new approaches in the future with the aim of improving *SM* and τ_{NAD} estimations. For instance, the implementation of the 3-P retrieval (*SM*, τ_{NAD} and the composite soil-canopy temperature) or the use of soil and canopy temperatures coming from other satellites or models in the SMOS-IC algorithm could be of special interest.

REFERENCES

Albergel, C., de Rosnay, P., Balsamo, G., Isaksen, L., Muñoz-Sabater, J., 2012. Soil Moisture Analyses at ECMWF: Evaluation Using Global Ground-Based In Situ Observations. J. Hydrometeorol. 13, 1442–1460. doi:10.1175/JHM-D-11-0107.1

Armstrong, R., Brodzik, M.J., Varani, A., 1997. The NSIDC EASE-Grid: Addressing the need for a common, flexible, mapping and gridding scheme. Earth Syst. Monit. 7, 6–7.

Brocca, L., Melone, F., Moramarco, T., Wagner, W., Naeimi, V., Bartalis, Z., Hasenauer, S., 2010. Improving runoff prediction through the assimilation of the ASCAT soil moisture product. Hydrol. Earth Syst. Sci. 14, 1881–1893. doi:10.5194/hess-14-1881-2010

Cano, A., Saleh, K., Wigneron, J.P., Antol??n, C., Balling, J.E., Kerr, Y.H., Kruszewski, A., Mill??n-Scheiding, C., S??bj??rg, S.S., Skou, N., L??pez-Baeza, E., 2010. The SMOS Mediterranean Ecosystem L-Band characterisation EXperiment (MELBEX-I) over natural shrubs. Remote Sens. Environ. 114, 844–853. doi:10.1016/j.rse.2009.11.019

De Lannoy, G.J.M., Reichle, R.H., Vrugt, J.A., 2014. Uncertainty quantification of GEOS-5 L-band radiative transfer model parameters using Bayesian inference and SMOS observations. Remote Sens. Environ. 148, 146–157. doi:10.1016/j.rse.2014.03.030

de Rosnay, P., Drusch, M., Vasiljevic, D., Balsamo, G., Albergel, C., Isaksen, L., 2013. A simplified Extended Kalman Filter for the global operational soil moisture analysis at ECMWF. Q. J. R. Meteorol. Soc. 139, 1199–1213. doi:10.1002/qj.2023

Entekhabi, D., Njoku, E.G., O'Neill, P.E., Kellogg, K.H., Crow, W.T., Edelstein, W.N., Entin, J.K., Goodman, S.D., Jackson, T.J., Johnson, J., Kimball, J., Piepmeier, J.R., Koster, R.D., Martin, N., McDonald, K.C., Moghaddam, M., Moran, S., Reichle, R., Shi, J.C., Spencer, M.W., Thurman, S.W., Tsang, L., Van Zyl, J., 2010. The soil moisture active passive (SMAP) mission. Proc. IEEE 98, 704–716. doi:10.1109/JPROC.2010.2043918

Escorihuela, M.J., Chanzy, A., Wigneron, J.P., Kerr, Y.H., 2010. Effective soil moisture sampling depth of L-band radiometry: A case study. Remote Sens. Environ. 114, 995–1001. doi:10.1016/j.rse.2009.12.011

Escorihuela, M.J., Kerr, Y.H., De Rosnay, P., Wigneron, J.P., Calvet, J.C., Lemaître, F., 2007. A simple model of the bare soil microwave emission at L-band. IEEE Trans. Geosci. Remote Sens. 45, 1978–1987. doi:10.1109/TGRS.2007.894935

Fernandez-Moran, R., Al-Yaari, A., Mialon, A., Mahmoodi, A., Al Bitar, A., De Lannoy, G., Lopez-Baeza, E., Kerr, Y., Wigneron, J.-P., 2017a. SMOS-IC: An alternative SMOS soil moisture and vegetation optical depth product. Remote Sens. 9, 457.

Fernandez-Moran, R., Wigneron, J.-P., De Lannoy, G., Lopez-Baeza, E., Parrens, M., Mialon, A., Mahmoodi, A., Al-Yaari, A., Bircher, S., Al Bitar, A., Richaume, P., Kerr, Y., 2017b. A new calibration of the effective scattering albedo and soil roughness parameters in

the SMOS SM retrieval algorithm. Int. J. Appl. Earth Obs. Geoinf. 62, 27–38. doi:10.1016/j.jag.2017.05.013

Fernandez-Moran, R., Wigneron, J.P., Lopez-Baeza, E., Al-Yaari, A., Coll-Pajaron, A., Mialon, A., Miernecki, M., Parrens, M., Salgado-Hernanz, P.M., Schwank, M., Wang, S., Kerr, Y.H., 2015. Roughness and vegetation parameterizations at L-band for soil moisture retrievals over a vineyard field. Remote Sens. Environ. 170, 269–279. doi:10.1016/j.rse.2015.09.006

Grant, J.P., Wigneron, J.P., De Jeu, R.A.M., Lawrence, H., Mialon, A., Richaume, P., Al Bitar, A., Drusch, M., van Marle, M.J.E., Kerr, Y., 2016. Comparison of SMOS and AMSR-E vegetation optical depth to four MODIS-based vegetation indices. Remote Sens. Environ. 172, 87–100. doi:10.1016/j.rse.2015.10.021

Grant, J.P., Wigneron, J.P., Van de Griend, A.A., Kruszewski, A., Søbjærg, S.S., Skou, N., 2007. A field experiment on microwave forest radiometry: L-band signal behaviour for varying conditions of surface wetness. Remote Sens. Environ. 109, 10–19. doi:10.1016/j.rse.2006.12.001

Kerr, Y.H., Waldteufel, P., Richaume, P., Wigneron, J.P., Ferrazzoli, P., Mahmoodi, A., Bitar, A. Al, Cabot, F., Gruhier, C., Juglea, S.E., Leroux, D., Mialon, A., Delwart, S., 2012. The SMOS Soil Moisture Retrieval Algorithm. Geosci. Remote Sens. 50, 1384–1403. doi:10.1109/TGRS.2012.2184548

Kerr, Y.H., Waldteufel, P., Wigneron, J.P., Martinuzzi, J.M., Font, J., Berger, M., 2001. Soil moisture retrieval from space: The Soil Moisture and Ocean Salinity (SMOS) mission. IEEE Trans. Geosci. Remote Sens. 39, 1729–1735. doi:10.1109/36.942551

Konings, A.G., Piles, M., R??tzer, K., McColl, K.A., Chan, S.K., Entekhabi, D., 2016. Vegetation optical depth and scattering albedo retrieval using time series of dual-polarized L-band radiometer observations. Remote Sens. Environ. 172, 178–189. doi:10.1016/j.rse.2015.11.009

Kurum, M., 2013. Quantifying scattering albedo in microwave emission of vegetated terrain. Remote Sens. Environ. 129, 66–74. doi:10.1016/j.rse.2012.10.021

Lawrence, H., Wigneron, J.-P., Demontoux, F., Mialon, A., Kerr, Y.H., 2013. Evaluating the Semiempirical H– Q Model Used to Calculate the L-Band Emissivity of a Rough Bare Soil. IEEE Trans. Geosci. Remote Sens. 51, 4075–4084. doi:10.1109/TGRS.2012.2226995

Lawrence, H., Wigneron, J.P., Richaume, P., Novello, N., Grant, J., Mialon, A., Al Bitar, A., Merlin, O., Guyon, D., Leroux, D., Bircher, S., Kerr, Y., 2014. Comparison between SMOS Vegetation Optical Depth products and MODIS vegetation indices over crop zones of the USA. Remote Sens. Environ. 140, 396–406. doi:10.1016/j.rse.2013.07.021

Masson, V., Champeaux, J.L., Chauvin, F., Meriguet, C., Lacaze, R., 2003. A global database of land surface parameters at 1-km resolution in meteorological and climate models. J. Clim. 16, 1261–1282. doi:10.1175/1520-0442-16.9.1261

Mironov, V., Kerr, Y., Member, S., Wigneron, J., Member, S., 2012. Temperature- and Texture-Dependent Dielectric Model for Moist Soils at 1 . 4 GHz 10, 1–5.

Mo, T., Choudhury, B.J., Schmugge, T.J., Wang, J.R., Jackson, T.J., 1982. A model for microwave emission from vegetation-covered fields. J. Geophys. Res. 87, 11229. doi:10.1029/JC087iC13p11229

Njoku, E.G., Kong, J.-A., 1977. Theory for passive microwave remote sensing of near-surface soil moisture. J. Geophys. Res. 82, 3108. doi:10.1029/JB082i020p03108

O'Neill, P., Chan, S., Njoku, E., Jackson, T., Bindlish, R., 2012. Soil Moisture Active Passive (SMAP) Algorithm Theoretical Basis Document (ATBD). SMAP Level 2 & 3 Soil Moisture (Passive), (L2_SM_P, L3_SM_P).

Parrens, M., Wigneron, J.-P., Richaume, P., Mialon, A., Al Bitar, A., Fernandez-Moran, R., Al-Yaari, A., Kerr, Y.H., 2016. Global-scale surface roughness effects at L-band as estimated from SMOS observations. Remote Sens. Environ. 181, 122–136.

Reichle, R.H., Koster, R.D., De Lannoy, G.J.M., Forman, B.A., Liu, Q., Mahanama, S.P.P., Toure, A., 2011. Assessment and enhancement of MERRA land surface hydrology estimates. J. Clim. 24, 6322–6338. doi:10.1175/JCLI-D-10-05033.1

Reul, N., Fournier, S., Boutin, J., Hernandez, O., Maes, C., Chapron, B., Alory, G., Quilfen, Y., Tenerelli, J., Morisset, S., Kerr, Y., Mecklenburg, S., Delwart, S., 2014. Sea Surface Salinity Observations from Space with the SMOS Satellite: A New Means to Monitor the Marine Branch of the Water Cycle. Surv. Geophys. 35, 681–722. doi:10.1007/s10712-013-9244-0

Schwank, M., Wigneron, J.P., López-Baeza, E., Völksch, I., Mätzler, C., Kerr, Y.H., 2012. L-band radiative properties of vine vegetation at the MELBEX III SMOS cal/val site. IEEE Trans. Geosci. Remote Sens. 50, 1587–1601. doi:10.1109/TGRS.2012.2184126

Talone, M., Portabella, M., Martinez, J., Gonzalez-Gambau, V., 2015. About the Optimal Grid for SMOS Level 1C and Level 2 Products. IEEE Geosci. Remote Sens. Lett. 12, 1630–1634. doi:10.1109/LGRS.2015.2416920

Van Der Schalie, R., Kerr, Y.H., Wigneron, J.P., Rodríguez-Fernández, N.J., Al-Yaari, A., Jeu, R.A.M. d., 2016. Global SMOS Soil Moisture Retrievals from The Land Parameter Retrieval Model. Int. J. Appl. Earth Obs. Geoinf. 45, 125–134. doi:10.1016/j.jag.2015.08.005

Wigneron, J.-P., Chanzy, A., de Rosnay, P., Rudiger, C., Calvet, J.-C., 2008. Estimating the Effective Soil Temperature at L-Band as a Function of Soil Properties. IEEE Trans. Geosci. Remote Sens. 46, 797–807. doi:10.1109/TGRS.2007.914806

Wigneron, J.P., Kerr, Y., Waldteufel, P., Saleh, K., Escorihuela, M.J., Richaume, P., Ferrazzoli, P., de Rosnay, P., Gurney, R., Calvet, J.C., Grant, J.P., Guglielmetti, M., Hornbuckle, B., Mätzler, C., Pellarin, T., Schwank, M., 2007. L-band Microwave Emission of the Biosphere (L-MEB) Model: Description and calibration against experimental data sets over crop fields. Remote Sens. Environ. 107, 639–655. doi:10.1016/j.rse.2006.10.014

Wigneron, J.P., Schwank, M., Baeza, E.L., Kerr, Y., Novello, N., Millan, C., Moisy, C., Richaume, P., Mialon, A., Al Bitar, A., Cabot, F., Lawrence, H., Guyon, D., Calvet, J.C., Grant, J.P., Casal, T., de Rosnay, P., Saleh, K., Mahmoodi, A., Delwart, S., Mecklenburg, S., 2012. First evaluation of the simultaneous SMOS and ELBARA-II observations in the

Mediterranean region. Remote Sens. Environ. 124, 26–37. doi:10.1016/j.rse.2012.04.014

LIST OF PUBLICATIONS

Peer-reviewed journal articles

Fernandez-Moran, R.; Al-Yaari, A.; Mialon, A.; Mahmoodi, A.; Al Bitar, A.; De Lannoy, G.; Rodriguez-Fernandez, N.; Lopez-Baeza, E.; Kerr, Y.; Wigneron, J.-P., 2017. SMOS-IC: An Alternative SMOS Soil Moisture and Vegetation Optical Depth Product. Remote Sens. 9, 457.

Fernandez-Moran, R.; Wigneron, J.-P.; De Lannoy, G.; Lopez-Baeza, E.; Parrens, M.; Mialon, A.; Mahmoodi, A.; Al-Yaari, A.; Bircher, S.; Al Bitar, A.; Richaume, P.; Kerr, Y., 2017. A new calibration of the effective scattering albedo and soil roughness parameters in the SMOS SM retrieval algorithm. Int. J. Appl. Earth Obs. Geoinf. 62, 27–38.

Wigneron, J.-P.; Jackson, T. J.; O'Neill, P.; De Lannoy, G.; Rosnay, P. de; Walker, J. P.; Ferrazzoli, P.; Mironov, V.; Bircher, S.; Grant, J. P.; Kurum, M.; Schwank, M.; Munoz-Sabater, J.; N. Das, A. R.; Al-Yaari, A.; Bitar, A. Al; **Fernandez-Moran, R**.; Lawrence, H.; Mialon, A.; Parrens, M.; Richaume, P.; Rodriguez-Fernandez, N.; Delwart, S.; Kerr., Y., 2017. Modelling the passive microwave signature from land surfaces: a review of recent results and application to the L-band SMOS & SMAP soil moisture retrieval algorithms. Remote Sens. Environ. 192, 238-262.

Parrens, M.; Wigneron, J.-P.; Richaume, P.; Al Bitar, A.; Mialon, A.; **Fernandez-Moran, R.**; Al-Yaari, A.; O'Neill, P.; Kerr, Y., 2017. Considering combined or separated roughness and vegetation effects in soil moisture retrievals. Int. J. Appl. Earth Obs. Geoinf. 55, 73–86.

Parrens, M.; Wigneron, J.-P.; Richaume, P.; Mialon, A.; Al Bitar, A**.; Fernandez-Moran**, R.; Al-Yaari, A.; Kerr, Y. H., 2016. Global-scale surface roughness effects at L-band as estimated from SMOS observations. Remote Sens. Environ. 181, 122–136.

Wang, S.; Wigneron, J.-P.; Jiang, L.-M.; Parrens, M.; Yu, X.-Y.; Al-Yaari, A.; Ye, Q.-Y.; **Fernandez-Moran, R.**; Ji, W.; 2015. Kerr, Y. Global-scale evaluation of roughness effects on C-Band AMSR-E observations. Remote Sens. 7, 5734–5757.

Fernandez-Moran, R.; Wigneron, J.-P.; Lopez-Baeza, E.; Al-Yaari, A.; Coll-Pajaron, A.; Mialon, A.; Miernecki, M.; Parrens, M.; Salgado-Hernanz, P. M.; Schwank, M.; Wang, S.; Kerr, Y. H., 2015. Roughness and vegetation parameterizations at L-band for soil moisture retrievals over a vineyard field. Remote Sens. Environ. 170, 269–279.

Fernandez-Moran, R.; Wigneron, J.-P.; Lopez-Baeza, E.; Miernecki, M.; Salgado-Hernanz, P.; Coll, M. A.; Kerr, Y. H.; Schwank, M., 2015. Validación a largo plazo de datos de nivel 3 de tierra de SMOS con medidas de ELBARA-II en la Valencia Anchor Station. Rev. Teledetec. 2015, 55–62.

Miernecki, M.; Wigneron, J. P.; Lopez-Baeza, E.; Kerr, Y.; De Jeu, R.; De Lannoy, G. J. M.; Jackson, T. J.; O'Neill, P. E.; Schwank, M.; **Fernandez Moran, R.**; Bircher, S.; Lawrence, H.; Mialon, A.; Al Bitar, A.; Richaume, P., 2014. Comparison of SMOS and SMAP soil moisture retrieval approaches using tower-based radiometer data over a vineyard field. Remote Sens. Environ. 154, 89–101.

Articles in international conferences proceedings

Fernandez-Moran, R.; Wigneron, J.-P.; De Lannoy, G.; Lopez-Baeza, E.; Parrens, M.; Mialon, A.; Mahmoodi, A.; Al-Yaari, A.; Bircher, S.; Al Bitar, A.; Richaume, P.; Kerr, Y., 2017. SMOS-IC: A Revised SMOS Product Based on a New Effective Scattering Albedo and Soil Roughness Parameterization. In IEEE International Geoscience and Remote Sensing Symposium (IGARSS); IEEE: Fort Worth, Texas, (USA).

Al-Yaari, A.; **Fernandez-Moran, R.**; Wigneron, J.-P.; Mialon, A., Mahmoodi, A.; Al Bitar, A.; Kerr, Y., 2017. First glance on a revised SMOS soil moisture retrieval algorithm: Evaluation with respect to ECMWF soil moisture simulations In IEEE International Geoscience and Remote Sensing Symposium (IGARSS); IEEE: Fort Worth, Texas, (USA).

Fernandez-Moran, R.; Wigneron, J.-P.; De Lannoy, G.; Lopez-Baeza, E.; Mialon, A.; Mahmoodi, A.; Parrens, M.; Al Bitar, A.; Richaume, P.; Kerr, Y., 2016. Calibrating the effective scattering albedo in the SMOS algorithm: Some first results. In IEEE International Geoscience and Remote Sensing Symposium (IGARSS); IEEE: Beijing (China), pp. 826–829.

Yin, C.; Lopez-Baeza, E.; Martin-Neira, M.; **Fernandez Moran, R.**; Peinado-Galan, N.; Navarro, E.; Egido, A.; Mollfulleda, A.; Li, W.; Cao, Y.; Zhu, B.; Yang, D., 2016. Intercomparison of soil moisture retrieved from GNSS-R and passive L-band radiometry at the Valencia Anchor Station. In International Geoscience and Remote Sensing Symposium (IGARSS); Beijing (China), pp. 3137–3139.

Al-Yaari, A.; Wigneron, J. P.; Ducharne, A.; Kerr, Y.; **Fernandez-Moran, R.**; Parrens, M.; Bi-tar, A. Al; Mialon, A.; Richaume, P., 2015. Evaluation of the most recent reprocessed SMOS soil moisture products: Comparison between SMOS level 3 V246 and V272. In IEEE International Geoscience and Remote Sensing Symposium (IGARSS); Milan (Italy), pp. 2493–2496.

Fernandez-Moran, R.; Wigneron, J.-P.; Lopez-Baeza, E.; Al-Yaari, A.; Bircher, S.; Coll-Pajaron, A.; Mahmoodi, A.; Parrens, M.; Richaume, P.; Kerr, Y., 2015. Analyzing the impact of using the SRP (Simplified roughness parameterization) method on soil moisture retrieval over different regions of the globe. In International Geoscience and Remote Sensing Symposium (IGARSS); Milan (Italy), pp. 5182–5185.

Al-Yaari, A.; Wigneron, J. P.; Ducharne, A.; Kerr, Y.; Wagner, W.; Reichle, R.; De Lannoy, G.; Bitar, A.; Dorigo, W.; Parrens, M.; **Fernandez, R.**; Richaume, P.; Mialon, A., 2014. Compared performances of microwave passive soil moisture retrievals (SMOS) and active soil moisture retrievals (ASCAT) using land surface model estimates (MERRA-LAND). In International Geoscience and Remote Sensing Symposium (IGARSS); Québec (Canada), pp. 2463–2466.

Wang, S.; Wigneron, J.-P.; Parrens, M.; Al-Yaari, A.; **Fernandez-Moran, R.**; Jiang, L.-M.; Zeng, J.-Y.; Kerr, Y., 2014. Evaluating roughness effects on C-band AMSR-E observations. In International Geoscience and Remote Sensing Symposium (IGARSS); Québec (Canada), pp. 3311–3314.

Fernandez-Moran, R.; Wigneron, J.-P.; Lopez-Baeza, E.; Salgado-Hernanz, P. M.; Mialon, A.; Miernecki, M.; Alyaari, A.; Parrens, M.; Schwank, M.; Wang, S.; Coll-Pajaron, A.; Lawrence, H.; Kerr, Y. H., 2014. Evaluating the impact of roughness in soil moisture and optical thickness retrievals over the VAS area. In International Geoscience and Remote Sensing Symposium (IGARSS); Québec (Canada), pp. 1947–1950.

Parrens, M.; Wigneron, J.-P.; Richaume, P.; Kerr, Y.; Wang, S.; Alyaari, A.; **Fernandez-Moran, R.**; Mialon, A.; Escorihuela, M. J.; Grant, J.-P., 2014. Global maps of roughness parameters from L-band SMOS observations. In International Geoscience and Remote Sensing Symposium (IGARSS); Québec (Canada), pp. 4675–4678.

Conference presentations

Talks

Fernandez-Moran, R.; Wigneron, J.-P.; De Lannoy, G.; Lopez-Baeza, E.; Parrens, M.; Mialon, A.; Mahmoodi, A.; Al-Yaari, A.; Bircher, S.; Al Bitar, A.; Richaume, P.; Kerr, Y., 2017. SMOS-IC: A Revised SMOS Product Based on a New Effective Scattering Albedo and Soil Roughness Parameterization. In IEEE International Geoscience and Remote Sensing Symposium (IGARSS); Fort Worth, Texas, (USA).

Al-Yaari, A.; **Fernandez-Moran, R.**; Wigneron, J.-P.; Mialon, A., Mahmoodi, A.; Al Bitar, A.; Kerr, Y., 2017. First glance on a revised SMOS soil moisture retrieval algorithm: Evaluation with respect to ECMWF soil moisture simulations. In IEEE International Geoscience and Remote Sensing Symposium (IGARSS); Fort Worth, Texas, (USA).

Fernandez-Moran, R., Wigneron, J. -P., De Lannoy, G., Lopez-Baeza, E., Mialon, A., Mahmoodi, A, Parrens, M., Al Bitar, A., Richaume, P., Kerr, Y., 2016. Calibration of the effective scattering albedo and roughness parameters in the SMOS retrieval algorithm. In 7th SMAP CAL/VAL workshop; New York (USA).

Fernandez-Moran, R., Wigneron, J.-P., Lopez-Baeza, E., Al-Yaari, A., Bircher, S., Coll-Pajaron, A., Mahmoodi, A., Parrens, M., Richaume, P., Kerr, Y., 2015. Analyzing the impact of using the SRP (Simplified Roughness Parameterization) method on soil moisture retrieval over different regions of the globe. In SMOS SM Progress Meeting; WSL-Birmensdorf, Zurich (Switzerland).

Fernandez-Moran, R.; Wigneron, J.-P.; Lopez-Baeza, E.; Al-Yaari, A.; Bircher, S.; Coll-Pajaron, A.; Mahmoodi, A.; Parrens, M.; Richaume, P.; Kerr, Y., 2015. Analyzing the impact of using the SRP (Simplified roughness parameterization) method on soil moisture retrieval over different regions of the globe. In International Geoscience and Remote Sensing Symposium (IGARSS); Milan (Italy).

Fernández-Morán, R., Wigneron, J.-P., Coll Pajarón, A., Kerr, Y., Miernecki, M., Salgado-Hernanz, P., Schwank, M., Lopez-Baeza. E., 2013. Towards a long-term dataset of ELBARA-II measurements in support of SMOS level-3 product and algorithm validation at the Valencia Anchor Station (MELBEX Experiment 2010-2013). In URSI-F Microwave Signatures; Espoo (Finland).

Posters

Fernandez-Moran, R.; Wigneron, J.-P.; De Lannoy, G.; Lopez-Baeza, E.; Mialon, A.; Mahmoodi, A.; Parrens, M.; Al Bitar, A.; Richaume, P.; Kerr, Y., 2016. Calibrating the effective scattering albedo in the SMOS algorithm: Some first results. In IEEE International Geoscience and Remote Sensing Symposium (IGARSS); IEEE: Beijing (China).

Fernandez-Moran, R., Wigneron, J.P., Lopez-Baeza, E., Al-Yaari, A., Bircher, S., Coll-Pajaron, A., Mahmoodi, A., Parrens, M., Richaume, P., Kerr, Y., 2015. Soil moisture retrieval at global scale using the SRP (Simplified Roughness Parameterization). In 2nd SMOS Science Conference; Madrid (Spain).

Fernandez-Moran, R., Wigneron, J.-P., Lopez-Baeza, E., Salgado-Hernanz, P.M., Kerr, Y., Mialon, A., Parrens, M. Miernecki, M., Coll-Pajaron, A. Alyaari, A., Wang, S. Schwank, M., 2016. Roughness parameterization for soil moisture optimum retrieval over the Valencia anchor station. In Recent Advances in Quantitative Remote Sensing (RAQRS). Torrent, Valencia (Spain).

Wang, S.; Wigneron, J.-P.; Parrens, M.; Al-Yaari, A.; **Fernandez-Moran, R.**; Jiang, L.-M.; Zeng, J.-Y.; Kerr, Y., 2014. Evaluating roughness effects on C-band AMSR-E observations. In International Geoscience and Remote Sensing Symposium (IGARSS); Québec (Canada).

Fernandez-Moran, R.; Wigneron, J.-P.; Lopez-Baeza, E.; Salgado-Hernanz, P. M.; Mialon, A.; Miernecki, M.; Alyaari, A.; Parrens, M.; Schwank, M.; Wang, S.; Coll-Pajaron, A.; Lawrence, H.; Kerr, Y. H., 2014. Evaluating the impact of roughness in soil moisture and optical

thickness retrievals over the VAS area. In International Geoscience and Remote Sensing Symposium (IGARSS); Québec (Canada).

Fernández-Morán, R., Wigneron, J.-P. Coll Pajarón, A., Kerr, Y., Miernecki, M., Salgado-Hernanz, P., Schwank, M., Lopez-Baeza, E., 2013. Towards a Long-term Dataset of ELBARA-II Measurements Assisting SMOS Level-3 Land Product and Algorithm Validation at the Valencia Anchor Station. In XV Congreso Asociación Española de Teledetección; Madrid (Spain).

COMPENDIUM OF PUBLICATIONS

ARTICLE 1: *ROUGHNESS AND VEGETATION PARAMETERIZATIONS AT L-BAND FOR SOIL MOISTURE RETRIEVALS OVER A VINEYARD FIELD*

This article was published in "Remote Sensing of Environment" in 2015. This journal currently has an impact factor of 6.265

Remote Sensing of Environment 170 (2015) 269–279

Contents lists available at ScienceDirect

Remote Sensing of Environment

journal homepage: www.elsevier.com/locate/rse

Roughness and vegetation parameterizations at L-band for soil moisture retrievals over a vineyard field

R. Fernandez-Moran [a,b], J.-P. Wigneron [b,*], E. Lopez-Baeza [a], A. Al-Yaari [b], A. Coll-Pajaron [a], A. Mialon [c], M. Miernecki [d], M. Parrens [b,c], P.M. Salgado-Hernanz [a], M. Schwank [e,f], S. Wang [b,g], Y.H. Kerr [c]

[a] University of Valencia, Faculty of Physics, Department of Earth Physics and Thermodynamics, Climatology from Satellites Group, Calle Dr Moliner, 50, Burjassot, 46100 Valencia, Spain
[b] INRA, UMR 1391 ISPA, Centre INRA Bordeaux Aquitaine, F-33140 Villenave d'Ornon, France
[c] CESBIO, CNES/CNRS/IRD/UPS, UMR 5126, 18 Avenue Edouard Belin, Toulouse, France
[d] University of Hamburg, Center for Marine and Atmospheric Science (ZMAW), Hamburg, Germany
[e] Swiss Federal Research Institute WSL, 8903 Birmensdorf, Switzerland
[f] Gamma Remote Sensing AG, 3073 Gümligen, Switzerland
[g] Institute of Remote Sensing and Digital Earth, Chinese Academy of Sciences, Beijing 100094, China

ARTICLE INFO

Article history:
Received 12 December 2014
Received in revised form 16 September 2015
Accepted 21 September 2015
Available online 6 October 2015

Keywords:
Microwave radiometry
L-band
Soil moisture
Soil roughness
Vegetation
L-MEB
SMOS

ABSTRACT

The capability of L-band radiometry to monitor surface soil moisture (SM) at global scale has been analyzed in numerous studies, mostly in the framework of the ESA SMOS and NASA SMAP missions. To retrieve SM from L-band radiometric observations, two significant effects have to be accounted for, namely soil roughness and vegetation optical depth. In this study, soil roughness effects on retrieved SM values were evaluated using brightness temperatures acquired by the L-band ELBARA-II radiometer, over a vineyard field at the Valencia Anchor Station (VAS) site during the year 2013. Different combinations of the values of the model parameters used to account for soil roughness effects (H_R, Q_R, N_{RH} and N_{RV}) in the L-MEB model were evaluated. The L-MEB model (L-band Microwave Emission of the Biosphere) is the forward radiative transfer model used in the SMOS soil moisture retrieval algorithm. In this model, H_R parameterizes the intensity of roughness effects, Q_R accounts for polarization effects, and N_{RH} and N_{RV} parameterize the variations of the soil reflectivity as a function of the observation angle, θ, respectively for both H (Horizontal) and V (Vertical) polarizations. These evaluations were made by comparing in-situ measurements of SM (used here as a reference) against SM retrievals derived from tower-based ELBARA-II brightness temperatures mentioned above. The general retrieval approach consists of the inversion of L-MEB. Two specific configurations were tested: the classical 2-Parameter (2-P) retrieval configuration where SM and τ_{NAD} (vegetation optical depth at nadir) are retrieved, and a 3-Parameter (3-P) configuration, accounting for the additional effects of the vineyard vegetation structure.

Using the 2-P configuration, it was found that setting N_{Rp} ($p = H$ or V) equals to -1 provided the best SM estimations in terms of correlation and unbiased Root Mean Square Error (ubRMSE). The assumption $N_{RV} = N_{RH} = -1$ simplifies the L-MEB retrieval, since the two parameters τ_{NAD} and H_R can then be grouped and retrieved as a single parameter (method here defined as the Simplified Retrieval Method (SRP)). The main advantage of the SRP method is that it is not necessary to calibrate H_R before performing the SM retrievals. Using the 3-P configuration, the results improved, with respect to SM retrievals, in terms of correlation and ubRMSE, as the structural characteristics of the vineyards were better accounted for. However, this method still requires the calibration of H_R, a disadvantage for operational applications. Finally, it was found that the use of in-situ roughness measurements to calibrate the roughness model parameters did not provide significant improvements in the SM retrievals as compared to the SRP method.

1. Introduction

Passive microwave radiometry at L-band (1–2 GHz) is one of the most efficient techniques to monitor surface soil moisture (SM) at global scale. Satellites such as ESA SMOS (Soil Moisture and Ocean Salinity) and NASA SMAP (Soil Moisture Active Passive) can provide global maps of soil moisture (Entekhabi, Njoku, et al. 2010; Kerr, Waldteufel, Richaume, et al., 2010; Kerr, Waldteufel, Wigneron, et al., 2010). The sensitivity of brightness temperature (TB) measured at horizontal ($p = H$) and vertical ($p = V$) polarization with respect to SM is due to the fact that soil emissivity in the microwave domain is highly related to the soil dielectric constant which is mainly determined by SM. TB is also affected by other factors such as soil texture and roughness (Jackson et al.,

* Corresponding author.

http://dx.doi.org/10.1016/j.rse.2015.09.006
0034-4257/

1980; Njoku & Entekhabi, 1996; Wigneron, Chanzy, De Rosnay, Rudiger, & Calvet, 2008), vegetation cover and litter (Grant et al., 2007; Jackson et al., 1980; Saleh, Wigneron, De Rosnay, Calvet, & Kerr, 2006), and by soil and vegetation temperatures (Wigneron et al., 2007). Measured TB generally increase with increasing soil roughness, while vegetation attenuates soil emission and adds its own contribution to the upwelling TB measured above the scene.

The effects of soil roughness at L-band have been evaluated in studies based on modeling (Lawrence, Wigneron, Demontoux, Mialon, & Kerr, 2013; Parrens et al., 2014; Ulaby et al., 1982; Schwank, Volksch, et al., 2010), satellite data (Patton & Hornbuckle, 2013), or in-situ data (Escorihuela, Chanzy, Wigneron, & Kerr, 2010; Mialon, Wigneron, De Rosnay, Escorihuela, & Kerr, 2012; Wigneron, Laguerre, & Kerr, 2001). In the SMOS retrieval algorithm, based on the inversion of L-MEB (Wigneron et al., 2007), a simple modeling approach based on four parameters (H_R, Q_R, N_{RH} and N_{RV}) was selected to model the roughness effects (Wang & Choudhury, 1981). This approach was generally found to be simple and accurate (Escorihuela et al., 2007; Mialon et al., 2012; Wang, O'Neill, Jackson, & Engman, 1983; Wigneron, Schmugge, Chanzy, Calvet, & Kerr, 1998; Wigneron et al., 2011).

In SM retrieval studies based on the inversion of L-MEB, the values of the four soil roughness parameters (H_R, Q_R, N_{RH} and N_{RV}) have to be estimated. Some studies have investigated the relationship between the empirical H_R parameter and soil physical parameters, such as the standard deviation σ of surface heights and the autocorrelation length Lc of the surface, based on experimental data (Choudhury, Schmugge, Chang, & Newton, 1979; Wigneron et al., 1998) or modeling approaches (Lawrence et al., 2013). The roughness parameters were calibrated for different types of land surfaces or land uses.

In this paper, optimal values of the four roughness parameters have been evaluated for the Valencia Anchor Station (VAS) region that is a long-term validation site for the SMOS products (Cano et al., 2010; Fernandez-Moran et al., 2014; Schwank, Wigneron, et al., 2012; Wigneron et al., 2012). The area is mainly composed of vineyards (65–70% cover fraction) and other Mediterranean vegetation species (shrubs, pine-, almond- and olive-trees, etc.). The European Space Agency (ESA) selected the VAS site for the installation of one of the three ELBARA-II prototype radiometers (Schwank, Wiesmann, et al., 2010) in September 2009 over a vineyard field that was called MELBEX-III (Mediterranean Ecosystem L-band Characterization Experiment), under the responsibility of the Climatology from Satellites Group of the University of Valencia. ELBARA-II is an automated L-band microwave radiometer system that accurately measures TB at horizontal (p = H) and vertical (p = V) polarizations over a range of observation angles θ (Schwank, Wiesmann, et al., 2010; Schwank et al., 2012).

In the VAS area, the vine phenological cycle extends from April to October and the surface remains under almost bare soil conditions for the rest of the year. Since a large part of the VAS area is dedicated to the production of wine, different agricultural practices are regularly performed along the year aiming at an optimal grape development. These agricultural practices include plowing, vine shoot pruning, tying up long branches to trellis wires, sulfate fertilization and grape harvest in October. Most of these practices, as well as strong rainfall events, usually lead to frequent and significant changes in soil roughness. These changing soil conditions and the opportunity to use long-term observations from ELBARA-II, make the VAS site a fairly adequate place to investigate the impact of changes in soil roughness conditions on the SM estimates retrieved from L-band microwave radiometry.

In this study, we evaluated several combinations of values of the four roughness parameters (H_R, Q_R and N_{Rp}, p = V, H) used to retrieve SM from multi-angular measurements made by ELBARA-II. The SM retrieval approach based on the inversion of L-MEB is also the basis for the SMOS level 2 soil moisture processor used to retrieve simultaneously vegetation optical depth (τ_{NAD}) and SM (Kerr et al., 2012; Wigneron et al., 2007). In a first step, several combinations of values of the roughness parameters were evaluated, by comparing SM retrievals with in-situ SM measurements, considered here as reference. The evaluation was made using all available ELBARA-II observations at 6 am and 6 pm during 2013 (323 days of full data; 42 days missing due to power input failures). In a second step, in-situ measurements were used to calibrate the values of the roughness parameters based on models developed by Lawrence et al. (2013). The evaluation was made over 13 dates during 2013 and the results were compared to those obtained in the first step of the study, using the Simplified Retrieval Method (SRP).

2. Materials

Results shown in this paper are based on measurements made with the ELBARA-II radiometer over the MELBEX-III site during 2013. This site, within the VAS region, is located at the "*Finca El Renegado*" (39° 31′ 18.18″ N, 1° 17′ 29.64″ W), a vineyard field of "Tempranillo" variety. The row spacing is 3 m and the spacing between plants is 2 m. The maximum LAI (Leaf Area Index) is usually reached in August being close to 2.2 $m^2 \cdot m^{-2}$ (Schwank et al., 2012; Wigneron et al., 2012). Several instruments are deployed over the site together with the ELBARA-II L-band radiometer and a number of automatic instruments used to characterize the soil and vegetation conditions. The year 2013 was selected in this study where we could gather a good dataset of SM automatic measurements together with an accurate monitoring of all agricultural practices performed over the vines.

ELBARA-II is a dual polarization L-band microwave radiometer with two measuring channels (1400–1418 MHz and 1409–1427 MHz) attached to a 23.5 dB gain horn antenna with a field of view of $\approx \pm 12°$ at −6 dB sensitivity (Schwank, Wiesmann, et al., 2010). The observed TB_p (p = H, V) used in this study are averages of the brightness temperature values measured in two 11 MHz frequency channels within the protected part (1400–1427 MHz) of the microwave L-band. The radiometer is placed on a 15 m high platform over the vineyard to measure TB_V and TB_H automatically for observation angles in the range of $\theta = 30°$–$150°$ (relative to nadir). The instrument footprint areas at −9 dB antenna sensitivity (corresponding to $\pm 9°$ around the antenna main direction) range from ≈ 33 m^2 at $\theta = 30°$ to ≈ 800 m^2 at $\theta = 70°$ (Fig. 1b in Schwank et al., 2012). The ELBARA-II system performs automated measurements following a protocol consisting of: (i) sky calibration measurements (every day at 23:55) at $\theta = 150°$, (ii) angular scans ($\theta = 30°, 35°, 40°, 45°, 50°, 55°, 60°, 65°, 70°$) every 30 min, and (iii) observations at a fixed angle of $\theta = 45°$ every hour at 10, 20, 40 and 50 min past the hour (Schwank et al., 2012). The measured multi-angular TB_p data were filtered out when the presence of radiofrequency interferences (RFI) was suspected. The filtering was made when either: (1) TB_p exceeds a maximum value (temperature of the air in kelvin) or is below a minimum value (set here at 50 K), (2) the brightness temperatures TB_p measured in the two frequency channels differ from more than 0.2 K, or (3) anomalies with the thermal stabilization of the instrument or short burst of RFI (e.g. from radars) were detected by a statistical analysis of the data samples at 800 Hz.

Two Delta-T ML2x soil moisture probes (ThetaProbes) are placed in the MELBEX-III site to estimate SM, 3 m away from the edge of the 30° ELBARA-II footprint. They provide the volumetric soil moisture (m^3 m^{-3}) of the top 0–5 cm soil layer. These probes are installed vertically in the soil and the calibration is based on results obtained by Wigneron et al. (2012) for a large range of SM conditions. One of the ThetaProbes is placed close to a vine stump and the other is in the middle of two rows. Averages of the measurements performed with these two probes were assumed to be representative of the soil moisture conditions in the MELBEX-III field site, and thus considered as the SM reference in this study. A larger number of probes is desirable to better estimate the average soil moisture value in the field. However, this was not feasible due to tractor operations and agricultural practices that regularly damaged the in-situ sensors (at the beginning of the experiment,

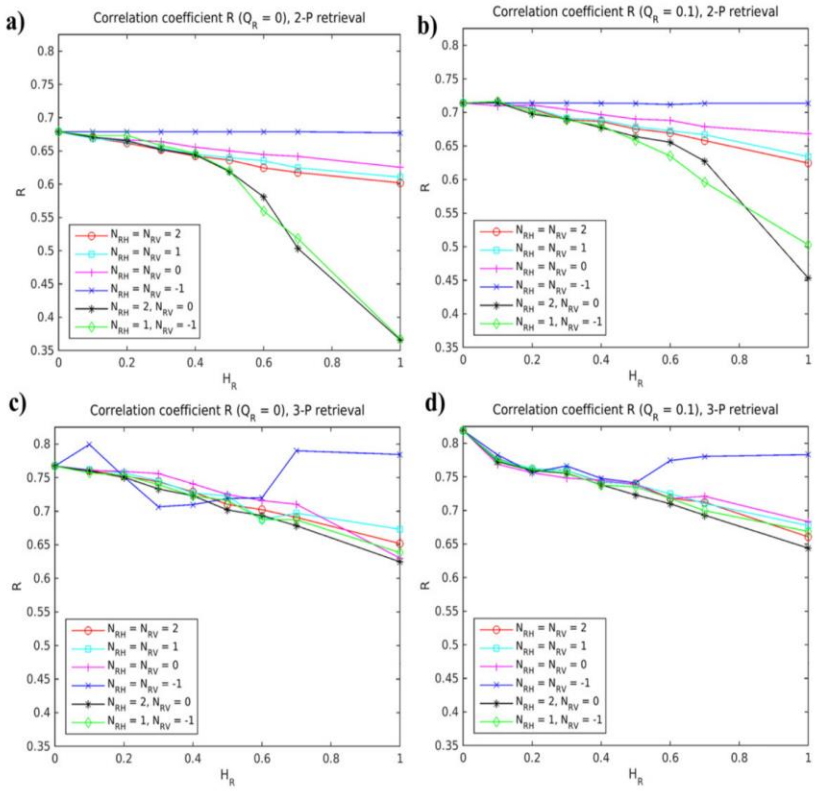

Fig. 1. Correlation coefficient *R* between retrieved SM values and measured SM values as a function of H_R for 2-P (a, b) and 3-P retrievals (c, d), and when Q_R is set equal to 0 (a, c) or 0.1 (b, d).

a network of 12 SM probes was set up within the ELBARA-II footprint (Schwank et al., 2012; Wigneron et al., 2012)). A needle board was used to estimate in-situ soil roughness conditions (Mialon et al., 2012). The board has 201 needles, at 1 cm spacing, free to move vertically following the local soil elevation profile. The measurement protocol consisted of eight repetitions, taking into consideration the perpendicular and parallel directions to the rows of vines, all inside the radiometer footprint. Then, standard deviation σ of surface heights and autocorrelation length *Lc* were computed from each measurement, and an average of the eight values was considered as an estimation of the synthetic roughness parameter *Zs* defined as $Zs = \sigma^2/Lc$ (Lawrence et al., 2013; Zribi, Gorrab, & Baghdadi, 2014).

In-situ soil roughness measurements were made for 13 dates during 2013, aiming at exploring soil roughness changes after major agricultural practices and rainfall events. Table 1 provides the corresponding dates and a brief description of the events that occurred during the days preceding the in-situ measurements. Precipitation during the year 2013 was obtained from the Caudete de las Fuentes rain gauge belonging to "Confederación Hidrográfica del Júcar" (Jucar River Basin Authority) (39° 32′ 48.97″ N, 1° 16′ 47.64″ W), less than 3 km away from the MELBEX-III site. As expected, as can be seen in Table 1, the main events influencing soil roughness were plowing and rainfall. There is generally an increase in the value of σ after plowing and a decrease after rainfall events.

In order to monitor changes in the vegetation conditions (growth cycle and senescence) at MELBEX-III, NDVI (Normalized Difference Vegetation Index) was obtained from MODIS (Moderate Resolution Imaging Spectroradiometer) after a moving window method was applied over the 16 day NDVI 1 km resolution composite MODIS product.

3. Theory

3.1. L-MEB model

SM retrievals were based on the inversion of the L-MEB model. L-MEB uses the zero-order τ-ω radiative transfer model (Mo, Choudhury, Schmugge, Wang, & Jackson, 1982) to simulate the thermal

Table 1
Roughness parameters derived from in-situ measurements in 2013 over the MELBEX-III site.

Date	Doy	Previous event	*Lc* (mm)	σ (mm)	*Zs* (cm)
20-02-2013	51	Light precipitation	89	18	0.3
12-03-2013	71	Not any practice	70	18	0.5
18-04-2013	108	Row plowing	77	25	0.8
23-05-2013	143	Plowing and sulfate fertilization	88	23	0.6
08-07-2013	189	Row plowing	43	23	1.3
15-07-2013	196	Heavy rain	75	14	0.3
22-07-2013	203	Long branch pruning	76	14	0.3
29-07-2013	210	Row plowing	52	25	1.2
20-09-2013	263	Not any practice	49	19	0.7
08-10-2013	281	Grape harvest (with combine harvester)	71	16	0.4
05-11-2013	309	Plowing half of the rows only	68	22	0.7
20-11-2013	324	Vine shoot pruning	79	21	0.5
17-12-2013	351	Plowing half of the rows and some steady precipitation	42	16	0.6

emission of a soil covered with vegetation. At thermal equilibrium, soil emissivity (e_{Gp}) at the observation angle θ can be computed from the corresponding soil reflectivity (r_{Gp}):

$$e_{Gp}(\theta) = 1 - r_{Gp}(\theta) \tag{1}$$

Rough soil reflectivity r_{Gp} is related to the reflectivity r_{Gp}^{*} (p = H, V) of a plane (specular) surface. The latter was computed from the Fresnel equations as a function of θ and of the soil dielectric constant (ε), which in turn was computed as a function of SM, soil effective temperature (T_G), and soil texture in terms of clay fraction (Mironov, Kerr, Wigneron, Kosolapova, & Demontoux, 2013). For the MELBEX-III site, Juglea et al. (2010) estimated the following soil fractions: sand (45%), silt (29%) and clay (26%). A semi-empirical approach developed originally by Wang and Choudhury (1981) was used to correct the specular reflectivities r_{GH}^{*} and r_{GV}^{*} from the roughness effects. The corresponding semi-empirical roughness model (referred to as the "QHN model" in the following) includes the four roughness parameters Q_R, H_R and N_{Rp} ($p = V, H$) (Wigneron et al., 2007):

$$r'_{GH}(\theta) = [1 - Q_R(\theta)]r^{*}_{GH}(\theta) + Q_R(\theta)r^{*}_{GV}(\theta) \tag{2}$$

$$r'_{GV}(\theta) = [1 - Q_R(\theta)]r^{*}_{GV}(\theta) + Q_R(\theta)r^{*}_{GH}(\theta) \tag{3}$$

$$r_{Gp}(\theta) = r'_{Gp}(\theta)\exp\left[-H_R\cos^{N_{Rp}}(\theta)\right] \tag{4}$$

The parameter H_R accounts for the decrease of the specular reflectivities r_{Gp}^{*} (p = H, V) due to soil roughness effects, Q_R accounts for polarization mixing effects, and N_{Rp} governs the changes in the angular dependence of reflectivity.

Using the τ-ω model (Eq. (5)), the emission from a soil covered with vegetation can be calculated for each polarization as a sum of (i) the direct upwelling vegetation emission, (ii) the upwelling soil emission attenuated by the canopy, and (iii) the downwelling vegetation emission reflected by the soil and attenuated again by the canopy layer.

$$TB_p(\theta) = (1-\omega_p)\left[1-\gamma_p(\theta)\right]\left[1+\gamma_p(\theta)r_{Gp}(\theta)\right]T_C + \left[1-r_{Gp}(\theta)\right]\gamma_p(\theta)T_G \tag{5}$$

where T_G and T_C are respectively the soil and vegetation effective temperature, γ_p is the vegetation transmissivity and ω_p (p = H, V) is the effective scattering albedo (Kurum, 2013). The latter is generally considered to be close to zero over low vegetation covers (Kurum, 2013; Wigneron et al., 2007). In this study, we set $\omega_p = 0$.

According to the Beer's law, vegetation transmissivity γ_P is related to τ_P as:

$$\gamma_p = \exp\left[-\tau_p/\cos(\theta)\right] \tag{6}$$

where the optical thickness (τ_p) at oblique observation angles $\theta > 0$ and polarization p = H, V is expressed as function of the optical thickness τ_{NAD} at nadir ($\theta = 0$):

$$\tau_p(\theta) = \tau_{NAD}\left[\sin^2(\theta)tt_p + \cos^2(\theta)\right] \tag{7}$$

where tt_V and tt_H are parameters used to quantify the dependence of τ_p on the incidence angle θ. The value $tt_H = 1$ or $tt_V = 1$ corresponds to the isotropic case for the Vertical or Horizontal polarization, where $\tau_H(\theta) = \tau_V(\theta) = \tau_{NAD}$. A value of $tt_P > 1$ or $tt_P < 1$ leads to an increase or decrease of τ_P as function of θ corresponding to anisotropic vegetation.

A single parameter called the composite soil-vegetation surface temperature T_{GC} (Jackson et al., 1980; Wigneron et al., 2007) was considered to account for both the soil effective temperature T_G and the vegetation canopy temperature T_C (Fernandez-Moran et al., 2014; Miernecki et al., 2014; Parrens et al., 2014; Wigneron et al., 2012). This assumption was made since retrievals were performed at 6 am and 6 pm, when the soil-vegetation temperature difference is small. In situ measurements of soil temperature profiles at VAS were discarded because they contained gaps in 2013. Values of T_{GC} were obtained from the ERA-INTERIM 0-7 cm soil temperature product from ECMWF (European Center for Medium range Weather Forecasting), with a temporal resolution of three hours and a spatial resolution of 1.5°. Following these assumptions, the τ-ω radiative transfer model (5) can be simplified yielding:

$$TB_p(\theta) = T_{GC}\left[1 - \gamma_p^2(\theta)r_{Gp}(\theta)\right] \tag{8}$$

Using Eqs. (2)–(4), (6)–(8), TB_P can be expressed as:

$$TB_p(\theta) = T_{GC}\left[1 - r'_{Gp}(\theta)\exp\left(-2\tau_{NAD}\frac{\cos^2(\theta) + tt_P\sin^2(\theta)}{\cos(\theta)} - H_R\cos^{N_{Rp}}(\theta)\right)\right] \tag{9}$$

3.2. Soil roughness parameterization

The soil roughness parameterization can be computed by the QHN model (Lawrence et al., 2013) requiring in-situ data as input parameters. More specifically, the parameters H_R, Q_R, N_{Rp} were derived from the values of the slope parameter $Zs = \sigma^2/Lc$ (σ = standard deviation of surface height, Lc = autocorrelation length of the surface) using six different methods as shown in detail in equations A–F of Lawrence et al. (2013), given in Table 2. In the present study, the parameters H_R, Q_R and N_{Rp} were calculated for the thirteen dates where in-situ roughness measurements were performed in 2013. These parameters were used to retrieve soil moisture at 6 am and 6 pm just after the roughness measurements were made. The results obtained with the 'Lawrence'

Table 2
Soil roughness parameterizations (Lawrence et al., 2013).

Parameterizations	Equations
A	$H_R = \begin{cases} 2.615(1-\exp(\frac{-Zs}{2.473})) & Zs \le 1.235 \\ 1.0279 & Zs > 1.235 \end{cases}$ $Q_R = 0.1771 H_R$ $N_{RH} = 1.615(1-\exp(\frac{-H_R}{0.359})) - 0.238$ $N_{RV} = 0.767 H_R - 0.099$
B	$H_R = \begin{cases} 2.265(1-\exp(\frac{-Zs}{2.023})), & Zs \le 1.253 \\ 1.046, & Zs > 1.253 \end{cases}$ $Q_R = 0.253 H_R$ $N_{RV} = 0.999 H_R - 0.54$ $N_{RH} = N_{RV} + 2.029 - 0.7457\,Zs$
C	$H_R = \begin{cases} 2.644(1-\exp(\frac{-Zs}{2.473})), & Zs \le 1.2391 \\ 1.042, & Zs > 1.2391 \end{cases}$ $Q_R = 0.118 H_R$ $N_R = 1.496(1-\exp(\frac{-H_R}{0.385})) - 0.241$ $N_{RH} = N_{RV}$
D	$H_R = \begin{cases} 2.689(1-\exp(\frac{-Zs}{2.556})), & Zs \le 1.2314 \\ 1.028, & Zs > 1.2314 \end{cases}$ $Q_R = 0$ $N_{RH} = 1.356(1-\exp(\frac{-H_R}{0.087})) - 0.602$ $N_{RV} = 1.759 H_R - 0.248$
E	$H_R = \begin{cases} 1.762(1-\exp(\frac{-Zs}{1.85})), & Zs \le 1.1894 \\ 0.836, & Zs > 1.1894 \end{cases}$ $Q_R = 0.050 H_R$ $N_{RH} = 0$ $N_{RV} = 0$
F	$H_R = \begin{cases} 2.62(1-\exp(\frac{-Zs}{2.993})), & Zs \le 1.1553 \\ 0.853, & Zs > 1.1553 \end{cases}$ $Q_R = 0$ $N_{RH} = 0$ $N_{RV} = 0$

parameterizations were compared with those obtained with the SRP method.

3.3. Simplified roughness parameterization (SRP)

Note that, for the specific case when $N_{RV} = N_{RH} = -1$, $Q_R = 0$, and vegetation is assumed as isotropic such that $tt_p = 1$ (p = H, V), Eq. (9) can be simplified as:

$$TB_p(\theta) = T_{GC}\left[1 - r^*_{Gp}(\theta)\exp(-2TR/\cos(\theta))\right] \quad (10)$$

where

$$TR = \tau_{NAD} + H_R/2 \quad (11)$$

In that case, vegetation (through the τ_{NAD} parameter) and roughness effects (through the H_R parameter) can be combined in the single parameter TR defined in Eq. (11). Thus, there is no need to attempt to decouple roughness and vegetation effects, which is a difficult task as suggested in many previous studies (Lawrence et al., 2013; Pardé et al., 2004; Patton & Hornbuckle, 2013). Moreover, in that case the chosen value for the H_R parameter has no impact on the SM retrievals: changes in the value of H_R have solely an impact on the retrieved values of τ_{NAD} but not on the retrieved values of SM. The specific 2-P retrieval case in which $N_{RV} = N_{RH} = -1$, $tt_V = tt_H = 1$ will be referred to as the 'simplified roughness parameterization' (SRP).

3.4. Soil moisture retrievals

In this study, SM estimates were retrieved from the ELBARA-II multi-angular observations $TB_p(\theta)$ following two retrieval configurations:

- *2-parameter (2-P) retrievals*: SM and τ_{NAD} were retrieved simultaneously while the parameters $tt_H = tt_V = 1$ were considered to represent isotropic vegetation structure. This configuration corresponds to the classical L-MEB inversion approach (Wigneron, Chanzy, Calvet, & Bruguier, 1995; Wigneron et al., 2003, 2007) and is currently used in the SMOS SM retrieval algorithm (Kerr et al., 2012).
- *3-parameter (3-P) retrievals*: SM, τ_{NAD} and the tt_V vegetation parameter were retrieved simultaneously (while $tt_H = 1$ was assumed), as in Wigneron et al. (2012) and Miernecki et al. (2014). Considering tt_V as a retrieved parameter allows accounting for the predominant vertical structure of the vine vegetation (mostly stems).

For both retrieval configurations, ELBARA-II measurements were used for the observation angles θ = 30, 35, 40, 45, 50, 55°. When some angles were missing (because of short electricity cuts or RFI), retrievals were carried out only if the available angular range (the difference between the highest and the lowest measurement angle) was at least 10°. It was found that only 13.5% of the dataset contained one or more missing angles over all the year at 6 am and 6 pm. The inversion of L-MEB is based on the minimization of a cost-function (CF) using a least-squares iterative algorithm (Wigneron et al., 2007):

$$CF = \frac{\sum (TB_{mes} - TB^*)^2}{\sigma(TB)^2} - \sum \frac{\sum \left(P_i^{ini} - P_i^*\right)^2}{\sigma(P_i)^2} \quad (12)$$

Where TB_{mes} are the brightness temperatures measured by ELBARA-II over all available angles and both polarizations (p = H, V), TB^* are the simulated brightness temperatures following Eq. (9), $\sigma(TB) = 1$ K is the standard deviation associated with TB_{mes} (Schwank et al., 2012), P_i^{ini} ($i = 1,\ldots, N$) are a priori estimates of the retrieved parameters P_i considered as initial values during the minimization of the cost-function CF, $\sigma(P_i)$ are the standard deviations associated with the initial guesses P_i^{ini} of the retrieved parameters P_i ($i = 1,\ldots, N$) and P_i^* ($i = 1,\ldots, N$) are the values of the retrieved parameters. After each SM retrieval, the RMSE between the ELBARA-II measurements (TB_{mes}) and the simulated brightness temperatures (T_{B_p}, Eq. (9)) was calculated (referred to as $RMSE_{TB}$). High errors in the retrieval process were filtered out by deleting SM values when $RMSE_{TB} > 12$ K, avoiding bad quality retrievals. These high errors are rare (no one was found) but they generally happen when the TB angular trend is noisy due to RFI effects, which were not detected and filtered, or to the sporadic presence of tractors and machines within the ELBARA-II footprint. Furthermore, SM values outside the range 0–0.5 $m^3 \cdot m^{-3}$ were rejected (Juglea et al., 2010). It happened only 1.5% of the retrievals.

4. Results

To assess performances of the SM retrievals for a number of different parameterizations of the soil roughness conditions, we compared corresponding SM retrievals (SM_{RM}) derived from the radiometric (RM) observations against in-situ measurements ($SM_{in\text{-}situ}$), considered here as the reference. The statistic scores used in this study are the correlation coefficient (R), the bias (B given by Eq. (13)), and the unbiased root mean square error ($ubRMSE$ given by Eq. (14)). The latter was computed as a function of the bias and the root mean square error ($RMSE$) (Entekhabi, Reichle, Koster and Crow, 2010b):

$$B = \sum_{i=1}^{n}\left(\frac{SM_{RM} - SM_{in-situ}}{n}\right) \quad (13)$$

$$ubRMSE = \sqrt{RMSE^2 - B^2} \quad (14)$$

Where n is the total number of SM retrievals considered in the evaluation.

4.1. Testing different roughness parameterizations

As shown in Table 1, surface roughness of the MELBEX-III site varies over the year and thus affects soil moisture retrievals. However, it is not possible to monitor the changes in σ and Lc over time at large spatial scales. For this reason, except when the 'simplified roughness parameterization' (SRP) is used (H_R is retrieved simultaneously to τ_{NAD} in that case), fixed values of the roughness parameters are assumed in this study. The resulting performances of the SM retrievals, in comparison with in-situ SM data used here as a reference, are analyzed in this section. Each statistic score (correlation R, bias B and unbiased root mean square error $ubRMSE$) was used separately to find which roughness parameterization leads to the "best" SM retrievals, considering highest R values, and lowest bias B and $ubRMSE$ values.

In a first step, various combinations of values of the roughness parameters used in the QHN model (H_R, Q_R and N_{Rp}) were explored. These values correspond to common ones used in the literature in this domain (Escorihuela et al., 2007; Miernecki et al., 2014; O'Neill, Chan, Njoku, Jackson, & Bindlish, 2012; Wigneron et al., 2007): $Q_R = \{0, 0.1\}$ and $(N_{RH}, N_{RV}) = \{(2, 2), (1, 1), (0, 0), (-1, -1), (2, 0), (1, -1)\}$. H_R values were fixed as $H_R = \{0, 0.1, 0.2, 0.3, 0.4, 0.5, 0.6, 0.7, 1\}$, in order to find which one performs best. Note that the case $N_{RH} = 2$, $N_{RV} = 0$ corresponds to the default parameterization used currently in the SMOS SM retrieval algorithm (Kerr, Waldteufel, Richaume, et al., 2010; Kerr, Waldteufel, Wigneron, et al., 2010, ATBD). The evaluations were made using all available ELBARA-II observations performed at 6 am and 6 pm during the year 2013. Since very little differences in the resulting SM were found when taking into account these times separately, both were considered simultaneously.

4.1.1. Results in terms of correlation

In Fig. 1 we show the correlation coefficients R between measured and retrieved SM values as a function of H_R for different values of Q_R and N_{Rp} (p = H, V), for 2-P and 3-P retrievals. For 2-P retrievals, it can

be seen that the 'simplified roughness parameterization' (SRP) configuration led to the highest correlation values in the case $Q_R = 0$ ($R = 0.68$) [Fig. 1a] or $Q_R = 0.1$ ($R = 0.71$) for all values of H_R [Fig. 1b]. In both cases, for all other roughness parameterizations than SRP, it can be noted that R decreases as H_R increases. As noted in Section 2.3, it can be seen that the retrieved value of SM does not depend on H_R for the SRP configuration. The same SM retrievals as the SRP method were found when setting $H_R = 0$ (in that case N_{RV} and N_{RH} have no influence on the SM retrievals, Eq. (9)). The two parameterizations, where the values of N_{RH} and N_{RV} are different, led to lower R values when $H_R \geq 0.4$. For 3-P retrievals (when tt_V is retrieved simultaneously with SM and τ_{NAD}) , it can be seen that the correlation coefficient R depends on H_R for the $N_{RH} = N_{RV} = -1$ parameterization (contrary to what was obtained for the 2-P retrievals). However, whatever the value of H_R used, considering 3-P parameters led to higher correlation values in comparison to 2-P retrievals. Furthermore, for a given roughness configuration, 3-P retrieval performed better in terms of correlation values than 2-P in all cases. Increasing values of H_R, led generally to a decrease in the R values (except when $N_{RH} = N_{RV} = -1$).

The correlation coefficients R between in-situ and retrieved SM are analyzed in detail in terms of the highest correlations in Table 3 considering separately 2-P and 3-P retrievals. In this table, highest R values are defined as values close to R_{max} (higher than R_{max} minus 0.04), where R_{max} is the maximum value of R, considering all tested parameterizations of the roughness parameters. 2-P and 3-P retrievals were analyzed separately. For instance, $R_{max} = 0.72$ was obtained for 2-P retrieval. If $N_{RH} = N_{RV} = 1$ and $Q = 0$, the condition $R \geq (R_{max}$ - 0.04) was fulfilled only for the case $H_R = 0$ and the corresponding value of R was $R = 0.68$. The values of H_R, Q_R, N_{RH} and N_{RV} that satisfy this condition are shown in Table 3. For 2-P retrievals, whatever the values of N_{RH}, N_{RV} and Q_R, values of H_R producing "best correlations" can be found. This is not the case for 3-P retrievals.

4.1.2. Results in terms of bias

In Fig. 2, we present the results of the bias B between measured and retrieved SM values. For 2-P retrievals, the range of bias values was similar when $Q_R = 0$ ($-0.046\ m^3 \cdot m^{-3}$ (SRP) $\leq B \leq +0.113\ m^3 \cdot m^{-3}$) and when $Q_R = 0.1$ ($-0.078\ m^3 \cdot m^{-3}$ (SRP) $\leq B \leq +0.077\ m^3 \cdot m^{-3}$). For both $Q_R = 0$ and $Q_R = 0.1$, it can be noted that the bias B increases, from negative to positive values, almost linearly as H_R increases. Setting $Q_R = 0.1$ generally led to lower retrieved SM values. When $Q_R = 0$, a bias B equals zero can be reached for values of H_R in the range $0.3 \leq H_R \leq 0.7$, depending on the values of N_{RH} and N_{RV}. When $Q_R = 0.1$, a bias equals zero can be reached for values of $H_R \geq 0.5$. The absolute value $|B|$ of the bias for the SRP method was found to be higher when $Q_R = 0.1$ ($B = -0.078\ m^3 \cdot m^{-3}$) in comparison with the case $Q_R = 0$ ($B = -0.046\ m^3 \cdot m^{-3}$).

Using 3-P retrievals, similar results to 2-P retrievals were obtained, except that lower SM values were retrieved generally ($-0.077\ m^3 \cdot m^{-3} \leq B \leq +0.051\ m^3 \cdot m^{-3}$ for $Q_R = 0$, and $-0.091\ m^3 \cdot m^{-3} \leq B \leq +0.040\ m^3 \cdot m^{-3}$ for $Q_R = 0.1$). For 3-P retrievals the range of bias values is slightly lower compared to 2-P retrievals. A bias equal to zero was achieved for the parameter range $0.5 \leq H_R \leq 0.8$ when $Q_R = 0$ and for $H_R > 0.6$ when $Q_R = 0.1$. For the specific parameterization $N_{RV} = N_{RH} = -1$, the bias is almost constant ($-0.080\ m^3 \cdot m^{-3} \leq B \leq -0.062\ m^3 \cdot m^{-3}$ for $Q_R = 0$, and $-0.091\ m^3 \cdot m^{-3} \leq B \leq -0.082\ m^3 \cdot m^{-3}$ for $Q_R = 0.1$). Table 4 provides the values of the roughness parameters leading to lowest bias values (defined here as $-0.02\ m^3 \cdot m^{-3} \leq B \leq +0.02\ m^3 \cdot m^{-3}$) for 2-P and 3-P retrievals. Only in the case of $N_{RH} = N_{RV} = -1$, the lowest value of B cannot be reached. It can be seen that the value of H_R required to obtain a bias close to zero, tends to increase when $Q_R = 0.1$, in comparison to the case $Q_R = 0$, and also when using 3-P retrievals instead of 2-P retrievals.

4.1.3. Results in terms of unbiased RMSE

Finally, we considered the results for the unbiased RMSE (*ubRMSE*) in Fig. 3. As observed in the previous figures, varying the value of H_R does not affect the *ubRMSE* values for the SRP parameterization (Fig. 3ab). For the other parameterizations, the *ubRMSE* values generally increase with increasing values of H_R.

For 2-P retrievals, the lowest value of *ubRMSE* was reached with SRP ($ubRMSE = 0.056\ m^3 \cdot m^{-3}$ for $Q_R = 0$ and $ubRMSE = 0.044\ m^3 \cdot m^{-3}$ for $Q_R = 0.1$) while the highest values were $ubRMSE = 0.106\ m^3 \cdot m^{-3}$ for $Q_R = 0$ and $ubRMSE = 0.097\ m^3 \cdot m^{-3}$ for $Q_R = 0.1$. Whatever the value of H_R, the parameterizations in which N_{RH} is not equal to N_{RV} produced higher *ubRMSE* values. For the 3-P retrievals, results were relatively similar to 2-P retrievals except that lower values of *ubRMSE* were obtained ($0.035\ m^3 \cdot m^{-3} \leq ubRMSE \leq 0.086\ m^3 \cdot m^{-3}$ for $Q_R = 0$, and $0.035\ m^3 \cdot m^{-3} \leq ubRMSE \leq 0.089\ m^3 \cdot m^{-3}$ for $Q_R = 0.1$). As for 2-P retrievals, the configurations leading to lowest *ubRMSE* values were those in which $N_{Rp} = -1$ (p = H, V). In summary and in terms of *ubRMSE*, 3-P retrievals provided improved results in comparison to 2-P retrievals, while setting $Q_R = 0.1$, instead of $Q_R = 0$, provided improved results only in the case of the 2-P retrievals.

In Table 5, the parameterizations providing best *ubRMSE* values (defined here as values of *ubRMSE* close to the lowest *ubRMSE* value ($ubRMSE_{min}$), i.e. $ubRMSE \leq ubRMSE_{min} + 0.02\ m^3\ m^{-3}$) are presented. For 2-P retrievals, best *ubRMSE* values could be obtained for values of $H_R \leq$ (0.1–0.7), while best *ubRMSE* values could be obtained for values of $H_R \leq 0.3$ for 3-P retrievals.

4.2. Illustration of the SRP results

In order to illustrate the retrieval results, Fig. 4 presents the retrieved SM values using the SRP method ($Q_R = 0$) as well as the simulated ECMWF SM values, in-situ measurements of SM and precipitation values registered by the rain gauge from "Confederación Hidrográfica del Júcar" (Jucar River Basin Authority) during the year 2013. Fig. 5 shows a scatter plot of the SM values retrieved from ELBARA-II using the SRP method and the SM measurements for the whole year 2013. As found earlier, retrieved SM values with the SRP method underestimates the corresponding in-situ measurements, in particular for low SM values. It should be noted that retrieved SM represents soil moisture of the ≈0–3 cm top surface layer (Escorihuela et al., 2010), while in-situ measurements (using Theta probes) are assumed to represent SM within the ≈0–5 cm top soil layer. Except during rainfall events, this thicker soil layer is believed to be generally wetter than the 0–3 cm top soil layer over the vineyard considered in this study. It seems that the bias B computed between the in-situ measurements and the retrieved SM values (Figs. 4 and 5) corroborate this hypothesis. For instance, it can be noted that lower B values were generally obtained during rain events in contrast to what is obtained during dry periods. During the days when the field was plowed, no anomalies can be noted in the SM values retrieved with the SRP method applied to the ELBARA-II data.

Table 3
Values of H_R, Q_R, N_{RH} and N_{RV} producing best correlation coefficients (i.e. $R \geq (R_{max}$ - 0.04)) in 2-P and 3-P retrievals.

		2-P retrieval		3-P retrieval	
N_{RH}, N_{RV}	Q_R	H_R	R	H_R	R
2, 2	0	0	0.68	–	–
2, 2	0.1	≤0.5	0.72	≤0.1	0.82
1, 1	0	0	0.68	≤0.1	0.82
1, 1	0.1	≤0.5	0.71	–	–
0, 0	0	0	0.68	–	–
0, 0	0.1	≤0.7	0.71	–	–
−1, −1	0	No matter	0.68	0, ≥0.7	0.80
−1, −1	0.1	No matter	0.71	≤0.1, ≥0.7	0.82
2, 0	0	0	0.68	–	–
2, 0	0.1	≤0.4	0.71	–	–
1, −1	0	0	0.68	–	–
1, −1	0.1	≤0.4	0.71	0	0.82

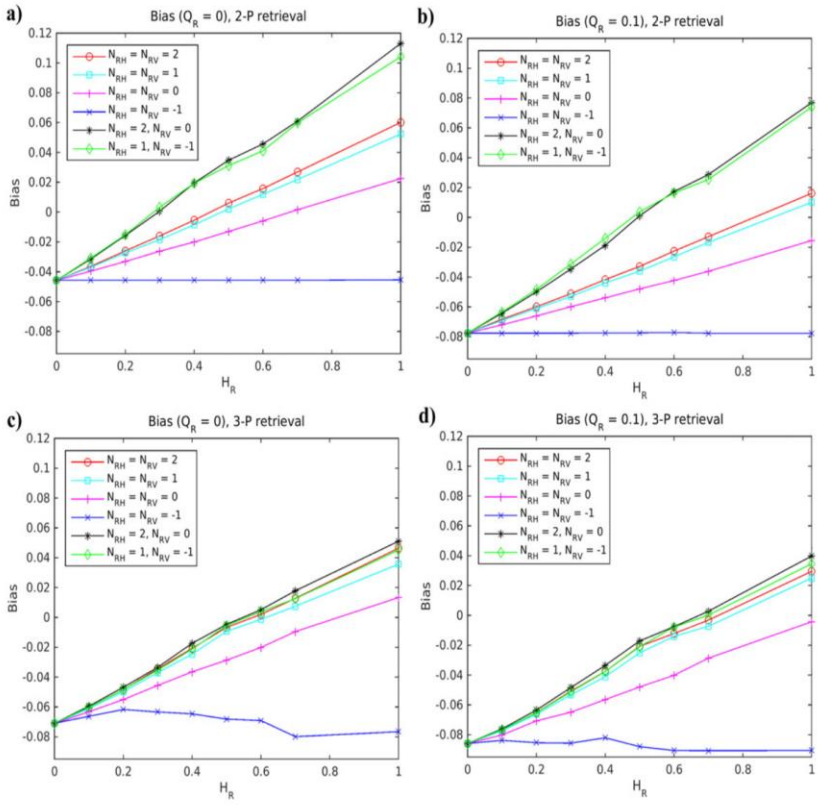

Fig. 2. Bias B between retrieved and in-situ measured SM as a function of H_R for 2-P (a, b) and 3-P retrievals (c, d), and when Q_R is set to 0 (a, c) or 0.1 (b, d).

4.3. Vegetation and roughness results

Even though the focus of this study is on soil moisture, it was interesting to evaluate the possible relationships between the retrievals of *TR* (defined in Eq. (11)) and τ_{NAD} with the soil and vegetation variables. The changes in the vegetation and roughness conditions in the field over 2013 and the retrievals of *TR* and τ_{NAD} for some specific configurations are presented in Fig. 6. The time changes in the NDVI values reflect the seasonal vegetation cycle of the vineyard field. The vegetation cycle starts at approximately Day of Year (DoY) 160, when NDVI increases as leaves start to appear, reaching a maximum value in summer ($\approx$0.4). Senescence begins on DoY $\approx$ 260. Fig. 6 illustrates the retrieved soil and vegetation parameters for two cases: *TR* obtained by the SRP method, and τ_{NAD} obtained using the 3-P retrieval, for the case $H_R = 0$, $Q_R = 0$ and $N_{Rp} = -1$. The values shown in Fig. 6 for H_R were calculated from in-situ observations using the formulation E from Lawrence et al. (2013) (see Table 2). The influence of the changes in the values of H_R (due to plowing in particular) on *TR* can be noted, as expected. However, the influence of the changes in the values H_R on vegetation optical depth τ_{NAD} can be noted too, which suggests that soil roughness and vegetation effects cannot be decoupled in the 3-P retrievals. For instance, this effect is very clear on DoY 189 when there is a significant increase in H_R, and therefore in *TR* and τ_{NAD} just after plowing. However, heavy rain events the following days significantly smoothed out soil conditions leading to a strong decrease in the retrieved H_R values. It seems that both *TR* and vegetation optical depth, τ_{NAD}, follows that decrease even though this cannot be explained by the vegetation conditions (no such change can be observed in NDVI). Other similar episodes showing the influence of the changes in H_R on the values of *TR* and τ_{NAD} occur on DoY 108 (increase in H_R) and DoY 281 (decrease in H_R).

So, it seems that changes in the soil roughness conditions have an impact on the values of both *TR* and τ_{NAD}, but the *TR* parameter seems to be more sensitive to these changes. Generally, the range of values of *TR* seems to be larger than that of τ_{NAD} over the vegetation cycle, in relation with an increased sensitivity of *TR* to the soil roughness effects.

An illustration of the vegetation anisotropy parameter tt_V retrieved with the 3-P approach is shown in Fig. 7 (the same 3-P configuration was used in both Figs. 6 & 7: $H_R = 0$, $Q_R = 0$, $N_{Rp} = -1$). Schwank et al. (2012) found that vegetation structure is more vertical in winter, due to the presence of the vine stocks only, leading to a higher difference between the values of tt_V and tt_H. In Fig. 7, there is a high variability in the retrieved values of the parameter tt_V and it is difficult to

Table 4
Values of H_R, Q_R, N_{RH} and N_{RV} producing lowest $B| \leq 0.02$ $m^3 \cdot m^{-3}$ in 2-P and 3-P retrievals.

		2-P retrieval		3-P retrieval	
N_{RH}, N_{RV}	Q_R	H_R	B ($m^3 \cdot m^{-3}$)	H_R	B ($m^3 \cdot m^{-3}$)
2, 2	0	0.3–0.6	−0.005	0.5–0.7	0.002
2, 2	0.1	≥0.7	−0.013	0.6–0.7	−0.003
1, 1	0	0.3–0.6	0.002	0.5–0.7	−0.001
1, 1	0.1	≥0.7	0.010	0.6–0.7	±0.001
0, 0	0	0.5–0.7	0.002	≥0.6	−0.009
0, 0	0.1	1	−0.016	1	−0.004
2, 0	0	0.2–0.4	0.001	0.4–0.7	−0.005
2, 0	0.1	0.4–0.6	0.001	0.5–0.7	0.003
1, −1	0	0.2–0.4	0.003	0.5–0.7	0.004
1, −1	0.1	0.4–0.6	0.004	0.6–0.7	0.000

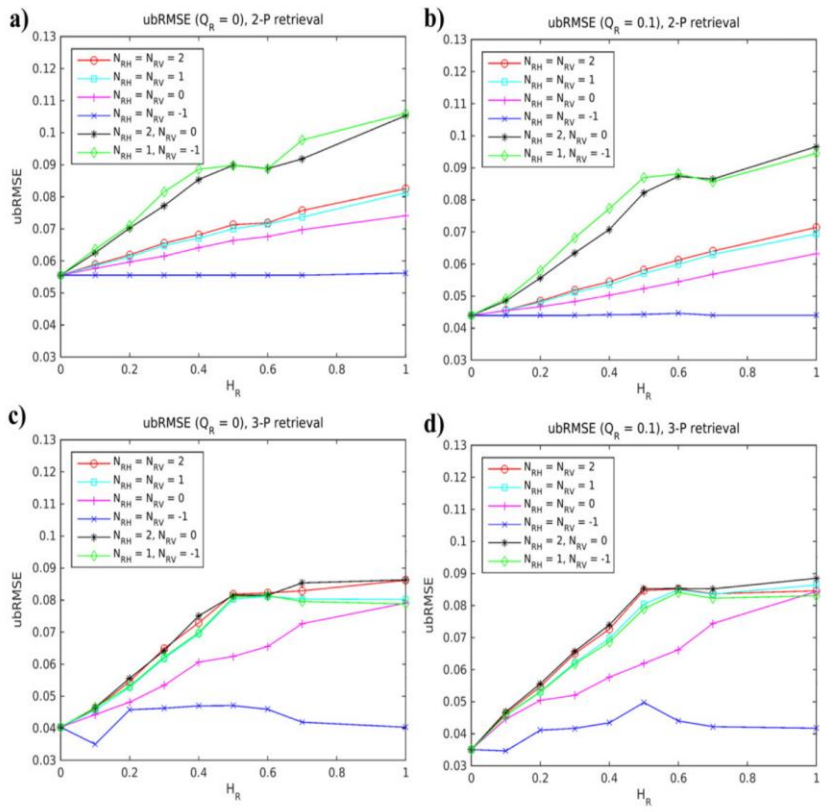

Fig. 3. Unbiased *RMSE* between retrieved SM values and measured SM values as a function of H_R for 2-P (a, b) and 3-P retrievals (c, d), and when Q_R is set equal to 0 (a, c) or 0.1 (b, d).

distinguish clear relationships between the changes in tt_V values and the phenological vegetation cycle. Nevertheless, higher tt_V values were retrieved during the early growing season, contrarily to summer with lower retrieved values. A lower variability in the retrieved values of tt_V can be noted during summer and winter, while higher variability of tt_V occurs during the period of vegetation changes (growth and senescence).

4.4. Roughness parameterizations calibrated from in-situ data

The six roughness parameterizations (A–F, Table 2) proposed by Lawrence et al. (2013) to compute H_R, Q_R, N_{RH} and N_{RV} from $Zs = \sigma^2/Lc$ (σ and Lc measured in-situ) were evaluated, and Table 6 shows the statistics scores (R, B, and *ubRMSE*) obtained from the comparison between in-situ measurements of SM and retrieved SM values (3-P retrieval). For the sake of comparison, results obtained with the SRP method (Section 2.2) are also shown in Table 6. Note that the different number of data given in Table 6 is due to the data filtering by $RMSE_{TB} > 12$ K as explained in Section 2.2.

Table 5
Values of H_R, Q_R, N_{RH} and N_{RV} producing best *ubRMSE* values (i.e. $ubRMSE \le ubRMSE_{min} + 0.02\ m^3 \cdot m^{-3}$) in 2-P and 3-P retrievals.

		2-P retrieval		3-P retrieval	
N_{RH}, N_{RV}	Q_R	H_R	*ubRMSE* ($m^3 \cdot m^{-3}$)	H_R	*ubRMSE* ($m^3 \cdot m^{-3}$)
2, 2	0	≤0.2	0.056	0–0.2	0.040
2, 2	0.1	≤0.7	0.044	0–0.1	0.035
1, 1	0	≤0.2	0.056	0–0.2	0.040
1, 1	0.1	≤0.7	0.044	0–0.2	0.035
0, 0	0	≤0.4	0.056	0–0.3	0.040
0, 0	0.1	No matter	0.044	0–0.3	0.035
−1, −1	0	No matter	0.056	No matter	0.040
−1, −1	0.1	No matter	0.044	No matter	0.035
2, 0	0	≤0.1	0.056	0–0.1	0.040
2, 0	0.1	≤0.3	0.044	0–0.1	0.035
1, −1	0	≤0.1	0.056	0–0.2	0.040
1, −1	0.1	≤0.2	0.044	0–0.2	0.035

In spite of higher absolute values of bias B and slightly higher values of *ubRMSE*, much better results were obtained generally in terms of the correlation coefficient (R) using the SRP method ($R = 0.86$). Parameterizations E and F corresponding to the case in which $N_{Rp} = 0$, led to the worst results in terms of correlation R and bias B among the parameterizations proposed by Lawrence et al. (2013), while parameterization D ($Q_R = 0$) led to a low correlation value ($R = 0.59$) but to the lowest bias ($B = -0.010\ m^3 \cdot m^{-3}$).

5. Discussion and conclusions

The aim of this study was to analyze the impact of several roughness parameterizations on SM retrievals. To this end, we used multi-angular TB_p observations (p = H, V) measured with the L-band ELBARA-II radiometer, in-situ measurements of SM, and in-situ roughness measurements performed in the MELBEX-III vineyard in the VAS area. Several values of the roughness parameters (H_R, Q_R, N_{RV}, N_{RH}) were tested as inputs for the L-MEB model when retrieving SM simultaneously with vegetation optical depth τ_{NAD} (2-P retrieval) and simultaneously with both τ_{NAD} and the vegetation anisotropy parameter tt_V (3-P retrieval).

It was found that when setting $N_{Rp} = -1$ (p = H, V) in the 2-P retrievals, the original formulation of the QHN model used to compute

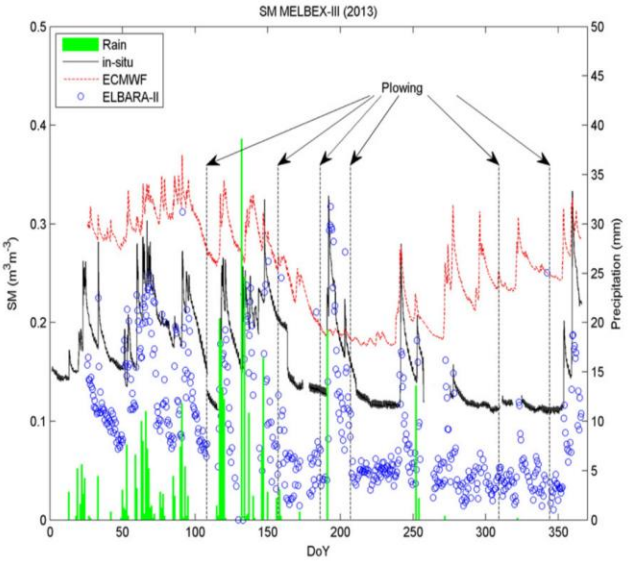

Fig. 4. Time variations in the values of the retrieved SM (SRP method), in-situ SM, SM from ECMWF modeling (European Center for Medium range Weather Forecasting) and daily precipitation from the Jucar River Basin Authority, in 2013 over the MELBEX-III site.

TB could be simplified, leading to the SRP method. In the SRP method, it is mathematically possible to account for the combined impact of soil roughness (H_R) and vegetation (τ_{NAD}) through a single parameter (*TR*). In that case H_R does not need to be calibrated, as it is included in the *TR* parameter defined in Eq. (11), which is retrieved simultaneously with SM. Based on the data set acquired over the VAS area in 2013, it was found that best SM retrievals in terms of correlation coefficient (*R*) and *ubRMSE* were obtained with the SRP method when compared with synchronous in-situ SM, considered here as the reference. Conversely, the lowest bias *B* was found with other combinations of the roughness parameters. Using the SRP configuration, the retrieved SM values underestimated the in-situ SM for all tested configurations (2-P or 3-P retrievals for $Q_R = 0$ or $Q_R = 0.1$) and the bias was in the range $-0.08\ m^3 \cdot m^{-3} \le B \le -0.04\ m^3 \cdot m^{-3}$. However as noted earlier, the sampling depths of the retrieved SM (≈0–2 cm) and of the in-situ measurements (≈0–5 cm) are not the same, which may affect the analyses in a way or another, and may have an impact, particularly, on the bias values (*B*) (Escorihuela et al., 2010). A study made by Rondinelli et al. (2015) analyzed this issue as well, concluding that the bias cannot be explained by the different sampling depths. However, the latter study was focused in the watershed of the South Fork Iowa River (relatively humid region) while the VAS is located in a semi-arid region where the differences between SM over the 0–2 cm top layer and deeper ones are more significant and cover longer periods, over most of the season of spring and summer.

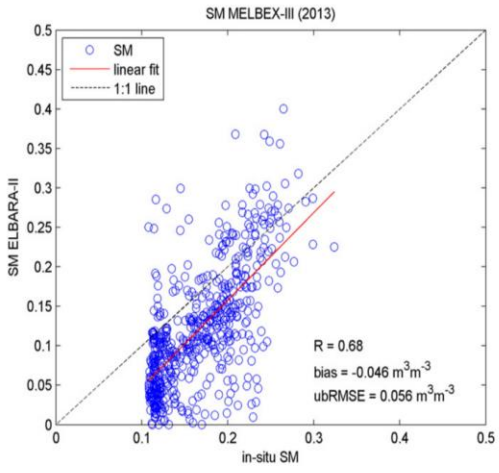

Fig. 5. Comparison between retrieved (SRP) and measured in-situ SM values in 2013 over the MELBEX-III site.

Considering the vegetation anisotropy parameter tt_V as a free parameter in the retrievals (3-P retrievals), generally led to improved results in terms of correlation *R* and *ubRMSE*, but the bias *B* between measured and retrieved SM data was generally larger. This improvement could be due to the fact that the specific structural characteristics of the vineyards, with a preferential vertical orientation of the vine stems and stocks, could be accounted for in the 3-P retrievals where the free parameter tt_V parameterizes the dependence of the optical depth at V-polarization (τ_V) on the incidence angle. Conversely, in 2-P retrievals, both tt_V and tt_H were set equal to $tt_V = tt_H = 1$, corresponding to isotropic conditions which could not account for the changes in the vegetation structure in relation with the vegetation cycle (growth and senescence) and the agricultural practices.

Although, over the vineyard field, the 3-P retrieval was found to be the most efficient approach in terms of correlation *R* and *ubRMSE*, this configuration presents the traditional disadvantages of requiring the calibration of the H_R parameter. However, note that in the case when $N_{RV} = N_{RH} = -1$, both the *R* and *ubRMSE* criteria were found to be only slightly dependent on the value of H_R.

In summary, for both 2-P and 3-P retrievals, it was found that the best approaches in terms of correlation coefficient *R* and *ubRMSE* were those corresponding to the case $N_{RV} = N_{RH} = -1$ (i.e. the SRP method in the case of 2-P retrievals). In both cases, the SM retrievals were either independent for 2-P retrievals (for SRP) or only slightly dependent for 3-P retrievals on the value of H_R. For all the other configurations, it was found that the correlation coefficient decreased and the *ubRMSE* increased for increasing values of H_R.

In a second step we used in-situ measurements of the roughness characteristics to estimate the model roughness parameters using relationships developed from numerical modeling approaches by Lawrence

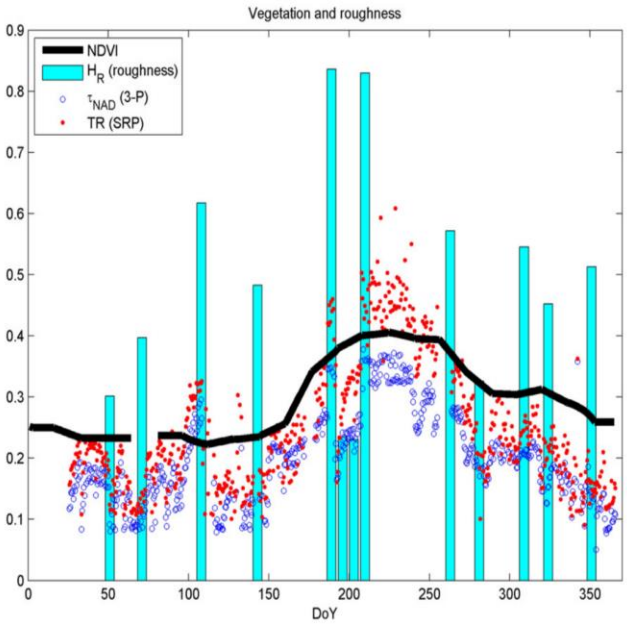

Fig. 6. Time series of soil and vegetation parameters over 2013: retrieved *TR* (Eq. (11)) using the SRP method and retrieved τ_{NAD} using the 3-P retrieval approach ($H_R = 0$, $Q_R = 0$, $N_{Rp} = -1$), H_R computed from in-situ measurements (Lawrence et al., 2013) and NDVI derived from MODIS observations (1 km, 16 days).

et al. (2013). The analysis of the statistical criteria showed that the obtained retrieval results with the Lawrence parameterizations, requiring information on the in-situ roughness conditions, provided better results in terms of bias and *ubRMSE* but poorer results in terms of correlation than those obtained with the SRP method.

In conclusion, the results of this study suggest that the use of the SRP method is an interesting approach to account for surface roughness effects in SM retrievals. The SRP method provided the best results in terms of correlation and unbiased RMSE among all the tested roughness parameterizations while the soil roughness parameter H_R does no longer need to be calibrated (as H_R is retrieved simultaneously with vegetation optical depth τ_{NAD}). More studies evaluating the improvement in SM retrievals using the SRP method from space borne observations will be crucial to consolidate this method as a feasible option in the determination of SM at global scale. In particular, errors due to uncertainties in the estimations of the L-MEB model input parameters (soil effective temperature, vegetation parameter tt_P, scattering albedo, etc.) over a large range of vegetation canopy types are to be further analyzed.

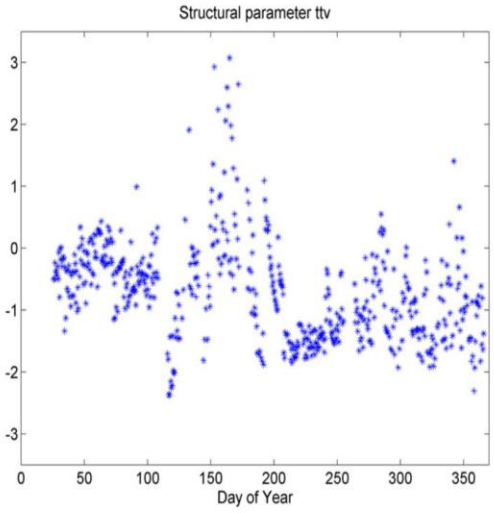

Fig. 7. Retrieved vegetation anisotropy parameter tt_V over the MELBEX-III site (3-P retrieval, $H_R = 0$, $Q_R = 0$, $N_{Rp} = -1$) in 2013.

Acknowledgments

ELBARA-II was lent by the European Space Agency (ESA) under the "ESA ELBARAII-3 L-band Radiometer System depCal/Val at the Valencia Anchor Station" (ESTEC ELBARA Loan Agreement 21013/07/NL/FF), and "Long-term ELBARA-II Assistance to SMOS Level-2 Land Product and Algorithm Validation. Accurate Monitoring of Vegetation Water Content and Surface Water Balance" (ESA ELBARA-II AO Proposal ID 11759).

This work is carried out within the framework of the project MIDAS-7/UVEG "Productos y Aplicaciones Avanzados de SMOS y Futuras Misiones (Parte UVEG)" from the Spanish Research Programme on Space, Spanish Ministry for Economy and Competitiveness, and of TOSCA-CNES (Centre National d'Etudes Spatiales) and ESA projects in the framework of the improvement of the SMOS algorithm (ESA ESL (Expert Support Laboratory) funding).

Table 6
Performance criteria in SM retrievals using roughness parameterizations calibrated from in-situ data and using the SRP method.

Parameterization	*R*	*B* ($m^3 \cdot m^{-3}$)	*ubRMSE* ($m^3 \cdot m^{-3}$)	Number of data
A	0.62	−0.036	0.061	11
B	0.63	−0.030	0.065	11
C	0.62	−0.036	0.061	11
D	0.59	−0.010	0.059	10
E	0.56	−0.042	0.053	10
F	0.55	−0.036	0.052	10
SRP	0.86	-0.062	0.069	9

References

Cano, A., Saleh, K., Wigneron, J. -P., Antolín, C., Balling, J. E., Kerr, Y. H., et al. (2010). The SMOS Mediterranean Ecosystem L-Band characterisation EXperiment (MELBEX-I) over natural shrubs. *Remote Sensing of Environment, 114*(4), 844–853.

Choudhury, B. J., Schmugge, T. J., Chang, A., & Newton, R. W. (1979). Effect of surface roughness on the microwave emission from soils. *Journal of Geophysical Research, 84*(C9), 5699–5706.

Entekhabi, D., Njoku, E. G., O'Neill, P. E., Kellogg, K. H., Crow, W. T., Edelstein, W. N., Entin, J. K., Goodman, S. D., Jackson, T. J., Johnson, J., et al. (2010o). The soil moisture active passive (SMAP) mission. *Proceedings of the IEEE, 98*(5), 704–716.

Entekhabi, D., Reichle, R. H., Koster, R. D., & Crow, W. T. (2010b). Performance metrics for soil moisture retrievals and application requirements. *Journal of Hydrometeorology, 11*, 832–840.

Escorihuela, M. J., Chanzy, A., Wigneron, J. -P., & Kerr, Y. (2010). Effective soil moisture sampling depth of L-band radiometry: A case study. *Remote Sensing of Environment, 114*, 995–1001.

Escorihuela, M. J., Kerr, Y., de Rosnay, P., Wigneron, J. -P., Calvet, J. -C., & Lemaître, F. (2007). A simple model of the bare soil microwave emission at L-band. *IEEE Transactions on Geoscience and Remote Sensing, 45*(7), 1978–1987.

Fernandez-Moran, R., Wigneron, J. -P., Lopez-Baeza, E., Salgado-Hernanz, P. M., Mialon, A., Miernecki, M., ... Kerr, Y. H. (2014n). Evaluating the impact of roughness in soil moisture and optical thickness retrievals over the VAS area. *Geoscience and remote sensing symposium (IGARSS), 2014 IEEE International* (pp. 1947–1950).

Grant, J. P., Wigneron, J. -P., Van de Griend, A. A., Kruszewski, A., Søbjærg, S. S., & Skou, N. (2007). A field experiment on microwave forest radiometry: L-band signal behaviour for varying conditions of surface wetness. *Remote Sensing of Environment, 109*(1), 10–19.

Jackson, T. J., et al. (1980). Profile soil moisture from space measurements. *Journal of the Irrigation and Drainage Division. American Society of Civil Engineers, 106*, 81–92.

Juglea, S., Kerr, Y. H., Mialon, A., Wigneron, J. -P., Lopez-Baeza, E., Cano, A., ... Delwart, S. (2010l). Modelling soil moisture at SMOS scale by use of a SVAT model over the Valencia anchor station. *Hydrology and Earth System Sciences, 14*, 831–846.

Kerr, Y. H., Waldteufel, P., Wigneron, J. -P., Cabot, F., Boutin, J., Escorihuela, M. J., et al. (2010,). The SMOS mission: New tool for monitoring key elements of the global water cycle. *Proceedings of the IEEE, 98*(5), 666–687.

Kerr, Y. H., Waldteufel, P., Richaume, P., Wigneron, J. -P., Ferrazzoli, P., Mahmoodi, A., ... Delwart, S. (2012l). The SMOS soil moisture retrieval algorithm. *IEEE Transactions on Geoscience and Remote Sensing, 50*(5), 1384–1403.

Kerr, Y., Waldteufel, P., Richaume, P., Wigneron, J. -P., Ferrazzoli, P., & Gurney, R. (2010). SMOS level 2 processor for soil moisture algorithm theoretical basis document (ATBD). *CESBIO, Toulouse, France, Tech. Rep. SO-TN-ESL-SM-GS-0001*.

Kurum, M. (2013). Quantifying scattering albedo in microwave emission of vegetated terrain. *Remote Sensing of Environment, 129*, 66–74.

Lawrence, H., Wigneron, J. -P., Demontoux, F., Mialon, A., & Kerr, Y. H. (2013). Evaluating the semiempirical H - Q model used to calculate the L-band emissivity of a rough bare soil. *IEEE Transactions on Geoscience and Remote Sensing, 51*(7), 4075–4084.

Mialon, A., Wigneron, J. -P., De Rosnay, P., Escorihuela, M. -J., & Kerr, Y. H. (2012). Evaluating the L-MEB model from long-term microwave measurements over a rough field, SMOSREX 2006. *IEEE Transactions on Geoscience and Remote Sensing, 50*(5), 1458–1467.

Miernecki, M., Wigneron, J. -P., Lopez-Baeza, E., Kerr, Y., De Jeu, R., De Lannoy, G. J. M., Jackson, T. J., O'Neill, P. E., Schwank, M., Fernandez-Moran, R., et al. (2014k). Comparison of SMOS and SMAP soil moisture retrieval approaches using tower-based radiometer data over a vineyard field. *Remote Sensing of Environment, 154*, 89–101.

Mironov, V., Kerr, Y., Wigneron, J. -P., Kosolapova, L., & Demontoux, F. (2013). Temperature- and texture-dependent dielectric model for moist soils at 1.4 GHz. *IEEE Geoscience and Remote Sensing Letters, 10*(3), 419–423.

Mo, T., Choudhury, B., Schmugge, T., Wang, J., & Jackson, T. (1982). A model for microwave emission from vegetation-covered fields. *Journal of Geophysical Research, 87*(C13), 11229–11237.

Njoku, E. G., & Entekhabi, D. (1996). Passive microwave remote sensing of soil moisture. *Journal of Hydrology, 184*(1), 101–129.

O'Neill, P., Chan, S., Njoku, E., Jackson, T., & Bindlish, R. (2012). Soil moisture active passive (SMAP) algorithm theoretical basis document (ATBD). SMAP level 2 & 3 soil moisture (Passive), (L2_SM_P, L3_SM_P). Initial Release, 1 http://smap.jpl.nasa.gov/files/smap2/L2&3_SM_P_InitRel_v1_filt2.pdf

Pardé, M., Wigneron, J. -P., Chanzy, A., Kerr, Y., Calvet, J. C., Waldteufel, P., ... Skou, N. (2004k). N-parameter retrievals from L-band microwave measurements over a variety of agricultural crops. *IEEE Transactions on Geoscience and Remote Sensing, 42*(6), 1168–1178.

Parrens, M., Wigneron, J. -P., Richaume, P., Kerr, Y., Wang, S., Alyaari, A., ... Grant, J. -P. (2014r). Global maps of roughness parameters from L-band SMOS observations. *Geoscience and remote sensing symposium (IGARSS), 2014 IEEE International* (pp. 4675–4678).

Patton, J., & Hornbuckle, B. (2013). Initial validation of SMOS vegetation optical thickness in Iowa. *IEEE Geoscience and Remote Sensing Letters, 10*(4), 647–651.

Rondinelli, W. J., Hornbuckle, B. K., Patton, J. C., Cosh, M. H., Walker, V. A., Carr, B. D., & Logsdon, S. D. (2015). Different rates of soil drying after rainfall are observed by the SMOS satellite and the South Fork in situ soil moisture network. *Journal of Hydrometeorology, 16*, 889–903.

Saleh, K., Wigneron, J. -P., De Rosnay, P., Calvet, J. -C., & Kerr, Y. (2006). Semi-empirical regressions at L-band applied to surface soil moisture retrievals over grass. *Remote Sensing of Environment, 101*(3), 415–426.

Schwank, M., Volksch, I., Wigneron, J. -P., Kerr, Y. H., Mialon, A., De Rosnay, P., & Matzler, C. (2010,). Comparison of two bare-soil reflectivity models and validation with L-band radiometer measurements. *IEEE Transactions on Geoscience and Remote Sensing, 48*(1), 325–337.

Schwank, M., Wiesmann, A., Werner, C., Mätzler, C., Weber, D., Murk, A., ... Wegmüller, U. (2010m). ELBARA II, an L-band radiometer system for soil moisture research. *Sensors MDPI, 10*, 584–612.

Schwank, M., Wigneron, J. -P., et al. (2012). L-band radiative properties of vine vegetation at the SMOS Cal/Val site MELBEX III. *IEEE Transactions on Geoscience and Remote Sensing, 50*(5), 1587–1601.

Ulaby, F. T., et al. (1982). *Microwave remote sensing: active and passive, radar remote sensing and surface scattering and emission theory*. Reading Mass: Addison-Wesley, 2.

Wang, J. R., & Choudhury, B. J. (1981). Remote sensing of soil moisture content over bare field at 1.4 GHz frequency. *Journal of Geophysical Research, 86*, 5277–5282.

Wang, J. R., O'Neill, P. E., Jackson, T. J., & Engman, E. T. (1983). Multifrequency measurements of the effects of soil moisture, soil texture, and surface roughness. *IEEE Transactions on Geoscience and Remote Sensing, GE-21*(1), 44–45.

Wigneron, J. -P., Calvet, J. -C., Pellarin, T., Van de Griend, A. A., Berger, M., & Ferrazzoli, P. (2003,). Retrieving near-surface soil moisture from microwave radiometric observations: current status and future plans. *Remote Sensing of Environment, 85*(4), 489–506.

Wigneron, J. -P., Chanzy, A., Calvet, J. -C., & Bruguier, N. (1995). A simple algorithm to retrieve soil moisture and vegetation biomass using passive microwave measurements over crop fields. *Remote Sensing of Environment, 51*(3), 331–341.

Wigneron, J. -P., Chanzy, A., De Rosnay, P., Rudiger, C., & Calvet, J. -C. (2008). Estimating the effective soil temperature at L-band as a function of soil properties. *IEEE Transactions on Geoscience and Remote Sensing, 46*(3), 797–807.

Wigneron, J. -P., Kerr, Y. H., Waldteufel, P., Saleh, K., Escorihuela, M. -J., Richaume, P., ... Schwank, M. (2007a). L-band microwave emission of the biosphere (L-MEB) model: description and calibration against experimental data sets over crop fields. *Remote Sensing of Environment, 107*(4), 639–655.

Wigneron, J. -P., Laguerre, L., & Kerr, Y. H. (2001). A simple parameterization of the L-band microwave emission from rough agricultural soils. *IEEE Transactions on Geoscience and Remote Sensing, 39*(8), 1697–1707.

Wigneron, J. -P., Schmugge, T., Chanzy, A., Calvet, J. -C., & Kerr, Y. H. (1998). Use of passive microwave remote sensing to monitor soil moisture. *Agronomie, 18*, 1–17.

Wigneron, J. -P., Chanzy, A., Kerr, Y. H., Lawrence, L., Shi, J. -C., Escorihuela, M. -J., ... Saleh, K. (2011). Evaluating an improved parameterization of the soil emission in L-MEB. *IEEE Transactions on Geoscience and Remote Sensing, 49*(4), 1177–1189.

Wigneron, J. -P., Schwank, M., López-Baeza, E., Kerr, Y. H., Novello, N., Millan, C., et al. (2012,). First evaluation of the simultaneous SMOS and ELBARA-II observations in the Mediterranean region. *Remote Sensing of Environment, 124*, 26–37.

Zribi, M., Gorrab, A., & Baghdadi, N. (2014). A new soil roughness parameter for the modelling of radar backscattering over bare soil. *Remote Sensing of Environment, 152*, 62–73.

ARTICLE 2: *A NEW CALIBRATION OF THE EFFECTIVE SCATTERING ALBEDO AND SOIL ROUGHNESS PARAMETERS IN THE SMOS SM RETRIEVAL ALGORITHM*

This article was published in "International Journal of Applied Earth Observation and Geoinformation" in 2017. This journal currently has an impact factor of 3.930

Int J Appl Earth Obs Geoinformation 62 (2017) 27–38

Contents lists available at ScienceDirect

Int J Appl Earth Obs Geoinformation

journal homepage: www.elsevier.com/locate/jag

A new calibration of the effective scattering albedo and soil roughness parameters in the SMOS SM retrieval algorithm

R. Fernandez-Moran[a,b,*], J.-P. Wigneron[a], G. De Lannoy[c,d], E. Lopez-Baeza[b], M. Parrens[e], A. Mialon[e], A. Mahmoodi[e], A. Al-Yaari[a], S. Bircher[e], A. Al Bitar[e], P. Richaume[e], Y. Kerr[e]

[a] INRA, UMR1391 ISPA, 33140 Villenave d'Ornon, Centre INRA Bordeaux Aquitaine, France
[b] University of Valencia, Faculty of Physics. Dept. of Earth Physics & Thermodynamics, Climatology from Satellites Group, 46100 Valencia, Spain
[c] NASA Goddard Space Flight Center, Code 610.1, Greenbelt, MD 20771, USA
[d] KU Leuven, Department of Earth and Environmental Sciences, Heverlee, B-3001, Belgium
[e] CESBIO, CNES/CNRS/IRD/UPS, UMR 5126, 18 Avenue Edouard Belin, Toulouse, France

ARTICLE INFO

Keywords:
L-band
Effective scattering albedo
Soil moisture
Soil roughness
SMOS

ABSTRACT

This study focuses on the calibration of the effective vegetation scattering albedo (ω) and surface soil roughness parameters (H_R, and N_{Rp}, p = H,V) in the Soil Moisture (SM) retrieval from L-band passive microwave observations using the L-band Microwave Emission of the Biosphere (L-MEB) model. In the current Soil Moisture and Ocean Salinity (SMOS) Level 2 (L2), v620, and Level 3 (L3), v300, SM retrieval algorithms, low vegetated areas are parameterized by ω = 0 and H_R = 0.1, whereas values of ω = 0.06 − 0.08 and H_R = 0.3 are used for forests. Several parameterizations of the vegetation and soil roughness parameters (ω, H_R and N_{Rp}, p = H,V) were tested in this study, treating SMOS SM retrievals as homogeneous over each pixel instead of retrieving SM over a representative fraction of the pixel, as implemented in the operational SMOS L2 and L3 algorithms. Globally-constant values of ω = 0.10, H_R = 0.4 and N_{Rp} = −1 (p = H,V) were found to yield SM retrievals that compared best with *in situ* SM data measured at many sites worldwide from the International Soil Moisture Network (ISMN). The calibration was repeated for collections of *in situ* sites classified in different land cover categories based on the International Geosphere-Biosphere Programme (IGBP) scheme. Depending on the IGBP land cover class, values of ω and H_R varied, respectively, in the range 0.08–0.12 and 0.1–0.5. A validation exercise based on *in situ* measurements confirmed that using either a global or an IGBP-based calibration, there was an improvement in the accuracy of the SM retrievals compared to the SMOS L3 SM product considering all statistical metrics (R = 0.61, bias = $-0.019\ m^3\ m^{-3}$, ubRMSE = $0.062\ m^3\ m^{-3}$ for the IGBP-based calibration; against R = 0.54, bias = $-0.034\ m^3\ m^{-3}$ and ubRMSE = $0.070\ m^3\ m^{-3}$ for the SMOS L3 SM product). This result is a key step in the calibration of the roughness and vegetation parameters in the operational SMOS retrieval algorithm. The approach presented here is the core of a new forthcoming SMOS optimized SM product.

1. Introduction

L-band (1.1–2 GHz) microwave radiometry is one of the main remote sensing techniques to monitor Soil Moisture (SM) worldwide, a key element of the global water cycle. SM is a physical parameter of interest for many hydrological applications (Brocca et al., 2010), weather and climate predictions (de Rosnay et al., 2013), agricultural applications (Guérif and Duke, 2000) and early warning of natural hazards.

SM in the first centimeters of the soil surface (~0–3cm) is strongly related to the measurements of the emitted Brightness Temperature (TB) at L-band (Escorihuela et al., 2010; Njoku and Kong, 1977). However, other parameters must be accounted for in order to produce accurate estimates of SM, such as soil and canopy temperatures, soil roughness, texture and the vegetation optical depth and effective scattering albedo (Wigneron et al., 2017). Currently, the SMOS Soil Moisture and Ocean Salinity (SMOS) mission from European Space Agency (ESA), launched in November 2009 (Kerr et al., 2012), and the Soil Moisture Active Passive (SMAP) mission from National Aeronautics and Space Administration (NASA), launched in January 2015 (Entekhabi et al., 2010a), provide global maps of soil moisture and vegetation optical depth τ_{NAD} (only operational in the case of SMOS for this latter). The vegetation optical depth is related to vegetation features such as water content and vegetation structure (Grant et al.,

* Corresponding author.
E-mail addresses: roberto.fernandez-moran@inra.fr, roberfm@gmail.com (R. Fernandez-Moran).

http://dx.doi.org/10.1016/j.jag.2017.05.013
Received 16 March 2017; Received in revised form 22 May 2017; Accepted 24 May 2017

2016).

SMOS uses an interferometric L-band radiometer which measures brightness temperature at different angles whereas SMAP was originally conceived to combine the radiometer (passive) information at a constant incidence angle with radar (active) information to improve spatial resolution (the radar stopped working on July 7, 2016). These continuous measurements improve our knowledge of the soil-water processes which link water, energy and carbon cycles over land in order to advance in the prediction of droughts, flooding and climate forecasts (Entekhabi et al., 2014).

The L-band Microwave Emission of the Biosphere (L-MEB) model is the core of the SMOS level 2 retrieval algorithm (Kerr et al., 2012). In this algorithm, the radiative transfer model (Mo et al., 1982) parameters related to soil roughness and some vegetation parameters (Wigneron et al., 2007, 2008; Grant et al., 2007) are considered to be time independent and their values are computed based on a land cover map (ECOCLIMAP, Masson et al., 2003). Likewise, the SMAP algorithm is based on the land use classification scheme of the International Geosphere-Biosphere Programme (IGBP), which is composed of 17 classes. In this algorithm, the vegetation optical depth is estimated through the vegetation water content (VWC, kg/m^2), calculated using both the Normalized Vegetation Difference Index (NDVI) and values from a look-up table based on the IGBP classification (O'Neill et al., 2012).

The first objective of this study was to investigate the impact of the effective scattering albedo, ω, on the soil moisture retrieval accuracy. The effective scattering albedo ω accounts for absorption and scattering effects within the vegetation canopy (Kurum, 2013a,b). The value of ω is currently assumed to be zero over low vegetation canopies (non-forested biomes) in the SMOS level 2 (L2) and level 3 (L3) algorithms and 0.06–0.08 over forests (Kerr et al., 2012). However, the value of ω assigned to low vegetation was based on the analysis of tower-based L-band radiometric measurements (Wigneron et al., 2007) limited to a few specific agricultural sites and it may not be accurate for all canopy types and for measurements made by space-borne sensors such as SMOS and SMAP (Kurum, 2013a,b; Konings et al., 2016; Wigneron et al., 2004). Few studies can be found in the literature investigating ω at a global scale. The study of Konings et al. (2016) provides values of ω = 0.02–0.04 over low vegetation and 0.03–0.06 over forested areas. On the other hand, Van der Schalie et al. (2016) applied the Land Parameter Retrieval Model (LPRM) on SMOS observations against modelled SM from MERRA-Land (MERRA) and ERA-Interim/Land (ERA) and found a value of ω = 0.12 globally. In the SMAP L2 algorithm, the values of ω are based on the vegetation type (O'Neill et al., 2012). Additionally, the SMAP level 4 product provides globally variable estimates of the effective scattering albedo (and all other parameters) (Reichle et al., 2016; de Lannoy et al., 2013).

The second objective of this study was to investigate the effects of the soil roughness parameters on SM retrievals. Presently, the modelling of the roughness effects in the level 2 SMOS retrieval algorithm is based on four parameters (H_R, Q_R, N_{RH} and N_{RV}) (Wigneron et al., 2007). The parameter H_R accounts for the decrease in the soil reflectivity due to soil roughness effects, Q_r accounts for polarization mixing effects, and N_{Rp} (p = H,V) accounts for the angular dependence of reflectivity. Some studies have been done over specific vegetation types. For instance, Wigneron et al. (2007) found values of H_R = 0.1–0.2 for soybean and wheat crops and ~ 0.7 for corn fields. Over Spain, Cano et al. (2010) estimated that H_R ~ 0.35 over Mediterranean vegetation. Regarding the Q_R parameter, Lawrence et al. (2013) found that Q_R = 0 is a reasonable value for cases where roughness conditions are not extreme. As for the parameters N_{RH} and N_{RV}, Escorihuela et al. (2007) and Lawrence et al. (2013) proposed a difference of $N_{RH} - N_{RV}$ ~ 2 for smooth surfaces and (~1–1.5) for rough soils. In the SMOS L2 and L3 SM retrieval algorithm, Q_R is fixed globally to 0, while N_{RH} and N_{RV} are set to 2 and 0 respectively. The value of H_R is defined based on the ECOCLIMAP classification schema, with H_R = 0.3 for forests and H_R = 0.1 for the rest of the cover types (Kerr et al., 2012). In the SMAP L2 SM algorithm, N_{Rp} (p = H,V) is considered to be equal to 2 and the value of H_R is provided based on the IGBP classes (Entekhabi et al., 2014). Some studies have suggested the possibility of combining soil roughness and vegetation contributions as a single parameter in the retrieval algorithm (Fernandez-Moran et al., 2015; Parrens et al., 2016; Parrens et al., 2017), due to the existing relationship between the two contributions (Patton and Hornbuckle, 2013). This is done by setting the value of the N_{Rp} (p = H,V) parameter equal to −1 at both polarizations and by considering that the effective scattering albedo ω is equal to 0.

To achieve the above-mentioned objectives, we investigated the calibration of the vegetation and soil roughness parameters (ω, H_R, N_{RH} and N_{RV}) based on SMOS SM retrievals. To simplify the retrieval process, the SMOS pixels were assumed to correspond to homogeneous surfaces over land as suggested by Wigneron et al. (2012), contrary to the currently operational SMOS L2 and L3 SM retrieval algorithms which use auxiliary data sets to characterize the pixel heterogeneity. The simplicity of the assumption of "homogeneous surface" allows to produce fast retrievals in order to perform very intensive and time consuming calibration processes as the one presented here.

In this study, retrieved values of SMOS SM were compared with *in situ* SM data measured at several sites worldwide available from the International Soil Moisture Network (ISMN) representing various land cover and soil types. The calibration was done by finding the values of the vegetation and soil roughness parameters which minimize the difference between the retrieved SM values and the *in situ* ISMN data, considering the following metrics: correlation (R), bias, root mean square error (RMSE) and unbiased RMSE (ubRMSE). We evaluated if the parameter calibration we computed changed depending on the degree of heterogeneity of the pixel.

In Section 2, the *in situ* data used in the study is presented along with the method which was followed for the calibration and the validation process. The Section 2.1 includes a description of the SMOS TB, soil temperature and soil texture data, as inputs required to run the L-MEB model. A description of the level 3 SMOS SM product, the IGBP classification and the *in situ* sites used for calibration is also covered in this section. The Section 2.2 describes the L-MEB model, SM retrievals and addresses the calibration and performance analysis steps. The results presented in Section 3 are divided in three subsections: calibration step of N_{RH} and N_{RV} (3.1), calibration step of ω and H_R (3.2) and analysis (3.3). Discussion and conclusions are given in Section 4.

2. Available data and applied methodology

In order to synthesize the content of this section, Fig. 1 shows a flow chart that helps the reader to follow the use of the data described in Sections 2.1.1 to 2.1.4 and the methodology, as explained in Sections 2.2.1 to 2.2.4.

2.1. Data

2.1.1. SMOS data

The main inputs of the L-MEB model inversion are the multi-angular dual-polarization SMOS TB observations. The SMOS L3 TB (Version 310) product which is produced by the Centre Aval de Traitement des Données (CATDS) was chosen in this study. The resolution of this product is 25 km and uses the Equal-Area Scalable Earth (EASE) grid 2.0 (Armstrong et al., 1997) whereas the resolution of the SMOS radiometer corresponds to a 43-km footprint on average (Kerr et al., 2012). TB is expressed at the top of the atmosphere (at H and V polarizations) and at predefined incidence angles, θ, from 2.5 to 62.5° (in 5° steps). Each TB at an incidence angle, θ, is estimated from a bin of SMOS TB observations at θ ± 2.5°; the standard deviation of those TB observations is given in the SMOS L3 TB product. The availability of the TB data at different angles depends on the day and the location, taking

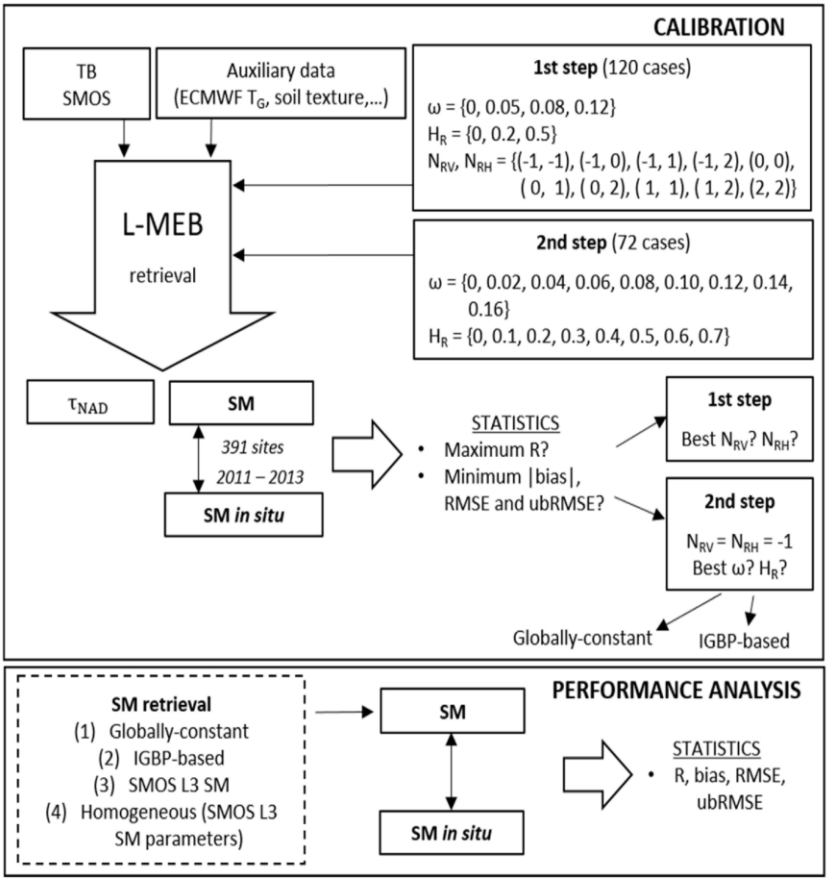

Fig. 1. Methodology flow chart.

into account the globe is fully imaged twice every three days. SMOS has a sun-synchronous orbit with a 06:00 LST ascending equator crossing time and 18:00 LST descending equator crossing time.

In this study, for each location and time (only ascending overpasses were used), the retrievals were performed only if the range of available incidence angles was larger than 10° (the retrieval error in SM decreases as the incidence angle range broadens: Wigneron et al., 2000), i.e. at least there was a difference of 10° between the largest and the smallest angle for each angle bin. Also, observations at incidence angles lower than 20° and larger than 55° were discarded as the former correspond to TB measurements of less quality outside of the optimal SMOS alias free field of view (Waldteufel et al., 2011) and the latter correspond to very large Earth antenna footprint (larger than 90 km × 50 km −3 dB ellipses) (Kerr et al., 2016). Although SMOS operates in a protected band, some regions around the world are strongly affected by Radio Frequency Interferences (RFI). This contamination could be due to several sources such as radars, radio transmitters, TV communications, wireless cameras or even other satellites (Oliva et al., 2012). In order to limit the impact of RFI effects and to improve the quality of the TB data which were selected for the SM retrievals, $TB_p(\theta)$ was filtered out when its standard deviation (given in the L3 TB SMOS product) exceeded radiometric accuracy by 5 K.

In this study, we also used the level 3 SMOS SM daily product (reprocessed R04, v300) for the performance analysis (Section 2.2.4). This product is processed by the CATDS and uses the EASE grid 2.0 with a spatial resolution of 25 km. The data quality index (DQX) present in this product estimates the retrieval quality; a maximum value of 0.06 $m^3 m^{-3}$ was established as an upper threshold (Al-Yaari et al., 2014a,b). In parallel, the RFI probability flag was used to filter out SM data contaminated by RFI. SM retrievals with an associated RFI probability higher than 10% were removed. Additionally, SM values below 0 and over 0.6 $m^3 m^{-3}$ (Dorigo et al., 2013) were filtered out.

In the operational SMOS L3 SM retrieval algorithm (similar to SMOS L2) (see Section 2.2.2), the total TB (TB_{total}) is simulated as the sum of several fractions contribution (F_{NO}: nominal, F_{FO}: forest, and others as urban, water, *etc.*), i.e. $TB_{TOTAL} = TB_{FNO} + TB_{FFO} + TB_{OTHERS}$. The FNO is a non-forest fraction where the retrieval can be done (bare soil, low vegetation, …). With the exception of some specific cases in which the SM retrieval is attempted over F_{FFO}, TB_{FFO} is computed from the SM value over the 0–7 cm layer coming from the ECMWF model to serve as auxiliary input to the retrieval over the nominal fraction FNO.

2.1.2. *ECMWF soil temperature and soil texture*

Soil temperatures were provided by the European Centre for Medium-range Weather Forecasting (ECMWF) for levels 1 (0–7 cm depth) and 3 (28–100 cm). It is based on the ERA-Interim dataset, which uses a numerical weather prediction (NWP) system (IFS − Cy31r2) to produce reanalyzed data (Berrisford et al., 2011). These data were reprocessed afterwards by the SMOS L3 preprocessor and provided on the EASE grid 2.0. Data from frozen soils were discarded, using the ECMWF level 1 surface temperatures as a threshold ($T < 275.3$ K). The effective soil temperature was computed from

the surface (level 1) and deep temperature (level 3) following the parameterization of Wigneron et al. (2001).

In the L-MEB model, the soil permittivity (ε) computation using the model by Mironov et al. (2013) requires the soil clay content at global scale; the latter information was obtained from a map provided on the EASE 2.0 grid computed from the Food and Agriculture Organization map (FAO, 1988), the same as the one used in the SMOS L3 algorithm (Al Bitar et al., 2017).

2.1.3. In situ data

In order to calibrate the effective scattering albedo and the soil roughness parameters over different cover types, the maximum number of *in situ* sites with a sufficiently long time series of soil moisture data was selected. Following this criteria, different sites were selected from the International Soil Moisture Network (ISMN) (Dorigo et al., 2011): Soil Climate Analysis Network (SCAN) in North America (Schaefer et al., 2007), Soil Moisture Observing System – Meteorological Automatic Network Integrated Application (SMOSMANIA) in the South of France (Calvet et al., 2007), African Monsoon Multidisciplinary Analysis (AMMA) in West Africa (Lebel et al., 2009), Valencia Anchor Station (VAS) in Spain (Wigneron et al., 2012), Red de Estaciones de Medición de la Humedad del Suelo (REMEDHUS) in Spain, (Leng et al., 2016), DAHRA in Senegal (Olsen et al., 2013), Atmospheric Radiation Measurement (ARM) in Central USA (Jin and Mullens, 2014), Plate Boundary Observatory (PBO_H2O) in North and Central America (Larson et al., 2008), SNOpack TELemetry (SNOTEL) in West USA, including Alaska (Serreze et al., 2001), The U.S. Climate Reference Network (USCRN) in the USA (Coopersmith et al., 2015), OzNet in Australia (Rüdiger et al., 2010) and four watersheds in the USA (Little Washita in Oklahoma, Little River in Georgia, Walnut Gulch in Arizona and Reynolds Creek in Idaho) (Jackson et al., 2012).

A total of 1001 *in situ* stations providing the volumetric soil moisture ($m^3\,m^{-3}$) of the top 0–5 cm soil layer were considered. The period of analysis was three years (2011–2013). For the global analysis of the statistical records, *in situ* stations with low quality data were discarded. For this purpose, we computed the p-value associated with the comparison of the SM retrievals and the *in situ* measurements. We accounted only for the stations fulfilling the condition p-value < 0.05 and $R > 0.3$ (for at least one of the cases of analysis) and for which the number of data available $N > 50$ (Al-Yaari et al., 2016). To ensure a proper inter-comparison, we used strictly the same number of data (namely the same dates) for all the retrieval configurations which were evaluated in terms of input values of effective scattering albedo and roughness parameters. Fig. 2 shows the locations of all stations: the *in situ* stations used for the calibration and performance analysis steps, and those discarded (as described in the following sections).

2.1.4. IGBP

The IGBP land cover classification scheme was developed during a series of meetings of the IGBP Land Cover Working Group in 1995 (Belward, 1996). The IGBP schema considers 17 different cover types. In this study, we used the 0.5 km Moderate-Resolution Imaging Spectroradiometer (MODIS)-based Global Land Cover Climatology map. It is based on 10 years (2001–2010) of the MODIS MCD12Q1 product, which contains land cover information. The map is generated by choosing, for each pixel, the land cover classification with the highest overall confidence from 2001 to 2010, as described in Broxton et al., 2014. This data has been re-gridded from the MODIS sinusoidal 0.5 km grid to a regular latitude-longitude grid (corresponding to a spatial resolution of 15 arc seconds. All IGBP pixels (0.5 km grid) contained in each SMOS L3 pixel (EASE 2.0 grid) were accounted for in order to calculate its composition, i.e. the percentage of each IGBP class within the SMOS L3 pixels.

2.2. Methodology

2.2.1. L-MEB model

Retrievals of SM from SMOS L-band measurements are based on the inversion of the L-MEB model. This model has been progressively refined and improved (Wigneron et al., 2017) and it is based on the zero-order τ-ω radiative transfer model (Mo et al., 1982). The latter simulates the thermal emission of a vegetated soil. The soil microwave emission expressed in terms of brightness temperature (TB_{Gp}, p = V, H) can be written as a function of the ground emissivity (e_{Gp}, p = H, V) and the effective soil temperature (T_G) as (Ulaby et al., 1981 & 1986):

$$TB_{Gp}(\theta) = e_{Gp}(\theta)\cdot T_G \quad (1)$$

The soil emissivity (e_{Gp}) at the observation angle θ can be computed from the corresponding soil reflectivity (r_{Gp}):

$$e_{Gp}(\theta) = 1 - r_{Gp}(\theta) \quad (2)$$

To model soil roughness effects, a semi-empirical approach was developed originally by Wang and Choudhury (1981) and modified to include the N_{RH} and N_{RV} parameters (Escorihuela et al., 2007;

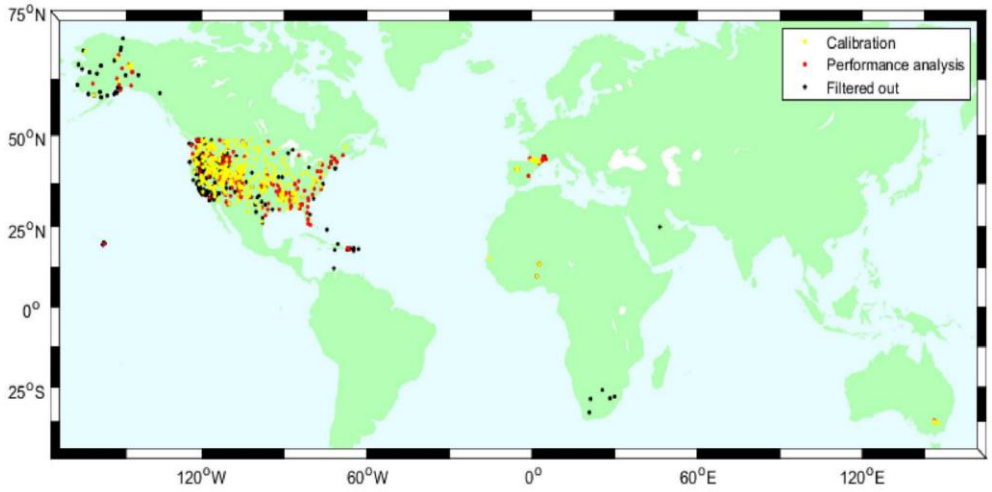

Fig. 2. *In situ* sites used for calibration (391), performance analysis (279, excluding the calibration sites) and filtered out (331).

Wigneron et al., 2007). The p-polarized soil reflectivity, r_{Gp} is given by:

$$r_{Gp}(\theta) = r'_{Gp}(\theta)\exp\left[-H_R\cos^{N_{Rp}}(\theta)\right] \quad (3)$$

where

$$r'_{GH}(\theta) = [1 - Q_R(\theta)]r^*_{GH}(\theta) + Q_R(\theta)r^*_{GV}(\theta) \quad (4)$$

$$r'_{GV}(\theta) = [1 - Q_R(\theta)]r^*_{GV}(\theta) + Q_R(\theta)r^*_{GH}(\theta) \quad (5)$$

where r'_{Gp} depends on the smooth surface reflectivity r^*_{Gp} (p = H, V), i.e. the reflectivity of a plane (specular) surface (Eqs. (4) and (5)). The latter can be computed from the Fresnel equations as a function of θ and soil permittivity (ε). The latter was computed as a function of SM, soil effective temperature (T_G), and soil texture in terms of clay fraction from the dielectric model of Mironov et al. (2013). This model is based on the Generalized Refractive Mixing Dielectric Model (GRMDM) and accounts for the measured dielectric spectra of moist soil samples for a given texture and temperature (Wigneron et al., 2017).

The semi-empirical roughness model includes four roughness parameters Q_R, H_R and N_{Rp} (p = H, V) (Wigneron et al., 2007). The parameter H_R accounts for the decrease of the specular reflectivity r^*_{Gp} (p = H, V) due to soil roughness effects, Q_r accounts for polarization mixing effects, and N_{Rp} (p = H, V) accounts for the change in the angular dependence of reflectivity caused by a rough surface.

From a large data set based on both experimental measurements and simulations, Lawrence et al. (2013) found that setting $Q_R = 0$ led to a simplified model with good performance in terms of both TB modelling and SM retrievals. The assumption of $Q_R = 0$ was made here, in line with SMOS L2 and L3 (Kerr et al., 2012; Al Bitar et al., 2017), SMAP (O'Neill et al., 2012) and LPRM (Van der Schalie et al., 2015) SM retrieval algorithms.

Using the τ-ω model, the emission of a soil covered with vegetation can be calculated for each polarization as a sum of: (i) the direct upwelling vegetation emission; (ii) the upwelling soil emission attenuated by canopy; (iii) the downwelling vegetation emission reflected by soil and attenuated again by the canopy layer:

$$TB_p(\theta) = (1 - \omega_p)[1 - \gamma_p(\theta)][1 + \gamma_p(\theta)r_{Gp}(\theta)]T_C + [1 - r_{Gp}(\theta)]\gamma_p(\theta)T_G \quad (6)$$

where T_G and T_C are the soil and vegetation effective temperatures, γ_p is the vegetation attenuation factor (also referred as vegetation transmissivity) and ω_P (p = H, V) is the effective scattering albedo (Kurum, 2013a,b). The latter is generally considered to be close to zero over low vegetation covers (Wigneron et al., 2007; Kurum, 2013a,b), while it is considered to be 0.08 for boreal forests and slightly lower for tropical forests (Rahmoune et al., 2013). In the following, ω_P is referred to as ω since we did not consider the dependence of the effective scattering albedo on polarization, as done in the SMOS L2 and L3, SMAP and LPRM algorithms.

According to Beer's law, the vegetation attenuation factor γ_p is related to τ_p as:

$$\gamma_p = \exp[-\tau_p/\cos(\theta)] \quad (7)$$

where the vegetation optical depth (τ_p) at observation angles $\theta > 0$ and polarization p = H, V is expressed as a function of the vegetation optical depth at nadir τ_{NAD} ($\theta = 0$):

$$\tau_p(\theta) = \tau_{NAD}[\sin^2(\theta)tt_p + \cos^2(\theta)] \quad (8)$$

where tt_V and tt_H quantify the dependence of τ_p on the incidence angle θ. The value $tt_H = tt_V = 1$ corresponds to the isotropic case for Vertical and Horizontal polarizations, where $\tau_H(\theta) = \tau_V(\theta) = \tau_{NAD}$. This assumption was made in this study, according to the SMOS L2 and L3 SM retrieval algorithm (Kerr et al., 2006).

2.2.2. SM retrieval

The retrieval of soil moisture relies on the inversion of the L-MEB model. The process involves the minimization of the following cost function (9), which accounts for all incidence angles between 20 and 55° and both polarizations (H and V):

$$x = \frac{\Sigma_{i=1}^{N}(TB_p(\theta)_{mes} - TB_p(\theta))^2}{\sigma(TB_p(\theta))^2} + \Sigma_{i=1}^{2}\frac{(P_i^{ini} - P_i)^2}{\sigma(P_i)^2} \quad (9)$$

where N is the number of observations for different viewing angles (θ), $TB_p(\theta)_{mes}$ is the measured value over the *in situ* sites (SMOS L3 pixels), $\sigma(TB_p(\theta))$ is the standard deviation associated with the brightness temperature measurements (taken from the SMOS L3 SM product), $TB_p(\theta)$ is the brightness temperature calculated using Eq. (6), P_i (i = 1, 2) is the value of the retrieved parameter (2-P parameter retrieval in this study, SM, τ_{NAD}); P_i^{ini} (i = 1, 2) is the initial value of each parameter in the retrieval process and corresponds to an a priori estimate of the parameter P_i; and $\sigma(P_i)$ is the standard deviation associated with this estimate. An initial value of 0.2 $m^3 m^{-3}$ was selected for SM and σ(SM), while it was equal to 0.5 for τ_{NAD} and 1 for $\sigma(\tau_{NAD})$.

Taking into account that retrievals were only considered at SMOS ascending orbit (around 6 am LST), a thermal equilibrium for the soil-vegetation layers can be assumed (Jackson, 1980; Wigneron et al., 2007). The atmospheric contribution was neglected in this study.

2.2.3. Calibration

The calibration process consists of two main steps and was carried out over three years of SMOS data (2011–2013). In the first step, our focus was on the calibration of the N_{Rp} (p = H, V) parameter. In the second one, it was on the calibration of the effective scattering albedo (ω) and the soil roughness parameter (H_R), using the value of N_{Rp} (p = H, V) which was previously calibrated.

In the first step, the SM retrievals were carried out over the calibration sites using a range of values of ω, H_R and N_{Rp} (p = H, V) as follows:

- ω = {0, 0.05, 0.08, 0.12}
- H_R = {0, 0.2, 0.5}
- N_{RV}, N_{RH} = {(-1, −1), (-1, 0), (-1, 1), (-1, 2), (0, 0), (0, 1), (0, 2), (1, 1), (1, 2), (2, 2)}

The range of values selected here correspond to common values of the model parameters used at L-band in the literature (Fernandez-Moran et al., 2015; Miernecki et al., 2014; Rahmoune et al., 2013; Wigneron et al., 2007; Escorihuela et al., 2007). The combination of inputs led to 120 (= 4 × 3 × 10) cases of analysis. Different statistical performance criteria were then computed: correlation coefficient (R), root mean square error (RMSE), bias and the unbiased root mean square error (ubRMSE), derived from the comparison between the retrieved soil moisture and the *in situ* SM measurements. As the focus in the first step was on the N_{Rp} (p = H, V) parameter, only a few values of ω and H_R were considered. Taking into account that the sampling depth of the *in situ* measurements (5 cm) does not correspond well to the estimated sampling depth of SM at L-band (~3 cm) (Escorihuela et al., 2010; Njoku and Kong, 1977), bias was considered as the less important metric in the calibration process (and RMSE by extension, due to its bias inclusion).

In the second step, the best N_{Rp} (p = H, V) estimate obtained from the first step was withheld and a new analysis was done considering the following values of ω and H_R (72 cases in total):

- ω = {0, 0.02, 0.04, 0.06, 0.08, 0.10, 0.12, 0.14, 0.16}
- H_R = {0, 0.1, 0.2, 0.3, 0.4, 0.5, 0.6, 0.7}

Each *in situ* site was classified according to the IGBP schema (see number of *in situ* stations for each class in Table 1). Only "representative" *in situ* stations of the SMOS L3 pixels to which they belong were selected. For that purpose, a filtering was applied according to the

Table 1
Total and filtered number of *in situ* stations used for calibration according to IGBP classes.

Class	Number of *in situ* stations	Number of "representative" stations for calibration
0 – Water	4	0
1 – Evergreen needle leaf forest	122	41
2 – Evergreen broadleaf forest	9	0
3 – Deciduous needle leaf forest	0	0
4 – Deciduous broadleaf forest	12	4
5 – Mixed forests	27	1
6 – Closed shrublands	2	0
7 – Open shrublands	100	25
8 – Woody savannas	59	16
9 – Savannas	4	1
10 – Grasslands	419	214
11 – Permanent wetland	7	0
12 – Croplands	119	63
13 – Urban and built-up	16	0
14 – Cropland/Natural Vegetation Mosaic	91	23
15 – Snow and ice	0	0
16 – Barren and sparsely vegetated	10	3
TOTAL	**1001**	**391**

following criteria:

- The IGBP class of the *in situ* station was the same as the predominant class of the L3 pixel (EASE 2.0 grid, 25 km to which it belongs).
- The predominant class covered at least 50% of the L3 pixel.
- The sum of the surface fraction of water, permanent wetland, urban and snow/ice classes represented less than 10% of the L3 pixel.

Table 1 shows the number of calibration candidate sites after applying the selection of "representative" stations.

Once the selection of "representative" stations was made, two calibrations were proposed: (1) globally-constant values of H_R, ω and N_{Rp} (p = H, V) across all *in situ* stations (2) specific values of H_R, ω and N_{Rp} (p = H, V) for each IGBP class (hereinafter "IGBP-based" calibration). Due to the lack of "representative" stations for some IGBP classes, the estimated parameters in those underrepresented classes were assigned the globally-constant values. Conversely, specific values were found for the following classes: evergreen needle leaf forest, open shrublands, woody savannas, grasslands, croplands, cropland/natural vegetation mosaic, and barren or sparsely vegetated.

2.2.4. Performance analysis

In the validation process, the SM retrievals obtained from the following four different approaches were compared to the *in situ* SM data: (1) a homogeneous retrieval using the globally-constant inputs (H_R, ω, N_{RH} and N_{RV}) obtained in the calibration phase, (2) the same as (1) where the values of the soil and vegetation parameters (H_R, ω, N_{RH} and N_{RV}) were estimated as a function of the IGBP land use class, (3) the SMOS L3 SM daily product (namely the official SMOS SM product available from the CATDS center) and (4) a homogeneous retrieval using the model parameter (H_R, ω, N_{RH} and N_{RV}) used in the SMOS L3 algorithm. For Cases (2) and (4), over a single pixel, each parameter P (H_R, ω, N_{RH} and N_{RV}) was weighted according to the percentage of each IGBP class as:

$$P = \sum P_i \cdot \frac{\%i}{100} \tag{10}$$

where P_i is the calibrated value of the parameter P for the class i and $\%_i$ is the percentage of the class i present within the SMOS L3 pixel.

After the filtering of *in situ* sites presented in Section 3, the analysis process was firstly performed over all the stations (670) and secondly over all sites excluding those employed in the calibration steps (279). Concerning data filtering, the same procedure as that described in the calibration Section 2.2.3 was applied. Additionally, the post filtering consisted of: (1) removing SM values out of the 0–0.6 $m^3\,m^{-3}$ range and (2) a quality control based on the RMSE value between the L3 TB SMOS and the L-MEB modelled TB (retrievals where RMSE was above 12 K were discarded as proposed in Wigneron et al. (2012)).

3. Results and discussion

3.1. Calibration of N_{Rp}

This section presents the results from the first step of the calibration process which focused on the calibration of the N_{Rp} (p = H, V)

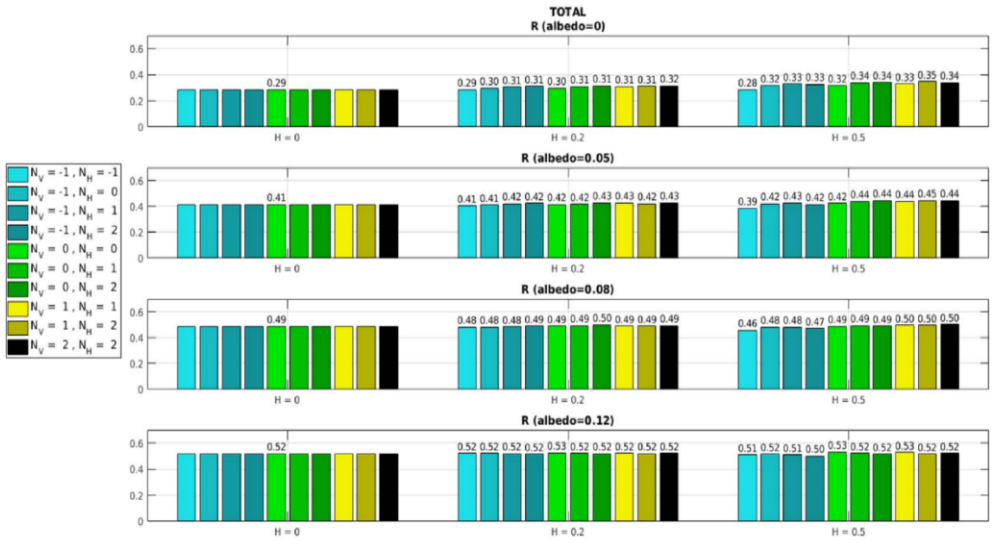

Fig. 3. Median correlation (all calibration sites: 391 stations) between *in situ* and retrieved SM for each H_R, ω and N_{Rp} (p = H, V) case.

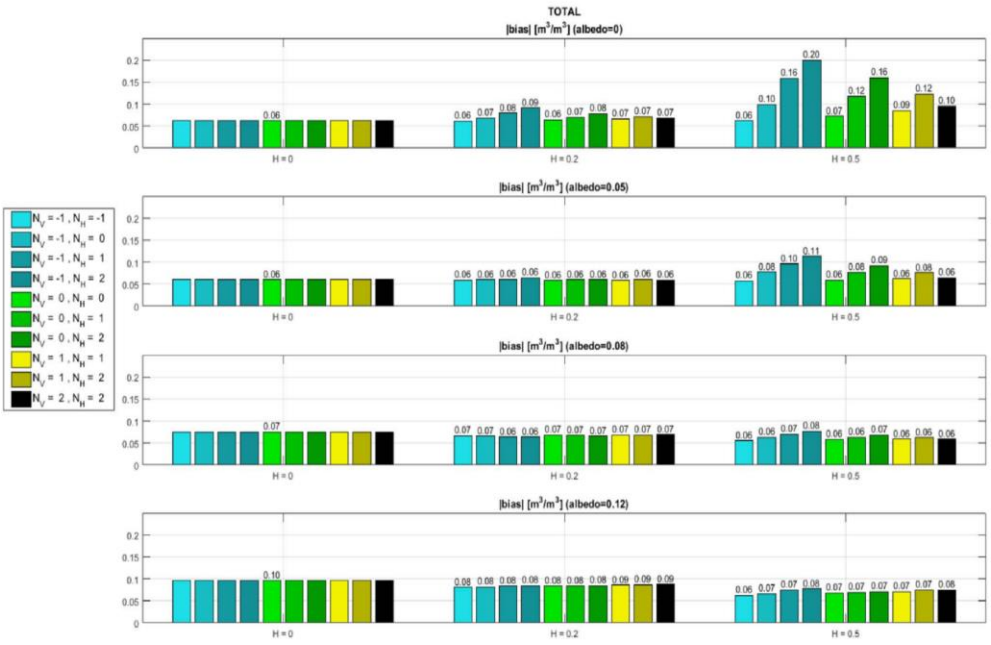

Fig. 4. Median absolute bias (all calibration sites: 391 stations) between *in situ* and retrieved SM for each H_R, ω and N_{Rp} (p = H, V) case.

parameter globally, as the behavior of this parameter was found to be rather similar across all IGBP classes. All results were obtained through a direct comparison between retrievals over rather homogeneous pixels and *in situ* measurements. Fig. 3 shows the median correlation values (R) for each retrieval case (considering 120 combinations of ω, H_R, N_{RH} and N_{RV} parameters). Values range from R = 0.28 (for the case ω = 0) to R = 0.53 (for the case ω = 0.12), highlighting the strong influence of effective scattering albedo on this metric. Conversely, for a given value of ω, changes in the values of H_R and N_{Rp} (p = H, V) do not lead to significant changes in the median value of R. Note that for H_R = 0, N_{Rp} has no influence on the retrievals, so all R values are the same.

In parallel to the correlation analysis, the absolute value of bias (|bias|) is shown in Fig. 4. The worst case (|bias| = 0.20) was found for ω = 0, H_R = 0.5, N_{RV} = −1 and N_{RH} = 2. The soil roughness parameter's impact on the absolute values of bias can be clearly noted, especially for the lowest albedo value (ω = 0). An increase in ω leads to higher |bias| values when H_R is set equal to zero. The best case (|bias| = 0.06) was found for several H_R and ω scenarios, namely: H_R = 0, ω = 0; H_R = 0, ω = 0.05; H_R = 0.5, N_{Rp} = −1 (p = H, V) and other cases in which there is a dependency of ω on the three parameters (ω, H_R and N_{Rp}, p = H, V). Furthermore, we can note the low impact of N_{Rp} (p = H, V) on |bias| when ω = 0.08–0.12. In any case, N_{Rp} = −1 (p = H, V) was the best choice to obtain the lowest |bias| values.

Fig. 5 shows, similarly to Figs. 3 and 4, the SM retrievals analysis in terms of unbiased root mean square error (ubRMSE). The ubRMSE and the bias together cover the information in the root mean square error (RMSE, Entekhabi et al., 2010b). Increasing values of ω yields lower ubRMSE values (from 0.11 − 0.18 for ω = 0 to 0.07 − 0.11 for ω = 0.12). Conversely, larger H_R tend to increase ubRMSE values and lead to larger differences between the different N_{Rp} (p = H, V) parameterizations. This effect becomes less remarkable as ω increases. As it was found for |bias|, N_{Rp} = −1 (p = H, V) generally leads to the lowest ubRMSE values for any given values of ω and H_R.

3.2. Calibration of ω and H_R

This section presents the second part of the calibration process. In the previous step it was shown that there was a low impact of N_{Rp} (p = H, V) on the correlation values between the retrieved and measured SM values for high values of ω.

Furthermore, it was found that the values of |bias| and ubRMSE between the retrieved and measured SM values were generally lower when N_{Rp} = −1 (p = H, V). Considering this result, hereinafter, N_{Rp} = −1 (p = H, V) was selected to be used in the second step of the calibration process, which consists in the calibration of the H_R and ω parameters (the subscript "p" for the N_{Rp} parameter will be dropped in the following). Two calibration approaches were evaluated in this study for the SM retrieval process: (i) a so-called "globally-constant" calibration, in which case globally-constant values of H_R, ω and N_R were estimated, and (ii) a so-called "IGBP-based" calibration, in which case values of H_R, ω and N_R were estimated for different land cover classes, tabulated by the IGBP classification scheme.

3.2.1. Globally-constant calibration

Fig. 6 shows the median metrics based on four criteria (R, bias, RMSE and ubRMSE) obtained through a direct comparison between the *in situ* SM measurements and SM retrievals over the calibration sites contained in rather homogeneous pixels. According to correlation results, the increase in ω leads to an increase in the values of R, whereas the effect of H_R on results is rather low. On the other hand, the bias values are clearly influenced by the values of both H_R and ω. For the case H_R = 0, increasing ω values from 0 to 0.16 leads to a significant decrease in bias values, from ~0 to $-0.11\,m^3\,m^{-3}$. A negative value of bias leads to an underestimation in the retrieved soil moisture as compared to the *in situ* measurements. Increasing the value of ω or decreasing the value of H_R leads to "dry" SM retrievals. To make an optimal choice in terms of bias reduction, a compromise has to be found between both values of H_R and ω. Regarding RMSE, an increase in both ω and H_R leads to decreasing errors. Regarding ubRMSE, it was observed that increasing ω and decreasing H_R tends to minimize this

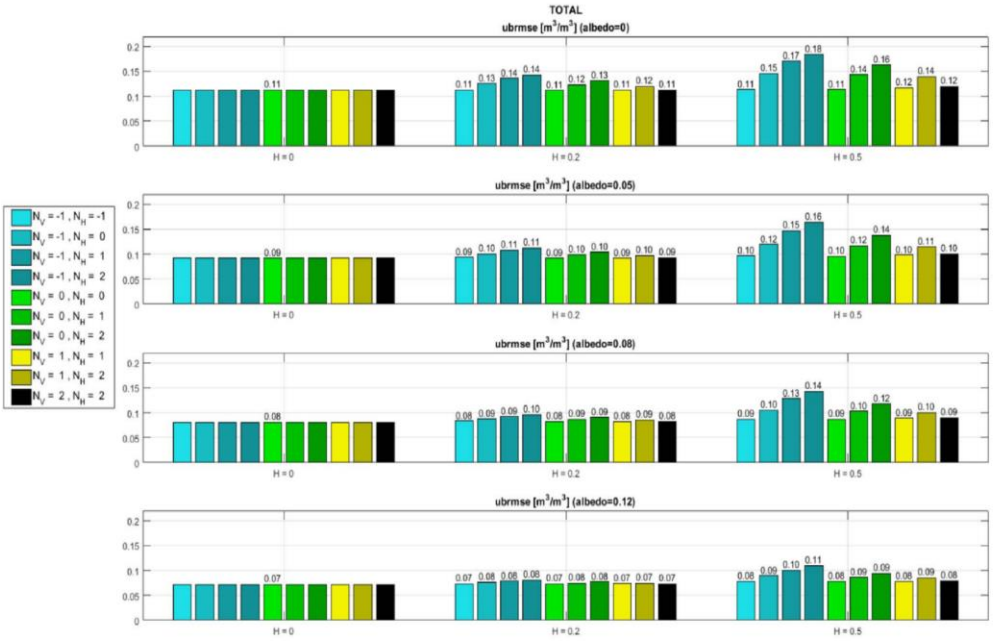

Fig. 5. Median ubRMSE (all calibration sites: 391 stations) between *in situ* and retrieved SM for each H_R, ω and N_{Rp} (p = H, V) case.

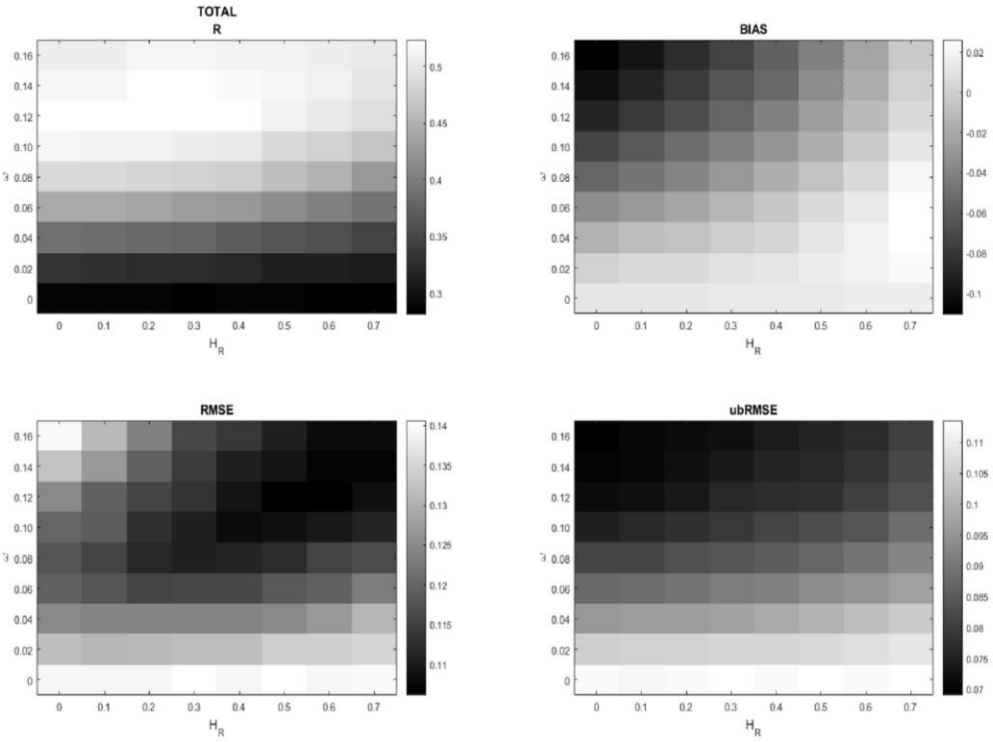

Fig. 6. Median R, bias, RMSE and ubRMSE (all calibration sites: 391 stations) between *in situ* and retrieved SM for each H_R and ω case ($N_R = -1$).

Table 2
Calibration of H_R and ω as a function of the vegetation IGBP classes ("IGBP-based" values).

IGBP Class	Number of filtered stations	ω	ω (SMAP L4)	H_R	H_R Parrens et al. (2017)
Evergreen needle leaf forest	41	0.10	0.12	0.4	0.35
Open shrublands	25	0.08	0.11	0.1	0.17
Woody savannas	16	0.12	0.13	0.4	0.35
Grasslands	214	0.10	0.07	0.5	0.13
Croplands	63	0.12	0.12	0.4	0.17
Cropland/Natural vegetation mosaic	23	0.12	0.15	0.5	0.22
Barren or sparsely vegetated	3	0.12	–	0.1	0.02

error. The largest impact of H_R on bias, RMSE and ubRMSE was found for high ω values (0.10 − 0.16).

In order to find a global calibration of the H_R and ω parameters, a best compromise among all statistical metrics was attempted by visual assessment of Fig. 6. Considering mainly two criteria (R and ubRMSE) a value of ω = 0.10 and H_R = 0.4 was estimated. Note that this H_R value might cause a slight drying effect (negative SM bias), which could be explained over many sites by the different sampling depth between the L-band space-borne observations and the *in situ* measurements.

3.2.2. IGBP-based calibration

In this section, instead of calibrating a single and global value of the soil and vegetation parameters ω and H_R, we estimated those parameters for different land cover classes, tabulated by the IGBP classification schema. Metrics were calculated following the same methodology as presented in Section 3.2.1 but now for subsets of *in situ* sites corresponding to each land cover class. Only classes including a representative number of calibration sites were considered, namely: evergreen needle leaf forest, open shrublands, woody savannas, grasslands, croplands, cropland/natural vegetation mosaic and barren or sparsely vegetated. Figs. 1S to 7S present the statistic records in terms of R, RMSE, bias, ubRMSE for each class.

The optimal values of ω (ranging from 0.08 to 0.12) were found to be relatively stable for the different IGBP vegetation classes and for the different statistical criteria and they are summarized in Table 2. These values are consistent with the ones computed by Van der Schalie et al. (2016), who found ω = 0.12 using the LPRM algorithm globally. The latter study showed that increasing ω produces increasing R and decreasing ubRMSE values, and a dry bias effect, exactly as we did in this study (see Figs. 1S to 7S). A saturation effect was also found for values of ω > 0.12. Moreover, our findings are consistent with the SMAP L4 ω product as well. This product was obtained through calibration with SMOS TB data (De Lannoy et al., 2013, 2014) and shows an average value of ω = 0.09 ± 0.07 depending on the IGBP class, as shown in Table 2. The values of SMAP L4 ω are slightly higher than the ones found in this study, with the exception of the grasslands class, for which SMAP L4 ω = 0.07 against 0.10 in the present study.

In terms of H_R, all classes presented similar and clear patterns, with exception of open shrublands. For that latter class, the only clear pattern was found for bias. The best compromise for all metrics was generally found when H_R = 0.4–0.5 with the exception of some low vegetation classes (open shrublands and barren or sparsely vegetated). For these latter, the best compromise was obtained with a rather low H_R value (~0.1) in order to avoid SM overestimation. The best R performances were obtained for croplands and cropland/natural vegetation; with a median R varying, respectively, from 0.58 to 0.72 and from 0.35 to 0.70. On the other hand, the poorest R value was obtained for the evergreen needle leaf forest and barren or sparsely vegetation classes (R varying respectively, from 0.2 to 0.4 and from 0.32 to 0.42 respectively).

Based on the analysis made above, the selected values of H_R for each vegetation class are summarized in Table 2. These values will be referred to as "IGBP-based" values, in contrast to the "globally-constant" values estimated in the previous section. This table also shows the H_R values which were found by Parrens et al. (2017), based on SMOS TB and Leaf Area Index (LAI) data from MODIS.

There is a good general agreement between the values computed by Parrens et al. (2017) and the ones found in the present study. As an exception, in the grasslands and cropland/natural vegetation mosaic classes, Parrens et al. (2017) found lower H_R values (0.13 and 0.22 respectively, instead of 0.5 for both vegetation cover types in this study).

3.3. Performance analysis

The calibration process, presented in the above section, was performed over a selection of *in situ* stations which were filtered based on criteria defined in Section 2.7 (only 391 stations out of a total of 1001 were selected). The selected stations correspond to SMOS pixels which are rather homogeneous and, as among others selection criteria, where the predominant class covers at least 50% of the L3 pixel.

In the present section, the calibrated values of the soil and vegetation parameters (ω, H_R and N_R) are tested. Two datasets were used in the computation of the statistics of this analysis:

- the whole collection of *in situ* sites, namely, all the selected *in situ* stations (391, corresponding to rather homogeneous SMOS L3 pixels) used for the calibration process plus all other *in situ* stations (670, corresponding to both rather homogeneous and heterogeneous SMOS L3 pixels), and
- exclusively *in situ* sites (279 stations) which were not previously accounted for in the calibration step (these *in situ* sites correspond to rather "heterogeneous" SMOS L3 pixels).

- In the performance analysis process, three cases were taken into account (Case (1) and (2) corresponds to the two "optimized" approaches which have been developed in this study):
- Case (1): SM retrievals using globally-constant calibrated values, namely ω = 0.10, H_R = 0.4 and N_R = −1.
- Case (2): SM retrievals using IGBP −based calibrated values, namely the calibrated values of soil roughness and ω which are dependent of the IGBP classes, as given in Table 2 and computed following equation 12.
- Case (3): the original SMOS L3 SM product.
- Case (4): SM retrievals over homogeneous pixels, as done in Case (1) and (2), but using the model parameters of the SMOS L3 algorithm, namely:
  - Forest class: ω = 0.06 and H_R = 0.3
- Other classes: ω = 0 and H_R = 0.1

Cases (1) (2) and (4) are thus based on SM retrievals under the consideration of homogeneous pixels. In those cases, SM and τ_{NAD} retrievals were performed over the whole pixel rather than over the fraction designated as either low vegetation or forest. Note that this approach is similar to the one considered in the AMSR-E (Owe et al., 2008), LPRM and SMAP level 2 SM algorithms.

The results are reported in Table 3 in terms of statistical criteria. It can be seen that the obtained results for configurations (a) and (b) are rather similar. This shows that our results are relatively independent on the selection of the *in situ* sites used in the calibration steps. Taking into account the configuration (a), slight differences between Case (1) and Case (2) were found, mainly in terms of R and bias values (R = 0.60, bias = $-0.023\ m^3\ m^{-3}$ and R = 0.61, bias = $-0.019\ m^3\ m^{-3}$ respectively). This result shows that the use of constant values of the soil and vegetation parameters ω, H_R and N_R is an interesting and simple

Table 3
Median statistical metrics for each case (considering all stations (a) and all stations except the ones used in calibration (b)).

	a			b		
CASE	R	bias ($m^3 m^{-3}$)	ubRMSE ($m^3 m^{-3}$)	R	bias ($m^3 m^{-3}$)	ubRMSE ($m^3 m^{-3}$)
(1) Globally-constant values of ω, H_R and N_R	0.60	−0.023	0.062	0.59	−0.022	0.061
(2) IGBP-based values of ω, H_R, N_R	0.61	−0.019	0.062	0.62	−0.019	0.061
(3) SMOS L3 SM	0.54	−0.034	0.070	0.54	−0.037	0.069
(4) Homogeneous (SMOS L3 SM ω, H_R, N_R)	0.44	0.028	0.086	0.39	0.035	0.089

alternative, as considering the dependence of these parameters on the IGBP classification do not lead to significant improvement in the results.

Compared to the SMOS L3 SM product, results for both approaches (1) and (2) show an improvement in all metrics. In particular, considering case (2) R improves by 0.07, and |bias| and ubRMSE errors decrease by 0.015 and 0.008 $m^3 m^{-3}$ respectively. However, this improvement cannot be explained by the use of homogeneous pixels, as Case (4) leads to poorer R (0.44) and ubRMSE (0.086 $m^3 m^{-3}$) than SMOS L3. The obtained statistical results highlight the impact of using the calibrated values obtained in Cases (1) and (2), as all metrics are poorer for Case (4). The inter-comparison of bias for Cases (3) and (4) is particularly interesting. The difference between these approaches lies fundamentally in the consideration of pixel heterogeneity. The median bias given by (3) is $-0.034\ m^3 m^{-3}$, meaning the SMOS L3 SM product underestimates SM. Nonetheless, the same approach under the assumption of "homogeneity" (4) leads to a wet bias equal to $0.028\ m^3 m^{-3}$.

Contrary to Case (4), the SMOS L3 SM retrieval algorithm does not consider the total TB contribution in the SM retrieval. As it was noted in Section 2.1.1, in both the SMOS L2 and L3 algorithms, TB is modelled over the forest fraction (TB_{FFO}) as a function of ECMWF SM as auxiliary information, when the retrieval is performed over the nominal fraction (TB_{FNO}). The well-known ECMWF SM overestimation compared to *in situ* SM values (Albergel et al., 2012) is causing a TB_{FFO} underestimation (Ulaby et al., 1981–1986). This underestimation may lead, by compensation, to an increase in the simulated value of TB_{FNO} during the inversion process. Considering that the SMOS L3 SM retrieval is performed mainly over the FNO, the resulting SM tends to decrease. Such an issue has been revealed over the Valencia Anchor Station site by Wigneron et al. (2012). This could partly explain the dry bias obtained by the SMOS L3 SM product (Case (3)) over some pixels including forested areas, despite the fact that assuming ω = 0 (FNO) or ω = 0.06 (FFO) instead of higher ω values (as the ones found in this study) leads to wetter SM retrievals.

To better evaluate the improvement obtained from the use of the IGBP-based approach (2) over the SMOS L3 SM product (3), Table 4 shows the percentage of *in situ* stations that performs best in each case in terms of maximum values of R and minimum values of |bias| and ubRMSE. The IGBP-based "optimized" approach is the best option for 84.4%, 57.0% and 86.1% of the *in situ* stations in terms of, respectively R, bias and ubRMSE values.

4. Conclusions

The main objective of this study was to calibrate the parameters which account for two crucial effects in the SM retrieval at L-band: soil roughness (in terms of H_R, N_{RH} and N_{RV} values) and vegetation (in terms of effective scattering albedo, ω). A large range of values of the latter parameters were used in order to retrieve soil moisture (SM) and vegetation optical depth (τ_{NAD}) over a large number of sites worldwide. The present study was carried out considering an optimized retrieval approach which is different from that used in the SMOS L3 SM retrieval algorithm. In this approach, pixels were assumed to be homogeneous (SM was retrieved over the whole SMOS pixel), while heterogeneity is accounted for in the SMOS L3 algorithm. The latter accounts for the surface fraction of the main cover types (bare soil and low vegetation, forest, water, urban, *etc.*) within each SMOS footprint depending on the incidence angles of the observations. However, the retrieval is only made over one fraction: either the nominal or forest fraction in some specific cases.

Long term SM retrievals were compared to *in situ* measurements obtained from the International Soil Moisture Network (ISMN) over the period 2011–2013, and were evaluated using different metrics (R, bias and ubRMSE). Note that, as the focus of this study was the optimization of the SM retrievals, the retrieval results concerning the τ_{NAD} parameter were not analyzed here. They will be presented and discussed in future studies. Some first results are described in Fernandez-Moran et al. (2017).

Finding the optimal retrieval values of the vegetation and soil parameters for the SM retrievals requires finding a compromise considering all the statistical metrics, i.e. the optimization of all of them (with a focus on R and ubRMSE). Performances of the SM retrievals, evaluated in terms of R, bias and ubRMSE, showed a high sensitivity of SM to ω and were found optimum for high ω values (ω ~ 0.10). On the contrary, the calibration of H_R required compromise between the performances obtained in terms of ubRMSE (lower for low H_R values) and of |bias| (lower for larger H_R values). It was found that increasing ω and decreasing H_R values led to drier SM retrievals. However, due to the different sampling depths of the *in situ* measurements (0–5 cm) and of the SMOS L-band observations (~0–3 cm), bias was considered as a second order criterion in the assessment of the results. Globally, a value of ω = 0.10, H_R = 0.4 and N_R = −1 (p = H, V) was found optimum at global scale. This finding is consistent with the work of Van der Schalie et al. (2016), who globally obtained ω equal to 0.12 after applying the Land Parameter Retrieval Model (LPRM) and evaluating SM retrievals against model datasets as MERRA-Land (MERRA) and ERA-Interim/Land (ERA). The latter study has also shown the low influence of soil roughness on the correlation statistics in terms of SM retrievals when ω = 0.12. Furthermore, the global map of the effective scattering albedo provided by the SMAP L4 product is in agreement with the findings of this study (ω = 0.09 ± 0.07). On the contrary, studies by Konings et al. (2016)

Table 4
Percentage of *in situ* stations where the best statistical metrics were obtained for each case (considering all stations (a) and all stations except the ones used in the calibration step (b)).

	a			b		
CASE	R	bias ($m^3 m^{-3}$)	ubRMSE ($m^3 m^{-3}$)	R	bias ($m^3 m^{-3}$)	ubRMSE ($m^3 m^{-3}$)
(2) IGBP-based values of ω, H_R, N_R	84.4%	57.0%	86.1%	79.1%	56.4%	85.3%
(3) SMOS L3 SM	15.6%	43.0%	13.9%	20.9%	43.6%	14.7%

found lower values (ω = 0.02–0.06) and the current set of effective scattering albedo in the SMOS L3 SM product is ω = 0.06–0.08 for forest and ω = 0 for the rest of the cover types.

All *in situ* sites used in this study were classified using the International Geosphere-Biosphere Programme (IGBP) land cover classification scheme, and then specific calibrated values of H_R, N_{Rp} (p = H, V) and ω were proposed for each class. Over the different IGBP classes, it was found that ω values are in a narrow range, from 0.08 to 0.12, whereas H_R ranged from 0.1 to 0.5. It is noticeable that the low H_R (~0.1) was associated to low vegetation cover types (open shrublands and barren or sparsely vegetated covers) whereas higher values, ranging from 0.4 to 0.5, were linked to the rest of IGBP classes. These results are in good agreement with the global map of H_R obtained by Parrens et al. (2017), who calibrated this parameter using SMOS retrievals and Leaf Area Index (LAI) data from MODIS as auxiliary data.

The calibrated soil roughness and effective scattering albedo values were used in an analysis *a posteriori*. This analysis was based on a comparison between the SM retrievals using the calibrated values and the SM data measured at the *in situ* sites. To evaluate the robustness of the calibration step two configurations were considered: a comparison using (a) all *in situ* sites and (b) all sites, excluding the ones (rather homogeneous) considered in the calibration step. Results obtained for both configurations (a) and (b) were generally very similar, which indicates the robustness of the calibrated values.

This analysis exercise confirmed that using either globally-constant or IGBP dependent parameters, there was improvement over the SMOS L3 SM product in terms of SM retrieval accuracies, as compared to the *in situ* SM data (R = 0.61, bias = $-0.019\ m^3 \cdot m^{-3}$ and ubRMSE = 0.062 for the IGBP-based calibration; R = 0.54, bias = $-0.034\ m^3 \cdot m^{-3}$ and ubRMSE = 0.070 for the SMOS L3 SM product). By comparing results obtained for the SMOS L3 SM product and the SMOS L3 SM product under the homogeneous approach we could show that this improvement could not be explained by the use of homogeneous pixels, but mainly by the use of the new model parameter calibration that we computed in this study. Nonetheless, the drying effect of the SMOS L3 SM algorithm retrieval due to the "heterogeneity" approach was demonstrated: considering the same model parameter calibration, the bias varied from $-0.034\ m^3\ m^{-3}$ when using the SMOS L3 SM algorithm (heterogeneous pixels) to $0.028\ m^3\ m^3$ when the homogeneous approach was used.

The findings presented in this study have important implications for the calibration of soil roughness and vegetation in the current Level 2 and 3 algorithms of the SMOS mission with potential implications for SMAP as well. An alternative SMOS product (referred to SMOS-INRA-CESBIO, or SMOS-IC for short) (Fernandez-Moran et al., 2017) based on the homogeneous retrieval approach and the new calibrated parameters presented here has been developed by Institut National de la Recherche Agronomique (INRA) and Centre d'Etudes Spatiales de la BIOsphère (CESBIO). One of the main advantages of this approach is its simplicity leading to the development of an efficient processor, capable of processing one year of data over a few hours. The dependence on the auxiliary data has also been reduced as compared to the L3 algorithm. Specifically, SMOS-IC does not use MODIS LAI and ECMWF SM data, whose tendency to SM overestimation is well-known (Albergel et al., 2012). Consequently, the products from the SMOS-IC approach are more aligned to SM products derived from other space-borne sensors (such as SMAP and AMSR-E), where the retrieval is done under the homogeneity assumption (Entekhabi et al., 2014; Ashcroft and Wentz, 2000; Owe et al., 2008). Future studies focusing on the global-scale validation of this product would be helpful to better understand its strengths and possible shortcomings.

Acknowledgements

The authors would like to thank the Terre Océan Surfaces Continentales et Atmosphère (TOSCA) CNES program and the European Space Agency (ESA) for funding this study. The authors acknowledge CATDS for the SMOSL3 dataset (http://catds.ifremer.fr) and the cooperation of the different soil moisture *in situ* networks in the International Soil Moisture Network (ISMN) project.

Appendix A. Supplementary data

Supplementary data associated with this article can be found, in the online version, at http://dx.doi.org/10.1016/j.jag.2017.05.013.

References

Al Bitar, A., Mialon, A., Kerr, Y., Cabot, F., Richaume, P., Jacquette, E., Quesney, A., Mahmoodi, A., Tarot, S., Parrens, M., Al-yaari, A., Pellarin, T., Rodriguez-Fernandez, N., Wigneron, J.−P., 2017. The Global SMOS Level 3 daily soil moisture and brightness temperature maps. Earth Syst. Sci. Data Discuss. 1–41.

Al-Yaari, A., Wigneron, J.-P., Ducharne, A., Kerr, Y.H., Wagner, W., De Lannoy, G., Reichle, R., Al Bitar, A., Dorigo, W., Richaume, P., Mialon, A., 2014a. Global-scale comparison of passive (SMOS) and active (ASCAT) satellite based microwave soil moisture retrievals with soil moisture simulations (MERRA-Land). Remote Sens. Environ. 152, 614–626.

Al-Yaari, A., Wigneron, J.-P., Ducharne, A., Kerr, Y., de Rosnay, H., de Jeu, P., Govind, R., Al Bitar, A., Albergel, A., Muñoz-Sabater, C., Richaume, J., Mialon, P., 2014b. Global-scale evaluation of two satellite-based passive microwave soil moisture datasets (SMOS and AMSR-E) with respect to Land Data Assimilation System estimates. Remote Sens. Environ. 149, 181–195.

Al-Yaari, A., Wigneron, J.-P., Kerr, Y., de Jeu, R., Rodriguez-Fernandez, N., van der Schalie, R., Bitar, Al, Mialon, A., Richaume, A., Dolman, P., Ducharne, A., 2016. Testing regression equations to derive long-term global soil moisture datasets from passive microwave observations. Remote Sens. Environ. 180, 453–464.

Albergel, C., de Rosnay, P., Balsamo, G., Isaksen, L., Muñoz-Sabater, J., 2012. Soil moisture analyses at ECMWF: evaluation using global ground-Based *In situ* observations. J. Hydrometeor 13, 1442–1460.

Armstrong, R., Brodzik, M.J., Varani, A., 1997. The NSIDC EASE-Grid: Addressing the need for a common, flexible, mapping and gridding scheme. Earth Syst. Monit. 7, 6–7.

Ashcroft, P., Wentz, F., 2000. Algorithm Theoretical Basis Document: AMSR Level-2A Algorithm, 706 Revised 03 November. Santa Rosa, Remote Sensing Systems, California USA.

Belward, A.E., 1996. The IGBP-DIS Global 1 Km Land Cover Data Set DISCover − Proposal and Implementation Plans. Report of the Land Cover Working Group of the IGBP-DIS. IGBP-DIS Working Paper 13. pp. 63.

Berrisford, P., Kållberg, P., Kobayashi, S., Dee, D., Uppala, S., Simmons, A.J., Poli, P., Sato, H., 2011. Atmospheric conservation properties in ERA-Interim. Q. J. R. Meteorolog. Soc. 137, 1381–1399.

Brocca, L., Melone, F., Moramarco, T., Wagner, W., Naeimi, V., Bartalis, Z., Hasenauer, S., 2010. Improving runoff prediction through the assimilation of the ASCAT soil moisture product. Hydrol. Earth Syst. Sci. 14 (10), 1881–1893.

Broxton, P., Zeng, X., Sulla-Menashe, D., Troch, P.A., 2014. A global land cover climatology using MODIS data. J. Appl. Meteor. Climatol. 53, 1593–1605.

Calvet, J.C., Fritz, N., Froissard, F., Suquia, D., Petitpa, A., Piguet, B., 2007. In situ soil moisture observations for the CAL/VAL of SMOS: The SMOSMANIA network. Int. Geosci. Remote Sens. Symp. (IGARSS) 1196–1199.

Cano, A., Saleh, K., Wigneron, J.-P., Antolín, C., Balling, J.E., Kerr, Y.H., et al., 2010. The SMOS mediterranean ecosystem L-band characterisation experiment (MELBEX-I) over natural shrubs. Remote Sens. Environ. 114 (4), 844–853.

Coopersmith, E.J., Cosh, M.H., Bindlish, R., Bell, J., 2015. Comparing AMSR-E soil moisture estimates to the extended record of the U.S: Climate Reference Network (USCRN). Adv. Water Resour. 85, 79–85.

De Lannoy, G.J.M., Reichle, R.H., Pauwels, V.R.N., 2013. Global calibration of the GEOS-5 L-band microwave radiative transfer model over non frozen land using SMOS observations. J. Hydrometeorol. 14, 765–785.

De Lannoy, G.J.M., Reichle, R.H., Vrugt, J.A., 2014. Uncertainty quantification of GEOS-5 L-band radiative transfer model parameters using Bayesian inference and SMOS observations. Remote Sens. Environ. 148, 146–157.

de Rosnay, P., Drusch, M., Vasiljevic, D., Balsamo, G., Albergel, C., Isaksen, L., 2013. A simplified Extended Kalman Filter for the global operational soil moisture analysis at ECMWF. Q. J. R. Meteorolog. Soc. 139 (674), 1199–1213.

Dorigo, W.A., Wagner, W., Hohensinn, R., Hahn, S., Paulik, C., Xaver, A., Gruber, A., Drusch, M., Mecklenburg, S., van Oeve-len, P., Robock, A., Jackson, T., 2011. The International Soil Moisture Network: a data hosting facility for global in situ soil moisture measurements. Hydrol. Earth Syst. Sci. 15, 1675–1698.

Dorigo, W.A., Xaver, A., Vreugdenhil, M., Gruber, A., Hegyiová, A., Sanchis-Dufau, A.D., Zamojski, D., Cordes, C., Wagner, W., Drusch, M., 2013. Global automated quality control of In situ soil moisture data from the international soil moisture network. Vadose Zone J. 12.

Entekhabi, D., Njoku, E.G., O'Neill, P.E., Kellogg, K.H., Crow, W.T., Edelstein, W.N., Entin, J.K., Goodman, S.D., Jackson, T.J., Johnson, J., et al., 2010a. The soil moisture active passive (SMAP) mission. Proc. IEEE 98 (5), 704–716.

Entekhabi, D., Reichle, R.H., Koster, R.D., Crow, W.T., 2010b. Performance metrics for soil moisture retrievals and application requirements. J. Hydrometeorol. 11, 832–840.

Entekhabi, D., Yueh, S., O'Neill, P., Kellogg, K., 2014. SMAP Handbook, JPL Publication

JPL 400–1567. Jet Propulsion Laboratory, Pasadena, California.
Escorihuela, M.J., Kerr, Y., de Rosnay, P., Wigneron, J.-P., Calvet, J.-C., Lemaître, F., 2007. A simple model of the bare soil microwave emission at L-band. IEEE Trans. Geosci. Remote Sens. 45, 1978–1987.
Escorihuela, M.J., Chanzy, A., Wigneron, J.-P., Kerr, Y., 2010. Effective soil moisture sampling depth of L-band radiometry: a case of study. Remote Sens. Environ. 114, 995–1001.
FAO, 1988. UNESCO Soil Map of the World, Revised Legend. World Resources Repor 60. pp. 138.
Fernandez-Moran, R., Wigneron, J.-P., Lopez-Baeza, E., Al-Yaari, A., Coll-Pajaron, A., Mialon, A., Miernecki, M., Parrens, M., Salgado- Hernanz, P., Schwank, M., et al., 2015. Roughness and vegetation parameterizations at L-band for soil moisture retrievals over a vineyard field. Remote Sens. Environ. 170, 269–279.
Fernandez-Moran, R., Al-Yaari, A., Mialon, A., Mahmoodi, A., Bitar, Al, De Lannoy, A., Rodriguez-Fernandez, G., Lopez-Baeza, N., Kerr, E., Wigneron, Y., 2017. SMOS-IC: an alternative SMOS soil moisture and vegetation optical depth product. Remote Sens. 9 (5), 457.
Grant, J.P., Wigneron, J.-P., Van de Griend, A.A., Kruszewski, A., Søbjærg, S.S., Skou, N., 2007. A field experiment on microwave forest radiometry: L-band signal behaviour for varying conditions of surface wetness. Remote Sens. Environ. 109 (1), 10–19.
Grant, J.P., Wigneron, J.P., De Jeu, R.A.M., Lawrence, H., Mialon, A., Richaume, P., Al Bitar, A., Drusch, M., van Marle, M.J.E., Kerr, Y., 2016. Comparison of SMOS and AMSR-E vegetation optical depth to four MODIS-based vegetation indices. Remote Sens. Environ. 172, 87–100.
Guérif, M., Duke, C., 2000. Adjustment procedures of a crop model to the site specific characteristics of soil and crop using remote sensing data assimilation Agriculture. Ecosyst. Environ. 81 (1), 57–69.
Jackson, T.J., Bindlish, R., Cosh, M.H., Zhao, T., Starks, P.J., Bosch, D.D., Seyfried, M., Moran, M.S., Goodrich, D.C., Kerr, Y.H., Leroux, D., 2012. Validation of soil moisture and Ocean Salinity (SMOS) soil moisture over watershed networks in the U.S. IEEE Trans. Geosci. Remote Sens. 50, 1530–1543.
Jackson, T.J., et al., 1980. Profile soil moisture from space measurements. J. Irrig. Drain. Div. Am. Soc. Civil Eng. 106, 81–92.
Jin, M.S., Mullens, T., 2014. A study of the relations between soil moisture, soil temperatures and surface temperatures using ARM observations and offline CLM4 simulations. Climate 2 (4), 279–295 (2014).
Kerr, Y.H., Waldteufel, P., Richaume, P., Davenport, I., Ferrazzoli, P., Wigneron, J.P., 2006. SMOS Level 2 Processor Soil Moisture Algorithm Theoretical Basis Document (ATBD). SM-ESL (CBSA). CESBIO, Toulouse (SO-TN-ESL-SM-GS-0001, V5. a, 15/03.).
Kerr, Y.H., Waldteufel, P., Richaume, P., Wigneron, J.P., Ferrazzoli, P., Mahmoodi, A., Al Bitar, A., Cabot, F., Gruhier, C., Juglea, S., Leroux, D., Mialon, A., Delwart, S., 2012. The SMOS soil moisture retrieval algorithm. IEEE Trans. Geosci. Remote Sens. 50 (5), 1384–1403.
Konings, A., Piles, M., Rötzer, K., McColl, K.A., Chan, S.K., Entekhabi, D., 2016. Vegetation optical depth and scattering albedo retrieval using time series of dual-polarized L-band radiometer observations. Remote Sens. Environ. 172, 178–189.
Kurum, M., 2013a. Quantifying scattering albedo in microwave emission of vegetated terrain. Remote Sens. Environ. 129, 66–74.
Kurum, M., 2013b. Quantifying scattering albedo in microwave emission of vegetated terrain. Remote Sens. Environ. 129, 66–74.
Larson, K.M., Small, E.E., Gutmann, E.D., Bilich, A.L., Braun, J.J., Zavorotny, V.U., 2008. Use of GPS receivers as a soil moisture network for water cycle studies. Geophys. Res. Lett. 35, L24405.
Lawrence, H., Wigneron, J.-P., Demontoux, F., Mialon, A., Kerr, Y.H., 2013. Evaluating the semiempirical H − Q model used to calculate the L-band emissivity of a rough bare soil. IEEE Trans. Geosci. Remote Sens. 51 (7), 4075–4084.
Lebel, T., Cappelaere, B., Galle, S., Hanan, N., Kergoat, L., Levis, S., Vieux, B., Descroix, L., Gosset, M., Mougin, E., Peugeot, C., Seguis, L., 2009. AMMA-CATCH studies in the Sahelian region of West-Africa: an overview. J. Hydrol. 375, 3–13.
Leng, P., Song, X., Duan, S.-B., Li, Z.-L., 2016. Preliminary validation of two temporal parameter-based soil moisture retrieval models using a satellite product and in situ soil moisture measurements over the REMEDHUS network. Int. J. Remote Sens. 37 (24), 5902–5917.
Masson, V., Champeaux, J.-L., Chauvin, F., Meriguet, C., Lacaze, R., 2003. A global database of land surface parameters at 1 km resolution in meteorological and climate models. J. Climate 16, 1261–1282.
Miernecki, M., Wigneron, J.-P., Lopez-Baeza, E., Kerr, Y., De Jeu, R., De Lannoy, G.J.M., Jackson, T.J., O'Neill, P.E., Schwank, M., Fernandez-Moran, R., et al., 2014. Comparison of SMOS and SMAP soil moisture retrieval approaches using tower-based radiometer data over a vineyard field. Remote Sens. Environ. 154, 89–101.
Mironov, V., Kerr, Y., Wigneron, J.-P., Kosolapova, L., Demontoux, F., 2013. Temperature- and texture-dependent dielectric model for moist soils at 1.4 GHz. IEEE Geosci. Remote Sens. Lett. 10 (3), 419–423.
Mo, T., Choudhury, B., Schmugge, T., Wang, J., Jackson, T., 1982. A model for microwave emission from vegetation-covered fields. J. Geophys. Res. 87 (C13), 11229–11237.
Njoku, E.G., Kong, J., 1977. A.Theory for passive microwave remote sensing of near-surface soil moisture. J. Geophys. Res. 82, 3108–3118.
O'Neill, P., Chan, S., Njoku, E., Jackson, T., Bindlish, R., 2012. SMAP Level 2 & 3 Soil Moisture (Passive) Algorithm Theoretical Basis Document, JPL D-66480. Jet Propulsion Laboratory, Pasadena, CA, USA Initial Release V1, October 2012.
Olsen, J.L., Ceccato, P., Proud, S.R., Fensholt, R., Grippa, M., Mougin, E., Ardö, J., Sandholt, I., 2013. Relation between seasonally detrended shortwave infrared reflectance data and land surface moisture in semi-arid sahel. Remote Sens. 5, 2898–2927.
Owe, M., De Jeu, R.A.M., Holmes, T.R.H., 2008. Multi-sensor historical climatology of satellite-derived global land surface moisture. J. Geophys. Res. 113, F01002.
Parrens, M., Wigneron, J.-P., Richaume, P., Mialon, A., Bitar, Al, Fernandez-Moran, A., Al-Yaari, R., Kerr, A., 2016. Global-scale surface roughness effects at L-band as estimated from SMOS observations. Remote Sens. Environ. 181, 122–136.
Parrens, M., Wigneron, J.-P., Richaume, P., Bitar, Al, Mialon, A., Fernandez-Moran, A., Al-Yaari, R., O'Neill, A., Kerr, Y., 2017. Considering combined or separated roughness and vegetation effects in soil moisture retrievals. Int. J. Appl. Earth Observ. Geoinform. 55, 73–86.
Patton, J., Hornbuckle, B., 2013. Initial validation of SMOS vegetation optical thickness in iowa. IEE Geosci. Remote Sens. Lett. 10 (4), 647–651.
Rüdiger, C., Western, A.W., Walker, J.P., Smith, A.B., Kalma, J.D., Willgoose, G.R., 2010. Towards a general equation for frequency domain reflectometers. J. Hydrol. 383 (3-4), 319–329.
Rahmoune, R., Ferrazzoli, P., Kerr, Y.H., Richaume, P., 2013. SMOS level 2 retrieval algorithm over forests: description and generation of global maps. IEEE J. Sel. Top. Appl. Earth Observ. Remote Sens. 6 (3), 1430–1439.
Reichle, R.H., DeLannoy, G.J.M., Liu, Q., Ardizzone, J.V., Chen, F., Colliander, A., Conaty, A., Crow, W., Jackson, T., Kimball, J., Koster, R.D., Smith, E.B., 2016. Soil Moisture Active Passive Mission L4_SM Data Product Assessment (Version 2 Validated Release). NASA GMAO Office Note, No. 12 (Version 1.0). National Aeronautics and Space Administration, Goddard Space Flight Center, Greenbelt, Maryland, USA.
Schaefer, G.L., Cosh, M.H., Jackson, T.J., 2007. The USDA Natural Resources Conservation Service Soil Climate Analysis Network (SCAN). J. Atmos. Ocean. Technol. 24, 2073–2077.
Serreze, M.C., Clark, M.P., Frei, A., 2001. Characteristics of large snowfall events in the montane western United States as examined using snowpack telemetry (SNOTEL) data. Water Resour. Res. 37, 675–688.
Ulaby, F.T., Moore, R.K., Fung, A.K., 1986. Microwave Remote Sensing — Active and Passive, Vol I, II, 1981-82., vol III Addison-Wesley Publishing Company, Artech House, Norwood, MA (1986).
Van der Schalie, R., Parinussa, R.M., Renzullo, L.J., Van Dijk, A.I.J.M., Su, C.-H., De Jeu, R.A.M., 2015. SMOS soil moisture retrievals using the land parameter retrieval model: evaluation over the murrumbidgee catchment, Southeast Australia. Remote Sens. Environ. 163, 70–79.
Van der Schalie, R., Kerr, Y.H., Wigneron, J.-P., Rodríguez-Fernández, N.J., Al-Yaari, A., de Jeu, R.A.M., 2016. Global SMOS soil moisture retrievals from the land parameter retrieval model. Int. J. Appl. Earth Observ. Geoinform. 45, 125–134.
Wang, J.R., Choudhury, B.J., 1981. Remote sensing of soil moisture content over bare field at 1.4 GHz frequency. J. Geophys. Res. 86, 5277–5282.
Wigneron, J.-P., Laguerre, L., Kerr, Y.H., 2001. A simple parameterization of the L-band microwave emission from rough agricultural soils. IEEE Trans. Geosci. Remote Sens. 39 (8), 1697–1707.
Wigneron, J.-P., Kerr, Y., Waldteufel, H., Saleh, P., Escorihuela, K., Richaume, M.-J., Ferrazzoli, P., de Rosnay, P., Gurney, P., Calvet, R., Guglielmetti, J.-C., Hornbuckle, M., Matzler, B., Pellarin, C., Schwank, T., 2007. L-band Microwave Emission of the Biosphere (L-MEB) Model: description and calibration against experimental data sets over crop fields. Remote Sens. Environ. 107 (4), 639–655.
Wigneron, J.-P., Chanzy, A., De Rosnay, P., Rudiger, C., Calvet, J.-C., 2008. Estimating the effective soil temperature at L-band as a function of soil properties. IEEE Trans. Geosci. Remote Sens. 46 (3), 797–807.
Wigneron, J.-P., Schwank, M., López-Baeza, E., Kerr, Y., Novello, H., Millan, N., et al., 2012. First Evaluation of the simultaneous SMOS and ELBARA-II observations in the Mediterranean region. Remote Sens. Environ. 124, 26–37.
Wigneron, J.-P., Jackson, T.J., O'Neill, P., De Lannoy, G., Rosnay, P., de Walker, J.P., Ferrazzoli, P., Mironov, V., Bircher, S., Grant, J.P., et al., 2017. Modelling the passive microwave signature from land surfaces: a review of recent results and application to the L-band SMOS & SMAP soil moisture retrieval algorithms. Remote Sens. Environ. 192, 238–262.

ARTICLE 3: *SMOS-IC: AN ALTERNATIVE SMOS SOIL MOISTURE AND VEGETATION OPTICAL DEPTH PRODUCT*

This article was published in "Remote Sensing" in 2017. This journal currently has an impact factor of 3.244

remote sensing

MDPI

Article

SMOS-IC: An Alternative SMOS Soil Moisture and Vegetation Optical Depth Product

Roberto Fernandez-Moran [1,2,*], Amen Al-Yaari [1], Arnaud Mialon [3], Ali Mahmoodi [3], Ahmad Al Bitar [3], Gabrielle De Lannoy [4], Nemesio Rodriguez-Fernandez [3], Ernesto Lopez-Baeza [2], Yann Kerr [3] and Jean-Pierre Wigneron [1]

1 INRA, Centre INRA Bordeaux Aquitaine, URM1391 ISPA, F-33140 Villenave d'Ornon, France; amen.alyaari@bordeaux.inra.fr (A.A.-Y.); jean-pierre.wigneron@inra.fr (J.-P.W.)
2 Climatology from Satellites Group, Faculty of Physics, Department of Earth Physics & Thermodynamics, University of Valencia, 46100 Valencia, Spain; Ernesto.Lopez@uv.es
3 CESBIO, CNES/CNRS/IRD/UPS, UMR 5126, 31401 Toulouse CEDEX 9, France; arnaud.mialon@cesbio.cnes.fr (A.M.); mahmoodi.ca@gmail.com (A.M.); ahmad.albitar@cesbio.cnes.fr (A.A.B.); nemesio.rodriguez-fernandez@univ-tlse3.fr (N.R.-F.); yann.kerr@cesbio.cnes.fr (Y.K.)
4 Department of Earth and Environmental Sciences, KU Leuven, Heverlee, B-3001, Belgium; gabrielle.delannoy@kuleuven.be
* Correspondence: roberto.fernandez-moran@inra.fr; Tel.: +33-7-5204-3085

Academic Editors: Prashant K. Srivastava and Prasad S. Thenkabail
Received: 1 March 2017; Accepted: 3 May 2017; Published: 9 May 2017

Abstract: The main goal of the Soil Moisture and Ocean Salinity (SMOS) mission over land surfaces is the production of global maps of soil moisture (SM) and vegetation optical depth (τ) based on multi-angular brightness temperature (TB) measurements at L-band. The operational SMOS Level 2 and Level 3 soil moisture algorithms account for different surface effects, such as vegetation opacity and soil roughness at 4 km resolution, in order to produce global retrievals of SM and τ. In this study, we present an alternative SMOS product that was developed by INRA (Institut National de la Recherche Agronomique) and CESBIO (Centre d'Etudes Spatiales de la BIOsphère). One of the main goals of this SMOS-INRA-CESBIO (SMOS-IC) product is to be as independent as possible from auxiliary data. The SMOS-IC product provides daily SM and τ at the global scale and differs from the operational SMOS Level 3 (SMOSL3) product in the treatment of retrievals over heterogeneous pixels. Specifically, SMOS-IC is much simpler and does not account for corrections associated with the antenna pattern and the complex SMOS viewing angle geometry. It considers pixels as homogeneous to avoid uncertainties and errors linked to inconsistent auxiliary datasets which are used to characterize the pixel heterogeneity in the SMOS L3 algorithm. SMOS-IC also differs from the current SMOSL3 product (Version 300, V300) in the values of the effective vegetation scattering albedo (ω) and soil roughness parameters. An inter-comparison is presented in this study based on the use of ECMWF (European Center for Medium range Weather Forecasting) SM outputs and NDVI (Normalized Difference Vegetation Index) from MODIS (Moderate-Resolution Imaging Spectroradiometer). A six-year (2010–2015) inter-comparison of the SMOS products SMOS-IC and SMOSL3 SM (V300) with ECMWF SM yielded higher correlations and lower ubRMSD (unbiased root mean square difference) for SMOS-IC over most of the pixels. In terms of τ, SMOS-IC τ was found to be better correlated to MODIS NDVI in most regions of the globe, with the exception of the Amazonian basin and the northern mid-latitudes.

Keywords: SMOS; L-band; Level 3; ECMWF; SMOS-IC; soil moisture; vegetation optical depth; MODIS; NDVI

1. Introduction

The estimation of surface soil moisture (SM) at global scale is a key objective for the recent L-band microwave missions SMOS (Soil Moisture and Ocean Salinity) (Kerr et al., 2012 [1]) and SMAP (Soil Moisture Active Passive) (Entekhabi et al., 2010 [2]). Measurements of soil moisture are needed for applications related to the study of climate change or agriculture (droughts, floods, etc.) and hydrological processes (Brocca et al., 2010 [3]) such as precipitation, infiltration, runoff and evaporation. Moreover, SM is considered as an Essential Climate Variable (ECV) and it is included in in the Climate Change Initiative (CCI) project (Hollmann et al., 2013 [4]). An ECV is defined as a physical, chemical or biological variable that critically contributes to the characterization of the Earth's climate.

The soil moisture of the first 2–3 cm soil layer is highly related to the soil emissivity at L-band through the soil permittivity. SMOS uses an interferometric radiometer, which delivers multi-angular brightness temperature measurements at L-band. Currently, various products are derived from the SMOS data at Level 2 (Kerr et al., 2012 [1]) and at Level 3 (Al Bitar et al., 2017 [5]), such as the SMOSL3 Brightness Temperature (SMOSL3 *TB*) and the SMOSL3 SM and τ products, with a 625 km^2 sampling. The SMOS SM retrieval algorithm, which is common to both SMOS Level 2 (L2) and Level 3 (L3) products, has been continuously improved since the launch of the satellite in 2009 (Kerr et al., 2001 [6]; Mialon et al., 2015 [7]; Al Bitar et al., 2017 [5]). It has been evaluated against several datasets from various space-borne sensors such as SMAP, the active Advanced Scatterometer (ASCAT), the Advanced Microwave Scanning Radiometer (AMSR-E) or different versions of the SMOS products (Al-Yaari et al., 2014 [8]; Al-Yaari et al., 2015 [9], 2017 [10], Kerr et al., 2016 [11]). All versions of the Level 2 (L2) and Level 3 (L3) products, are based on the inversion of the L-band Microwave Emission of the Biosphere (L-MEB) radiative transfer model (Wigneron et al., 2017 [12], thus retrieving two main parameters: soil moisture and vegetation optical depth at nadir (τ).

The SMOS τ is a measure of the attenuation of the microwave radiations by the vegetation canopy at L-band. Vegetation is commonly studied at optical or infrared frequencies. However, the longer wavelength of L-band sensors allows penetration of the radiations within the canopy. Thus, τ can be related to different vegetation features such as forest height (Rahmoune et al., 2013 [13], 2014 [14]), vegetation structure (Schwank et al., 2005 [15], 2012 [16]), water content (Jackson and Schmugge, 1991 [17], Mo et al., 1982 [18], Wigneron et al., 1995 [19]; Grant et al., 2012 [20]), sapflow (Schneebeli et al., 2011 [21]) and leaf fall (Guglielmetti et al., 2008 [22]; Patton et al., 2012 [23]). Furthermore, some vegetation indices can also be related to τ such as the Leaf Area Index (LAI) (Wigneron et al., 2007 [24]) and the normalized difference vegetation index (NDVI) (Grant et al., 2016 [25]). Note that some studies have also demonstrated the notable influence of soil roughness on the retrieved values of the τ parameter at both local and regional scales (Patton et al., 2013 [23]; Fernandez-Moran et al., 2015 [26]; Parrens et al., 2017 [27]).

The L-MEB model has been progressively refined and improved (Wigneron et al., 2011 [28], 2017 [12]). The SMOS L2 and L3 algorithms are based on a bottom-up approach where the *TB* contributions of 4 x 4 km land cover surfaces are convoluted using the antenna pattern to upscale the *TB* simulations to the sensor resolution. The use of such a bottom-up approach to retrieve SM and τ presents two main drawbacks. First, this approach is impacted by the uncertainties associated with the higher resolution auxiliary files, like the land cover maps, which are used to characterize the pixel heterogeneity. Second, the approach is more time consuming as the exact antenna patterns have to be applied for each view angle.

In this study, an alternative SMOS product is presented, hereinafter referred to as SMOS-IC (SMOS-INRA-CESBIO). This product is based on a simplified approach developed by INRA (Institut National de la Recherche Agronomique) and CESBIO (Centre d'Etudes Spatiales de la BIOsphère) and differs from the operational SMOS Level 2 and Level 3 products in four main ways:

I The main objective of this product is to be as independent as possible from auxiliary data. The SMOS-IC algorithm does not take into consideration pixel land use and assumes the pixel to

be homogeneous as suggested by Wigneron et al., 2012 [29]. The SM and τ retrieval is performed over the whole pixel rather than over the fraction designated as either low vegetation or forest. Note that this approach is similar to the one considered in the development of the AMSR-E and SMAP SM algorithms (O'Neill et al., 2012 [27]). By simplifying the retrieval approach, the SMOS-IC product becomes independent of the ECMWF soil moisture information currently used as auxiliary information to estimate *TB* in the subordinate pixel fractions of heterogeneous pixels in the operational SMOS L2 and L3 algorithms (Kerr et al., 2012 [1]).

II In relation to the above point, in some cases, the Level 2 and Level 3 algorithms use values of LAI derived from MODIS [30] to initialize the value of optical depth in the inversion algorithm (Kerr et al., 2012 [1]). In SMOS-IC, this is not implemented, and the initialization of optical depth in the inversion algorithm is based on a very simple approach (given in the following) and is completely independent of the MODIS data.

III SMOS-IC uses as input SMOS Level 3 fixed angle bins Brightness Temperature (*TB*) data at the top of the atmosphere and contains different flags allowing to filter SM retrievals accounting for the quality of the input *TB* data and for the *TB* angular range in the L-MEB inversion. SMOS-IC does not make use of the computationally expensive corrections based on angular antenna patterns to account for pixel heterogeneity as in the L2 and L3 retrieval algorithms.

IV New values of the effective vegetation scattering albedo (ω) and soil roughness parameters (H_R, N_{RV}, and N_{RH}) are considered in the SMOS-IC product. This change is based on the results of Fernandez-Moran et al. (2016) [31] who calibrated the L-MEB vegetation and soil parameters for different land cover types based on the International Geosphere-Biosphere Programme (IGBP) classes, as well as the findings of Parrens et al. (2016) [32] who computed a global map of the soil roughness H_R values. The calibration of Fernandez-Moran et al. (2016) [31] was obtained by selecting the values of the parameters (H_R, N_{RV}, N_{RH}, and ω) which optimized the SMOS SM retrievals, with respect to the in situ SM values measured over numerous sites obtained from ISMN (International Soil Moisture Network). The parameter values resulting from this new calibration differ from those used in the current SMOS L2 and L3 products. Values currently used in the SMOS L2 and L3 algorithms (Kerr et al., 2012 [1]) were defined before launch from literature. Over forested areas, values were updated but not over low vegetation. Consequently, in Version 620 of the L2 (and Version 300 for L3) algorithm, ω is still assumed to be zero over low vegetation canopies and ω ~0.06–0.08 over forests. Similarly, H_R is equal to 0.3 for forests and H_R = 0.1 for the rest of the cover types, whereas N_{RH} and N_{RV} are respectively set to 2 and 0 at global scale.

An evaluation and calibration of SMOS-IC at local scale was performed in Fernandez-Moran et al. (2016) [31]. The present study aims at presenting SMOS-IC and illustrating the main features of the SMOS-IC SM and τ products at global scale, in comparison to the current SMOSL3 product. To achieve this, the SMOS-IC and SMOSL3 SM products were compared against the ECMWF SM product for ease of comparison. Furthermore, NDVI (Rouse et al., 1974 [33]) from the Moderate-Resolution Imaging Spectroradiometer (MODIS) was used as a vegetation index to analyze the seasonal changes in the τ products from both SMOS-IC and SMOSL3. The NDVI index which is derived from optical observations cannot be directly compared to the τ product, which is derived from microwave observations. It must be noted that the L-band TB observations are almost insensitive to green leaves (Guglielmetti et al., 2007 [34], Santi et al., 2009 [35]), and τ is related to the vegetation water content (VWC, kg/m^2) of the whole vegetation layer. However, the NDVI index is a good indicator of the vegetation density and it can be used to interpret the seasonal changes in the SMOS τ product at large scale over low vegetation as found by Grant et al. (2016) [25], but with some caveats: saturation effects at high levels of vegetation density, sensitivity to the effects of snow and soil reflectivity (Qi et al., 1994 [36]), etc. It may be noted that NDVI is the proxy used for estimating τ in the current operational algorithm of the SMAP mission (O'Neill et al., 2012 [37]).

In Section 2, we present a description of both SMOS algorithms (SMOSL3 and SMOS-IC) and of the MODIS NDVI and ECMWF SM datasets. The inter-comparison of the SMOS products in terms of soil moisture and vegetation optical depth is given in Section 3. The inter-comparison covers almost six years of data, from 2010 to 2015, excluding the commissioning phase (the first six months of 2010; Corbella et al., 2011 [38]). Discussion and conclusions are presented in Section 4.

2. Materials and Methods

2.1. SMOSL3 Brightness Temperature, Soil Moisture and Vegetation Optical Depth

At Level 3, there are different SMOS products (Al Bitar et al., 2017 [5]). In this study, we used the SMOS L3 products which include *TB*, τ and SM (version 300) data produced by the CATDS (Centre Aval de Traitement des Données SMOS) (Al Bitar et al., 2017 [5]). These products are available in the NetCDF format and on the Equal-Area Scalable Earth (EASE) 2.0 grid (Armstrong et. al, 1997 [39]) with a 625 km^2 sampling [40]. The SMOSL3 *TB* is measured at the top of the atmosphere and provided in the surface reference frame (i.e., *H* and *V* polarizations) at angles ranging from 2.5 ± 2.5 to 62.5 ± 2.5. Ascending (~06:00 LST at the equator) and descending (~18:00 LST) orbits are processed separately. The Level 3 processor uses the same physically based forward model (L-MEB) as the ESA SMOS Level 2 processor (Kerr et al., 2012 [1], Kerr et al., 2013 [41]) for the retrieval of both SM and τ from dual polarization (*H*, *V*) and multi-angular SMOS measurements. The retrieval algorithm consists of the minimization of the differences between observed and modeled Level 1 *TB* (through the L-MEB forward model) in a Bayesian cost function, which accounts for the observation uncertainty, and also contains a prior parameter constraint. One of the characteristics of the *TB* modeling is the consideration of surface heterogeneity. The total modeled *TB* is simulated as the sum of *TB* contributions from several fractions (nominal or low vegetation, forest, and others as urban, water, etc.). In most of the cases, the SM retrieval is estimated from the *TB* contribution which corresponds to areas with low vegetation (nominal fraction), while the *TB* forest contribution is computed using ancillary data such as ECMWF SM. In other cases, the retrieval is performed entirely over the forest fraction. Dynamic changes as freezing or rainfall events are considered through ancillary weather data from ECMWF.

The SMOSL3 τ and SM retrievals are provided at different temporal resolutions: daily, 3-days, 10-days, and monthly averaged (Kerr et al., 2013 [41]; Jacquette et al., 2010 [42]). The quality of the SMOSL3 product containing SM and τ data is improved by the use of multi-orbit retrievals (Al Bitar et al., 2017 [5]). The SMOS ascending (06:00 LST) and descending (18:00 LST) orbits are processed separately in this product in order to better account for the diurnal effects (surface, total electron content which drives Faraday rotation and sun corrections) and, in some areas, radio frequency interferences (RFI) effects (Oliva et al., 2012 [43]) and sun glint impacts at L-band (Khazâal et al., 2016 [44]).

In SMOS-IC, we used the SMOS L3 *TB* product as input to the inversion algorithm. This product, which includes many corrections, is very easy and convenient to use (conversely, the L2 and L3 algorithms are based on L1 C TB data, which include multi-incidence angle brightness temperatures at the top of the atmosphere with a spatial resolution grid of 15 km).

2.2. SMOS-IC

2.2.1. Model Description

As for the L2 and L3 algorithms, in SMOS-IC, the retrieval of the soil moisture and vegetation optical depth at nadir is based on the L-MEB model inversion (Wigneron et al., 2007 [24]). The retrieval is performed over pixels which are considered as entirely homogeneous; in other words, a single representative value of each input model parameter is used for the whole pixel.

In L-MEB, the simulation of the land surface emission is based on the τ-ω radiative transfer model (Mo et al., 1982 [18]) using simplified (zero-order) radiative transfer equations. The model represents the soil as a rough surface with a vegetation layer. The modeled *TB* from the soil vegetation medium is

calculated as the sum of the direct vegetation emission, the soil emission attenuated by the canopy and the vegetation emission reflected by the soil and attenuated by the canopy following Equation (1). The atmospheric contribution is neglected.

$$TB_P(\theta) = (1-\omega)\Big[1-\gamma_P(\theta)\Big]\Big[1+\gamma_P(\theta)r_{GP}(\theta)\Big]T_C + \Big[1-r_{GP}(\theta)\Big]\gamma_P(\theta)T_G \quad (1)$$

where θ is the incidence angle, r_{GP} is the soil reflectivity, T_G and T_C are the soil and canopy effective temperatures (K), γ_p is the vegetation transmissivity (or vegetation attenuation factor) and ω is the effective scattering albedo (polarization effects are not taken into account for this parameter).

Soil roughness effects are parameterized through a semi-empirical approach initially developed by Wang and Choudhury (1981) [45] and refined in more recent studies (Escorihuela et al., 2007 [46]; Lawrence et al., 2013 [47]; Parrens et al., 2016 [27]). The roughness modeling in SMOS-IC is based on three parameters (H_R, N_{RH} and N_{RV}) and the calculation of the soil reflectivity r_{GP} is given by:

$$r_{GP}(\theta) = r^*_{GP}(\theta)exp\Big[-H_R{\cdot}cos^{N_{RP}}(\theta)\Big] \quad (2)$$

where r^*_{GP} (P = H, V) is the reflectivity of a plane (specular) surface, which is computed from the Fresnel equations (Ulaby, 1982 [48]) as a function of θ and of the soil dielectric constant (ε), expressed as a function of SM, soil clay fraction and soil temperature using the model developed by Mironov et al. (2012) [49]. H_R accounts for the decrease of r_{GP} due to soil roughness effects and its value was estimated from global maps computed by Parrens et al. (2016) [32]. The values of N_{RP} (P = H, V) have been calibrated in Fernandez-Moran et al. (2015, 2016) [31,50]. Optimized values of $N_{RP} = -1$ (P = H, V) were obtained over low vegetation and $N_{RH} = 1$ and $N_{RV} = -1$ over forests.

Under the assumption of isotropic conditions and no dependence of the vegetation optical depth on polarization, the vegetation attenuation factor γ_P can be computed using the Beer's law as:

$$\gamma_p = exp\Big[-\tau/cos(\theta)\Big] \quad (3)$$

The retrieval of SM and τ involves the minimization of the following cost function x:

$$x = \frac{\sum_{i=1}^{N}\left(TB_p(\theta)_{mes} - TB_p(\theta)\right)^2}{\sigma(TB)^2} + \sum_{i=1}^{2}\frac{\left(P_i^{ini} - P_i\right)^2}{\sigma(P_i)^2} \quad (4)$$

where N is the number of observations for different viewing angles (θ) and both polarizations (H, V), $TB_P(\theta)_{mes}$ is the measured value over the SMOS pixels from the SMOSL3 TB product (presented in Section 2.2.2), $\sigma(TB)$ is the standard deviation associated with the brightness temperature measurements (this parameter was set to the constant value of 4 K in this study), $TB_P(\theta)$ is the brightness temperature calculated using Equation (1), P_i (i = 1, 2) is the value of the retrieved parameter (SM, τ); P_i^{ini} (i = 1, 2) is an a priori estimate of the parameter P_i; and $\sigma(P_i)$ is the standard deviation associated with this estimate. A constant initial value of 0.2 m^3/m^3 was considered for SM and $\sigma(SM)$ and the value of τ_{NAD} was set equal to a yearly average value (computed from previous runs) and $\sigma(\tau_{NAD})$ was computed as follows:

$$\sigma(\tau_{NAD}) = min(0.1 + 0.3{\cdot}\tau_{NAD},\ 0.3) \quad (5)$$

2.2.2. Effective Vegetation Scattering Albedo, Soil Roughness and Soil Texture Parameters

One of the most important features of the SMOS-IC product is the ability to test new calibrated values of ω (Fernandez-Moran et al, 2016 [31]) and H_R (Parrens et al., 2016 [32]. Table 1 presents these values for SMOS-IC and SMOSL3 V300 as a function of the IGBP land category classes. It must be noted that SMOSL3 V300 uses the ECOCLIMAP classification (Masson et al., 2003 [51]) and that in new versions of SMOSL3, IGBP land use maps could be used.

In SMOS-IC, the retrieval of SM and τ is performed over the totality of each pixel and the input parameters H_R and ω are consequently constant values for the whole pixel. However, due to the heterogeneity present in all pixels, the input H_R and ω parameters used in the retrieval are calculated by linear weighting the H_R and ω contribution according to the percentage of each IGBP class within the pixel based on the values provided in Table 1. For instance, if a pixel is covered by 60% of grasslands and 40% of croplands, the effective vegetation scattering albedo considered for that pixel is calculated as follows: $\omega = 0.60 \times 0.10 + 0.40 \times 0.12 = 0.108$. The assumption of linearity, which is questionable, was made here as it leads to a very simple correction, and as no other more physical and general formulation was available.

The soil texture in terms of clay content is obtained in the SMOS-IC product from the Food and Agriculture Organization map (FAO, 1988) [52]. This map is re-gridded in the same EASE 2.0 grid used by SMOSL3.

Table 1. Calibrated Values of ω and H_R as a Function of the IGBP Land Category Classes for SMOS-IC and SMOSL3.

Class	ω (SMOS-IC)	ω (SMOSL3 V300)	H_R (SMOS-IC)	H_R (SMOSL3 V300)
1—Evergreen needle leaf forest	0.06	0.06–0.08 *	0.30	0.30
2—Evergreen broadleaf forest	0.06	0.06–0.08 *	0.30	0.30
3—Deciduous needle leaf forest	0.06	0.06–0.08 *	0.30	0.30
4—Deciduous broadleaf forest	0.06	0.06–0.08 *	0.30	0.30
5—Mixed forests	0.06	0.06–0.08 *	0.30	0.30
6—Closed shrublands	0.10	0.00	0.27	0.10
7—Open shrublands	0.08	0.00	0.17	0.10
8—Woody savannas	0.06	0.00	0.30	0.10
9—Savannas	0.10	0.00	0.23	0.10
10—Grasslands	0.10	0.00	0.12	0.10
11—Permanent wetland	0.10	0.00	0.19	0.10
12—Croplands	0.12	0.00	0.17	0.10
13—Urban and built-up	0.10	0.00	0.21	0.10
14—Cropland/Natural Vegetation'Mosaic	0.12	0.00	0.22	0.10
15—Snow and ice	0.10	0.00	0.12	0.10
16—Barren and sparsely vegetated	0.12	0.00	0.02	0.10

* $\omega = 0.08$ over boreal forests, $\omega = 0.06$ over other forest types.

2.2.3. Quality Flags

The data filtering of the SMOS-IC product can be done through different scene and processing flags which are summarized in Tables 2 and 3. The scene flags indicate the presence of moderate and strong topography, frozen soil or polluted scene. *TB* data for pixels where the sum of the water, urban and ice fractions are higher than 10% are considered as polluted scene. For ECMWF soil temperatures below 273 K, the soil is considered as frozen. The processing flags help to filter out all cases suspected to give dubious results. Retrievals for which the RMSE values between the measured (L3 *TB*) and the L-MEB modeled *TB* data are larger than 12 K can be filtered out as suggested in Wigneron et al. (2012) [29]. These retrievals and the SM retrievals, which are out of the physical range (0–1 m^3/m^3), are flagged using a processing flag (Table 3).

In order to extend the number of retrievals and the spatial coverage of the retrievals of SM and τ, scene and processing flags were not all considered in this study. More details about the data filtering used in this study are given in Section 2.4.1.

Table 2. Description of the SMOS-IC Scene Flags.

Scene Flags	Description
Presence of moderate topography	Same filter as SMOSL3 V300
Presence of strong topography	Same filter as SMOSL3 V300
Polluted scene	Water, urban and ice fractions (according to the IGBP classification) represent less than 10% of the pixel
Frozen scene	Soil temperature < 273 K

Table 3. Description of the SMOS-IC Processing Flags.

Processing Flags	Description
SM retrieved successfully	
SM retrieved successfully but not recommended	RMSE < 12 K
Failed retrieval	SM < 0 or SM > 1 m^3/m^3

2.3. ECMWF and MODIS Data

The ECMWF dataset used in this study for the SM product inter-comparison was obtained from the SMOSL3 SM pre-processor. This ECMWF product has a spatial resolution of 625 km^2 and 1-day temporal resolution, using the same EASE 2.0 grid and interpolated in time and space to fit the SMOSL3 sampling resolutions. It is based on the ERA-Interim dataset. ERA-Interim uses a numerical weather prediction (NWP) system (IFS-Cy31r2) to produce reanalyzed data (Berrisford et al., 2011) [53].

The ECMWF soil surface (Level 1, top 0–7 cm soil layer) and soil deep temperature (Level 3, 28–100 cm) are used in the computation of the effective soil temperature for the SMOS-IC and SMOSL3 SM products following the parameterization of Wigneron et al. (2001) [54]. It is worth noting that, unlike the SMOSL3 SM product, the SMOS-IC processor does not use the ECMWF SM product to compute contributions from the fixed fractions (i.e., fraction of the scene over which the SM retrieval is not performed), and is only considered for evaluation purpose in this study. The ECMWF SM product represents the top 0–7 cm surface layer and it has been frequently compared to retrieved SM at global scale (Al-Yaari et al., 2014 [55]; Albergel et al., 2013 [56]; Leroux et al., 2014) [57]. ECMWF SM was found by Albergel et al. (2012) [58] to represent very well the SM variability at large scales. It is also known to give erroneous values in some areas (Louvet et al., 2015 [59]; Kerr et al., 2016 [11]).

The NDVI product used in this study was obtained from the 16-day NDVI MODIS Aqua and Terra data (MOD13A2), with a 1 km resolution. This product was re-gridded in the EASE 2.0 grid in order to make it comparable with SMOS-IC and SMOSL3 SM. Different studies have shown that τ at microwave frequencies has high spatial correspondences with MODIS NDVI (De Jeu and Owe, 2003 [60]; Andela et al., 2013 [61]) and also temporal correspondences regarding both seasonal and inter-annual scales (Tian et al., 2016a [62], 2016b [63]) even though both products have shown sensitivity to different aspects of the vegetation dynamics (Grant et al., 2016 [25]).

2.4. Inter-Comparison

The inter-comparison was made for both SMOS-IC and SMOSL3 products by direct comparison between SM (m^3/m^3) and τ, respectively, the ECMWF SM and MODIS NDVI products. This section explains the filtering, which was applied to the latter datasets and the metrics used in the evaluation process.

2.4.1. Data Filtering

In the evaluation step, only ascending SMOS SM retrievals were selected (Al-Yaari et al., 2014 [8,55]). For SMOS-IC retrievals, only *TB* values whose standard deviations were within radiometric accuracy were kept (*TB* with a standard deviation exceeding 5 K plus the *TB* radiometric accuracy were filtered out). Moreover, only retrievals meeting the following conditions were considered: (i) made

in the range of incidence angles of 20° to 55°; and (ii) with a range of angular values exceeding 10° (to ensure a sufficient sampling of the angular distribution).

For the SMOSL3 SM product, a quality index (DQX) estimates the retrieval quality. In this study, data with DQX > 0.06 m^3/m^3 were excluded. In parallel, the Level 3 RFI probability flag was used to filter out SM data contaminated by RFI. SM retrievals with an associated RFI probability higher than 20% and frozen areas were removed (surface temperature < 273 K). The SMOS-IC and SMOSL3 retrievals of SM and τ used in the study were inter-compared for the same dates. This means that all the Level 3 flags were implicitly applied to both the SMOS-IC and SMOSL3 data. For both SMOS products (SMOSL3 and SMOS-IC), SM values out of the range 0–0.6 m^3/m^3 (Dorigo et al., 2013 [64]) and τ values out of the range 0–2 were filtered out. We only considered pixels with temporal series of at least 15 values for the product inter-comparison.

In order to compare τ with MODIS NDVI, the daily τ values were re-gridded to 16-day mean values produced every 8 days following the same methodology as described in Grant et al. (2016) [25].

2.4.2. Metrics

For evaluation purposes, the following metrics were used: Pearson correlation coefficient (R), bias, root mean square difference (*RMSD*) and unbiased RMSD (*ubRMSD*). Equations for the calculation of the SM metrics are the following:

$$R = \frac{\sum_{i=1}^{n}\left(SM_{EC(i)} - \overline{SM_{EC}}\right)\left(SM_{SMOS(i)} - \overline{SM_{SMOS}}\right)}{\sqrt{\sum_{i=1}^{n}\left(SM_{EC(i)} - \overline{SM_{EC}}\right)^2 \sum_{i=1}^{n}\left(SM_{SMOS(i)} - \overline{SM_{SMOS}}\right)^2}} \quad (6)$$

$$bias = \overline{(SM_{SMOS} - SM_{EC})} \quad (7)$$

$$RMSD = \sqrt{\overline{(SM_{SMOS} - SM_{EC})^2}} \quad (8)$$

$$ubRMSD = \sqrt{RMSD^2 - bias^2} \quad (9)$$

where n is the number of SM data pairs, SM_{SMOS} is the SMOS SM product (SMOSL3 SM or SMOS-IC) and SM_{EC} is the ECMWF SM. The use of *RMSD* instead of root mean square error (RMSE) should be noted as ECMWF SM contain errors and cannot be considered as the "true" ground SM value (Al-Yaari et al., 2014 [55]). In this study, only significant correlations were considered by means of a p-value filtering for SM retrievals, i.e., pixels where the p-value was above 0.05 were filtered out.

In order to evaluate τ, R was calculated as follows:

$$R = \frac{\sum_{i=1}^{n}\left(NDVI_i - \overline{NDVI}\right)\left(\tau_{SMOS(i)} - \overline{\tau_{SMOS}}\right)}{\sqrt{\sum_{i=1}^{n}\left(NDVI_i - \overline{NDVI}\right)^2 \sum_{i=1}^{n}\left(\tau_{SMOS(i)} - \overline{\tau_{SMOS}}\right)^2}} \quad (10)$$

where τ_{SMOS} is the vegetation optical depth at nadir (τ) retrieved from the SMOSL3 or SMOS-IC product.

3. Results and Discussion

3.1. Soil Moisture

Figure 1 shows the values of the temporal mean SM over the globe and over the period 2010–2015 for the three SM datasets considered in this study: (a) SMOS-IC; (b) SMOSL3 SM; and (c) ECMWF. It should be kept in mind that ECMWF SM is representative of the first 0–7 cm of the soil surface (Albergel et al., 2012 [65]) and the inherent nature of the simulated soil moisture (Koster et al., 2009 [66]) is different to that measured by the SMOS satellite observations, which are sensitive to the first ~0–3 cm of the soil surface (Escorihuela et al., 2010 [67]; Njoku and Kong et al., 1977 [68]). In Figure 1,

ECMWF SM must be analyzed in terms of spatial patterns rather than absolute values. Although the images in Figure 1a,b, have many similarities, some spatial patterns shown by the ECMWF SM product are in better agreement with SMOS-IC than with SMOS L3 SM. For instance, over the Appalachian region in the Eastern US, SMOSL3 SM shows a dry area, whereas SMOS-IC SM is closer to ECMWF, as these regions are known to be relatively wetter than the regions of west and midwest (Sheffied et al., 2004 [69]; Fan et al., 2004 [70]). This was partly explained by differences between ECOCLIMAP and IGBP and the use of ECMWF SM data in Mahmoodi et al., 2015 [71]. On the other hand, drier retrievals were found for SMOS-IC in the intertropical regions of Africa, for instance over the savannas and grasslands of Sahel. Over these regions SMOS-L3 SM is closer to ECMWF SM than SMOS-IC SM.

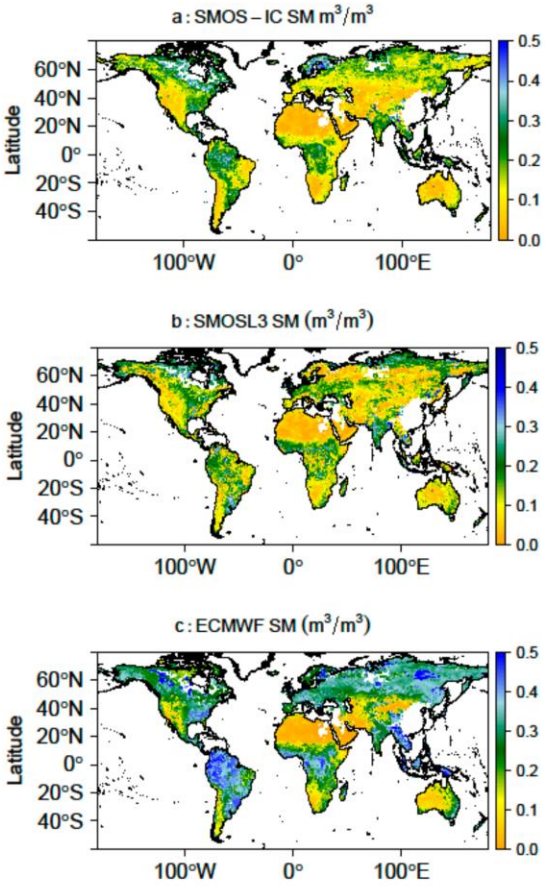

Figure 1. Temporal mean of soil moisture (m^3/m^3) during 2010–2015: (**a**) SMOS-IC (SMOS-INRA-CESBIO); (**b**) SMOSL3 SM (Level 3 SMOS soil moisture); and (**c**) ECMWF (European Center for Medium range Weather Forecasting) data. White values mean "no valid SMOS data".

Figure 2 displays different time series metrics derived from the direct comparison between SMOSL3 SM (Figure 2a) and SMOS-IC SM (Figure 2b) with ECMWF SM for 2010–2015. According to correlation (R) results, lowest R values were found in forests for both products. A lower number of negative R values were found between the SMOS-IC and ECMWF SM products. Conversely, SMOSL3 SM yielded negative correlations with ECMWF SM over several forest regions, namely the boreal forests of Alaska, Canada and Russia, and the tropical forests of Amazon and Congo basins. Over the non-forested biomes, R values were also found to be generally higher for SMOS-IC, when compared to

SMOSL3 SM. Substantial differences were found in terms of RMSD and ubRMSD. In general, lower values were obtained for the SMOS-IC product, especially over the intertropical regions of America and Africa (in terms of ubRMSD) and the boreal forests of Eurasia (in terms of RMSD). On the other hand, results do not show important differences in terms of bias between the two SMOS products. Both SMOS-IC and SMOSL3 SM products are generally much drier than ECMWF SM, except over some arid and semi-arid areas (deserts in central Asia and Australia, and Sahara in northern Africa) and north of Canada. However, SMOS-IC shows a wet bias in Northern Europe, which cannot be noted for SMOSL3. The general negative values of the bias can be partly explained by the difference between the sampling depth of the SMOS observations (~0–3 cm top soil layer) and the top soil layer considered in the modeled ECMWF SM (0–7 cm top soil layer). Considering this difference, the distinct SM bias patterns shown in Figure 2 should be interpreted with care.

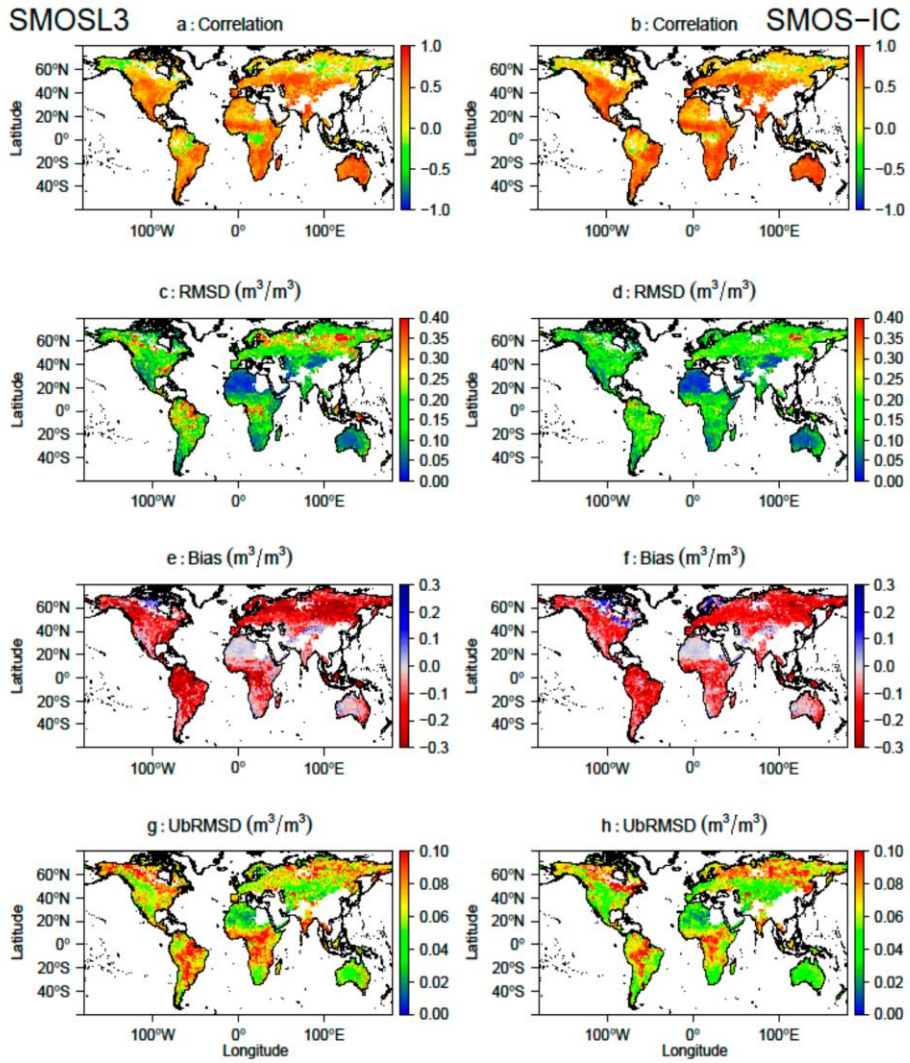

Figure 2. Pixel-based statistics during 2010–2015 computed between ECMWF SM simulations and: SMOSL3 SM (**left**); and SMOS-IC (**right**) SM retrievals: (**a**,**b**) correlation coefficient; (**c**,**d**) Root Mean Square Deviation (RMSD); (**e**,**f**) bias; and (**g**,**h**) unbiased Root Mean Square Deviation (ubRMSD).

A seasonal statistical analysis that separates cold and warm seasons was carried out and led to similar results to the ones presented above (Figure S1). Figure S1 shows that the ubRMSD is lower in the cold season, i.e., January–March (JFM) in the Northern Hemisphere and July–September (JAS) in the South Hemisphere.

Figure 3 is focused on the results in terms of correlation and ubRMSD, considered as first order criteria. It displays a world map which shows where the best correlation coefficient (R) and ubRMSD are obtained by comparing ECMWF SM with SMOS-IC SM (red) or SMOSL3 SM (blue) in the period 2010–2015. Areas where the result differs by less than 0.02 in terms of R values between SMOSL3 SM and SMOS-IC are represented in green color. This threshold is different for the ubRMSD metric and it was set to 0.005 m^3/m^3. It can be seen that the red color is dominant, meaning that SMOS-IC SM is generally closer to ECMWF in terms of temporal dynamics but there are some exceptions. For instance, regions colored in blue (SMOSL3 is closer to ECMWF than SMOS-IC) can be found for the ubRMSD metric, in northeastern Europe and northern Asia. It should be noted here that only pixels with significant correlations, i.e., p-value < 0.05 and a number of data >15 are presented.

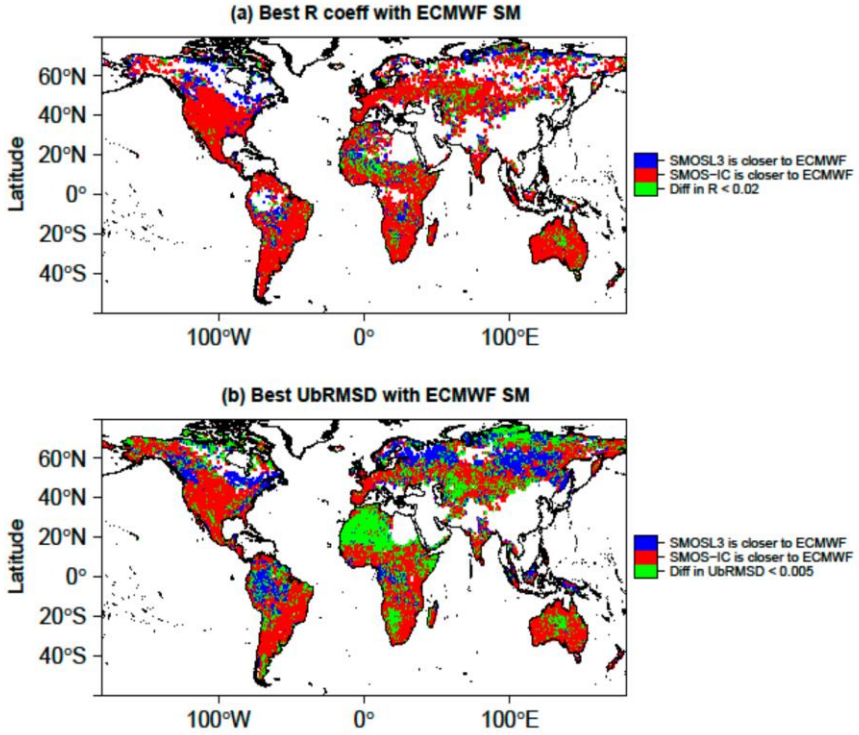

Figure 3. Comparison of the SMOS SM products with respect to ECMWF showing: (**a**) where SMOS-IC SM (red) or SMOSL3 SM (blue) leads to the best correlation coefficient, or where the difference in R < 0.02 (green) among both SMOS products; and (**b**) where SMOS-IC SM (red) or SMOSL3 SM (blue) lead to the lowest ubRMSE or where the difference in ubRMSD < 0.005 (green).

Figure 4 shows the spatial differences between SMOSL3 and SMOS-IC SM in terms of bias and ubRMSD. It can be observed that the most significant differences for bias were found for forest regions (Amazon and Congo basins, Boreal forests, etc.), where SMOSL3 is drier. In these areas, ubRMSD is also higher, contrary to deserts or barren regions as the Sahara or Central Australia, where the ubRMSD is close to zero.

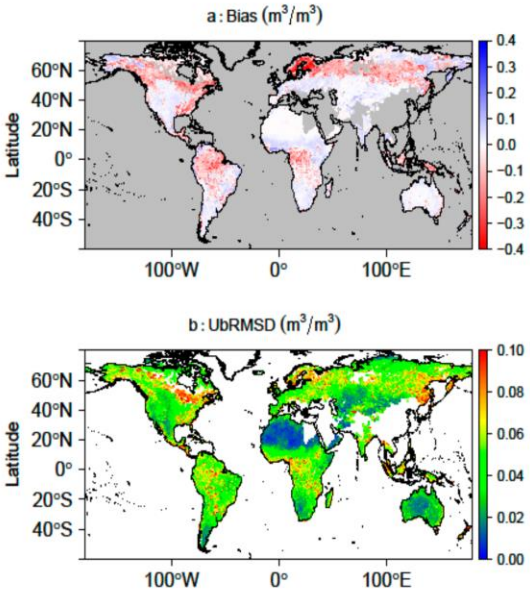

Figure 4. Mean bias (SMOSL3 minus SMOS-IC SM) and ubRMSD between SMOSL3 and SMOS-IC SM for 2010–2015.

In order to better assess the range of R and ubRMSD values, the dispersion diagrams displayed in Figure 5 show the scatter plot of both metrics for all pixels and for both SMOS products (SMOS-IC and SMOSL3 SM). In terms of correlation, the R values are generally larger for SMOS-IC. There are also a number of pixels where SMOSL3 SM yields negative correlations, whereas R is positive for SMOS-IC. In terms of ubRMSD, the largest number of pixels with lower ubRMSD corresponds to the SMOS-IC SM product.

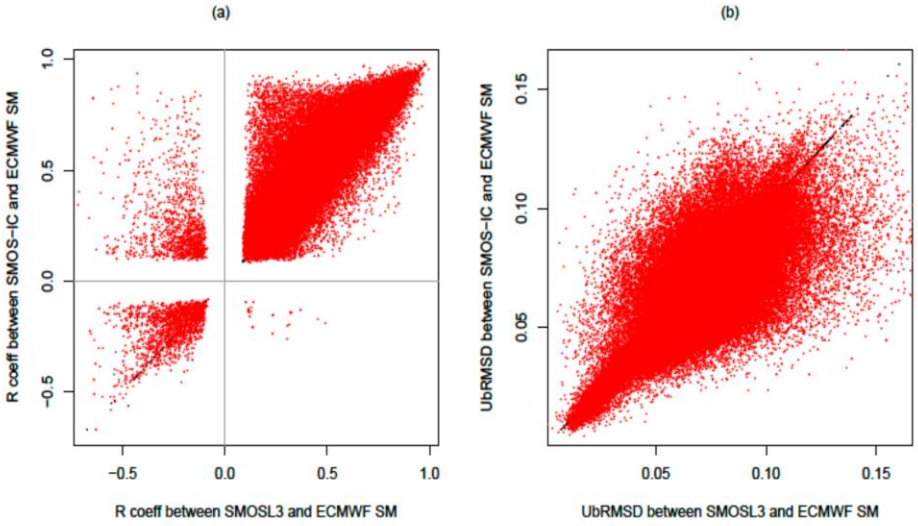

Figure 5. Scatter plot of correlation: (**a**) and ubRMSD values; (**b**) obtained by comparing both SMOS-IC and SMOSL3 SM to ECMWF SM.

3.2. Vegetation Optical Depth

The evaluation of the accuracy of the τ values retrieved from SMOS at global scale is not a simple issue due to the absence of a consensus on the reference values to be considered at large scale coming from models or in situ measurements. Some studies have been done at local scale. For instance, over croplands and grasslands, τ values at L-band vary generally between 0 and 0.6 (Saleh et al., 2006 [72], Wigneron et al., 2007 [24]). Over forests and from L-band radiometer measurements, Ferrazzoli et al. (2002) [73] found maximum values of τ ~0.9, and Grant et al. (2008) [74] found values of τ ~0.6–0.7 for a mature pine forest stand in *les Landes* forest in France, and τ ~1 for a mature deciduous (beech) canopy in Switzerland.

Figure 6 shows a global map of the temporal mean of the retrieved τ values for both SMOS-IC and SMOSL3 products. Both products show τ values that are sensitive to vegetation, as the highest τ values were found for the main boreal and tropical forests, and the minimum for dry areas, such as Inner Asia or Australia. It must be noted that the τ values coming from the SMOSL3 product were slightly larger than those obtained by the SMOS-IC product.

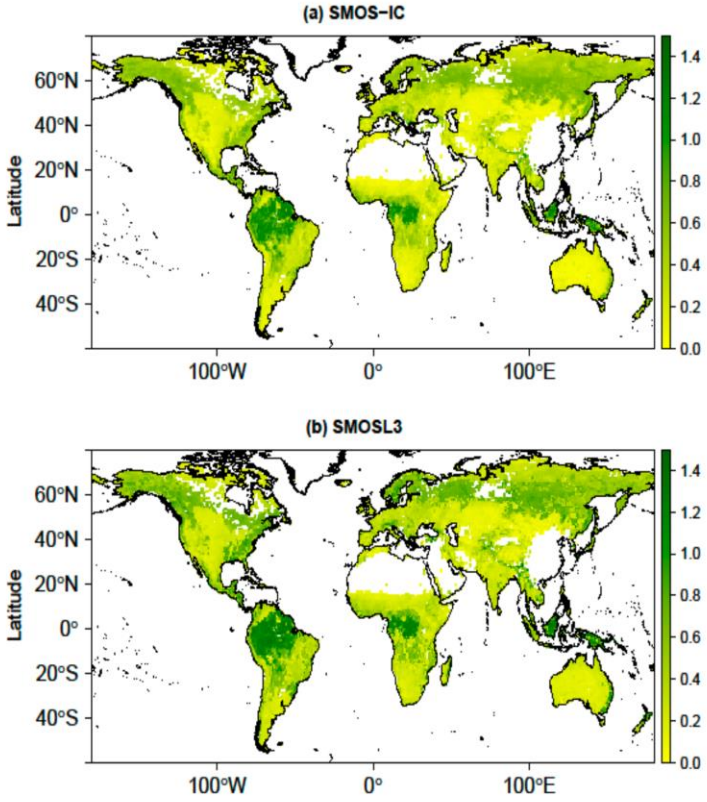

Figure 6. Temporal mean of τ during 2010–2015: (**a**) SMOS-IC; and (**b**) SMOSL3.

In order to identify possible patterns, Figure 7 shows a global map which illustrates the differences of τ between both SMOS datasets (SMOSL3 minus SMOS-IC). This result shows that the greatest differences between both τ datasets were found over some regions of the Northern Hemisphere, such as the east of USA, the north of Europe and also in the Amazon basin.

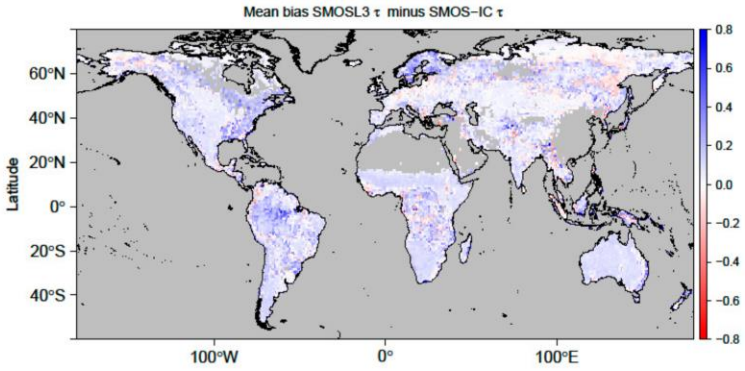

Figure 7. Mean bias: SMOSL3 τ minus SMOS-IC τ for 2010–2015.

Figure 8 shows the correlations obtained by comparing the SMOSC-IC and SMOSL3 τ datasets to MODIS NDVI. All correlations values are presented here including those not significant as done by Grant et al. (2016) [25]. It can be noted that slightly higher correlation values are generally obtained with SMOS-IC especially in the west of Mexico, the northeastern regions of Brazil and some parts of the Sahel. Conversely, slightly higher R values were obtained in western and central Europe with SMOSL3. The lowest correlations were found generally over forests for both SMOS products; a result which can be partly related to the tendency of NDVI to saturate for high biomass and LAI values. However, higher R values were obtained with SMOS-IC for some areas of the boreal forests and the tropical forests of Africa.

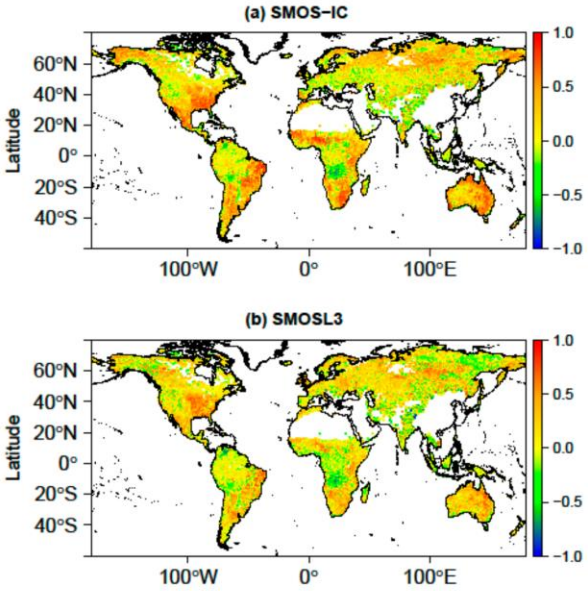

Figure 8. Correlation (R) values obtained between SMOS-IC τ and MODIS NDVI (**a**); and between SMOSL3 τ and MODIS NDVI (**b**).

In order to evaluate how NDVI represents the spatial differences in vegetation density, Figure 9 represents the spatial relation between NDVI and SMOS-IC and SMOSL3 τ. The results demonstrate that there is a general positive trend relating the spatial patterns of τ and NDVI. The latter saturates for

values of τ larger than ~0.7. It can be seen that the positive trend relating τ and NDVI is more distinct for SMOS-IC than for SMOSL3.

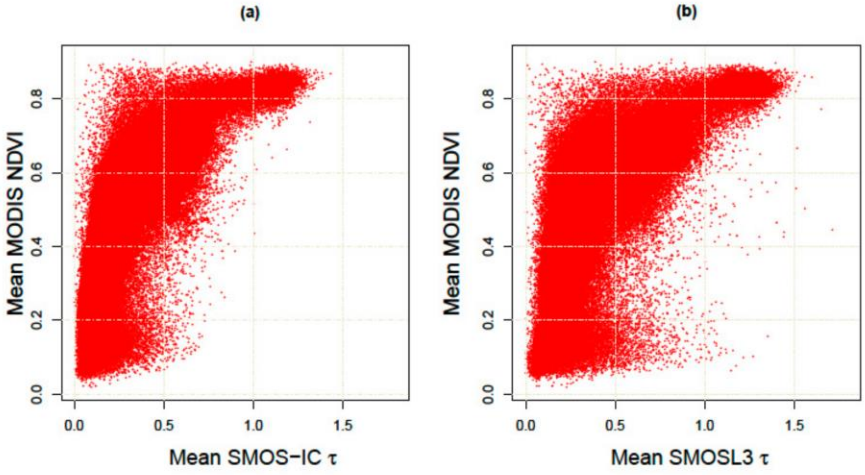

Figure 9. Scatter plot showing the spatial relationship between mean MODIS NDVI and mean SMOS-IC τ (**a**); and mean SMOSL3 τ (**b**).

Figure 10 presents a global map that shows for each pixel which τ dataset (SMOSL3 or SMOS-IC) leads to the largest correlation (R) values with MODIS NDVI. Over northern mid-latitudes, larger correlations were generally obtained with SMOSL3. However, except for these regions, the highest R values were generally obtained with SMOS-IC while no clear patterns were found in terms of longitude. Figure 11 shows a dispersion diagram in order to assess the range of correlation values found for both SMOS τ datasets against MODIS NDVI. The diagram generally yields positive correlations, although a non-negligible number of negative correlations can be noted for both SMOS products. The negative correlation values between τ and NDVI are difficult to explain. In some cases, negative values were found in dense forest areas and can be related to the saturation of NDVI for large biomass values (Grant et al., 2016 [25]).

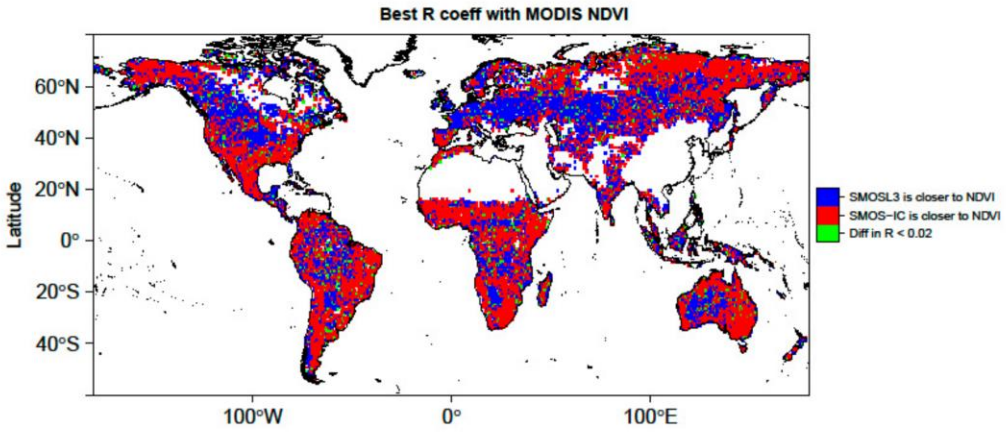

Figure 10. Comparison of SMOS-IC and SMOS-L3 τ products with respect to MODIS NDVI: higher correlation (R) values between SMOS-IC τ and MODIS NDVI (red) or between SMOSL3 τ and MODIS NDVI (blue) and where the difference in R < 0.02 (green).

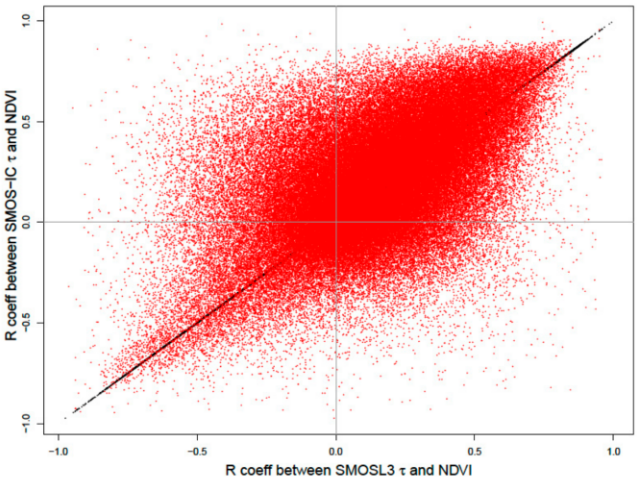

Figure 11. Scatter plot showing correlation values obtained between SMOS-IC τ and MODIS NDVI against correlation values obtained between the τ from SMOSL3 and MODIS NDVI.

4. Summary and Conclusions

The main objective of this study is to present an alternative SMOS SM and τ product, referred to as SMOS-IC, and compare it with model data. In terms of soil moisture, the presentation is based on an inter-comparison between SMOS-IC, the official Level 3 SMOS SM product (SMOSL3, V300), and a modeled SM product (ECMWF SM). The SMOS-IC product is based on the retrieval of SM and τ over pixels treated as homogeneous by means of the L-MEB model inversion. SMOS-IC uses the multi-angular and dual-polarization SMOSL3 *TB* product as the main input for the L-MEB model inversion. The L-MEB model input parameters (effective vegetation scattering albedo ω and the roughness parameter H_R) are estimated as a function of IGBP land category classes which compose the pixel. These parameter values are derived from previous analyses made by Fernandez-Moran et al. (2016) [31] and global maps of the roughness H_R parameter estimated by Parrens et al. (2016) [32]. Conversely, the SMOSL3 product considers different fractions over the pixel and performs SM and τ retrievals over the main fraction of the pixel (usually low vegetation) or over forests in some cases. In the SMOSL3 retrieval algorithm, the *TB* value of the pixel fraction, which is not considered in the retrieval (the forest fraction in general), is estimated based on auxiliary ECMWF SM data. This specific approach may lead to dry SM bias in forested regions, as noted by Wigneron et al. (2012) [29]. Currently, in the SMOSL3 V300 retrieval algorithm, the values of the vegetation and soil roughness parameters differ mainly between forest and low vegetation categories.

The SMOSL3 and SMOS-IC soil moisture retrievals were compared globally against ECMWF SM data for the period 2010–2015. This evaluation extends the work of Fernandez-Moran et al. (2016) [31] who evaluated a preliminary version of the SMOS-IC product at local scale using numerous in situ SM stations from ISMN and found higher R and lower ubRMSE with SMOS-IC than with the SMOSL3 V300 product. At global scale, both the SMOS-IC and SMOSL3 SM products were generally found to be drier than the ECMWF SM product. However, the different layers considered in the modeled ECMWF SM (top 0–7 cm soil layer) with respect to the remotely sensed SMOS SM (~top 0–3 cm soil layer), as well as the inherently different nature of simulated soil moisture (Koster et al., 2009 [66]), makes it difficult to truly assess the performance of the SMOS products in terms of bias at global scale. In terms of temporal variations, higher correlation values and lower ubRMSD values were generally found between SMOS-IC SM and ECMWF SM, than between SMOSL3 SM and ECMWF SM.

The ECMWF SM dataset is not "truth", and a larger inter-comparison of SMOS-IC and SMOSL3 against other modeled SM products such as MERRA (Modern-Era Retrospective analysis for Research

and Applications) (Reichle et al., 2011 [75]) or remotely sensed data (such as SMAP, AMSR-E, and ASCAT) should be made in the future to confirm the very preliminary results found here. In terms of τ values, the SMOS-IC and SMOSL3 τ products were compared to MODIS NDVI values over 2010–2015 in terms of correlation values. The SMOS-IC τ product presents a slightly lower range of values (~0–1.3) than the one obtained with the SMOSL3 τ product (~0–1.5). These ranges of τ values (obtained for both SMOSL3 and SMOS-IC) are in good agreement with the ranges of retrieved τ values based on in situ L-band radiometric measurements (τ ~0.6–1.0) performed over mature coniferous and deciduous forests in Europe. In general, higher correlation values were obtained between SMOS-IC τ and MODIS NDVI, than between SMOSL3 τ and MODIS NDVI.

The τ results should also be interpreted with care: the NDVI index is derived from optical sensors while the τ index is derived from L-band microwave measurements and therefore can sense deeper through the vegetation canopy. Moreover, the NDVI index is used to monitor the green vegetation, while the τ index is related to the whole vegetation water content (including stems, trunks, branches and senescent vegetation elements). Thus, at L-band, the NDVI index (as the LAI index) is only a proxy, which is used to provide an estimate of τ over rather low vegetation covers during the vegetation growth (O'Neill et al, 2012 [37]; Wigneron et al., 2007 [24]; Lawrence et al., 2014 [76]; Grant et al., 2016 [25]). A larger inter-comparison of the SMOS-IC and SMOSL3 τ products against different vegetation datasets (remotely sensed products, LAI, forest biomass) should be made in the future to confirm the results found in this study.

As for the Level 2 and 3 algorithms, based on rather complex and detailed concepts and auxiliary datasets, the simple SMOS-IC algorithm will be improved regularly and will be used to improve the L2 and L3 SMOS retrieval algorithms. These different approaches are complementary and a regular inter-comparison analysis between them should be of great benefit to improve the L-MEB inversion, and ultimately the SM and τ products retrieved from the SMOS observations.

Supplementary Materials: The following are available online at www.mdpi.com/2072-4292/9/5/457/s1, Figure S1: Pixel-based ubRMSD during 2010–2015 computed between ECMWF SM simulations and: SMOSL3 SM (**left**); and SMOS-IC (**right**) SM retrievals: (**a**,**b**) January-March (JFM); (**c**,**d**) July-September (JAS).

Acknowledgments: The authors would like to thank the TOSCA (Terre Océan Surfaces Continentales et Atmosphère) CNES program and the European Space Agency (ESA) for funding this study. The authors acknowledge CATDS for the SMOSL3 dataset (http://catds.ifremer.fr) and the cooperation of the different soil moisture in situ networks of the International Soil Moisture Network (ISMN) project.

Author Contributions: Jean-Pierre Wigneron and Roberto Fernandez-Moran designed the SMOS-IC product with the helpful contribution of CESBIO. Arnaud Mialon and Ali Mahmoodi optimized the code, improved the data format and processed the dataset at CESBIO. Amen Al-Yaari made the analysis of the IC data and produced all the figures; Yann Kerr. Gabrielle de Lannoy, Ahmad Al Bitar, Nemesio Rodriguez-Fernandez and Ernesto Lopez-Baeza provided scientific expertise. Roberto Fernandez-Moran and Jean-Pierre Wigneron wrote the paper.

Conflicts of Interest: The authors declare no conflicts of interest.

References

1. Kerr, Y.H.; Waldteufel, P.; Richaume, P.; Wigneron, J.P.; Ferrazzoli, P.; Mahmoodi, A.; Al Bitar, A.; Cabot, F.; Gruhier, C.; Juglea, S.E.; et al. The SMOS Soil Moisture Retrieval Algorithm. *Geosci. Remote Sens.* **2012**, *50*, 1384–1403. [CrossRef]
2. Entekhabi, D.; Njoku, E.G.; O'Neill, P.E.; Kellogg, K.H.; Crow, W.T.; Edelstein, W.N.; Entin, J.K.; Goodman, S.D.; Jackson, T.J.; Johnson, J.; et al. The soil moisture active passive (SMAP) mission. *Proc. IEEE* **2010**, *98*, 704–716. [CrossRef]
3. Brocca, L.; Melone, F.; Moramarco, T.; Wagner, W.; Naeimi, V.; Bartalis, Z.; Hasenauer, S. Improving runoff prediction through the assimilation of the ASCAT soil moisture product. *Hydrol. Earth Syst. Sci.* **2010**, *14*, 1881–1893. [CrossRef]
4. Hollmann, R.; Merchant, C.J.; Saunders, R.; Downy, C.; Buchwitz, M.; Cazenave, A.; Chuvieco, E.; Defourny, P.; De Leeuw, G.; Forsberg, R.; et al. The ESA climate change initiative: Satellite data records for essential climate variables. *Bull. Am. Meteorol. Soc.* **2013**, *94*, 1541–1552. [CrossRef]

5. Al Bitar, A.; Mialon, A.; Kerr, Y.; Cabot, F.; Richaume, P.; Jacquette, E.; Quesney, A.; Mahmoodi, A.; Tarot, S.; Parrens, M.; et al. The Global SMOS Level 3 daily soil moisture and brightness temperature maps. *Earth Syst. Sci. Data Discuss.* **2017**, in press. [CrossRef]
6. Kerr, Y.H.; Waldteufel, P.; Wigneron, J.P.; Martinuzzi, J.M.; Font, J.; Berger, M. Soil moisture retrieval from space: The Soil Moisture and Ocean Salinity (SMOS) mission. *IEEE Trans. Geosci. Remote Sens.* **2001**, *39*, 1729–1735. [CrossRef]
7. Mialon, A.; Richaume, P.; Leroux, D.; Bircher, S.; Al Bitar, A.; Pellarin, T.; Wigneron, J.P.; Kerr, Y.H. Comparison of Dobson and Mironov dielectric models in the SMOS soil moisture retrieval algorithm. *IEEE Trans. Geosci. Remote Sens.* **2015**, *53*, 3084–3094. [CrossRef]
8. Al-Yaari, A.; Wigneron, J.P.; Ducharne, A.; Kerr, Y.H.; Wagner, W.; De Lannoy, G.; Reichle, R.; Al Bitar, A.; Dorigo, W.; Richaume, P.; et al. Global-scale comparison of passive (SMOS) and active (ASCAT) satellite based microwave soil moisture retrievals with soil moisture simulations (MERRA-Land). *Remote Sens. Environ.* **2014**, *152*, 614–626. [CrossRef]
9. Al-Yaari, A.; Wigneorn, J.P.; Ducharne, A.; Kerr, Y.; Fernandez-Moran, R.; Parrens, M.; Al Bitar, A.; Mialon, A.; Richaume, P. Evaluation of the most recent reprocessed SMOS soil moisture products: Comparison between SMOS level 3 V246 and V272. In Proceedings of the 2015 IEEE International Geoscience and Remote Sensing Symposium (IGARSS), Milan, Italy, 26–31 July 2015.
10. Al-Yaari, A.; Wigneron, J.-P.; Kerr, Y.; Rodriguez-Fernandez, N.; O'Neill, P.E.; Jackson, T.J.; De Lannoy, G.J.M.; Al Bitar, A.; Mialon, A.; Richaume, P.; et al. Evaluating soil moisture retrievals from ESA's SMOS and NASA's SMAP brightness temperature datasets. *Remote Sens. Environ.* **2017**, *193*, 257–273. [CrossRef]
11. Kerr, Y.H.; Al-Yaari, A.; Rodriguez-Fernandez, N.; Parrens, M.; Molero, B.; Leroux, D.; Bircher, S.; Mahmoodi, A.; Mialon, A.; Richaume, P.; et al. Overview of SMOS performance in terms of global soil moisture monitoring after six years in operation. *Remote Sens. Environ.* **2016**, *180*, 40–63. [CrossRef]
12. Wigneron, J.-P.; Jackson, T.J.; O'Neill, P.; De Lannoy, G.; de Rosnay, P.; Walker, J.P.; Ferrazzoli, P.; Mironov, V.; Bircher, S.; Grant, J.P.; et al. Modelling the passive microwave signature from land surfaces: A review of recent results and application to the L-band SMOS & SMAP soil moisture retrieval algorithms. *Remote Sens. Environ.* **2017**, *192*, 238–262.
13. Rahmoune, R.; Ferrazzoli, P.; Kerr, Y.H.; Richaume, P. SMOS level 2 retrieval algorithm over forests: Description and generation of global maps. *IEEE J. Sel. Top. Appl. Earth Obs. Remote Sens.* **2013**, *6*, 1430–1439. [CrossRef]
14. Rahmoune, R.; Ferrazzoli, P.; Singh, Y.K.; Kerr, Y.H.; Richaume, P.; Al Bitar, A. SMOS retrieval results over forests: Comparisons with independent measurements. *IEEE J. Sel. Top. Appl. Earth Obs. Remote Sens.* **2014**, *7*, 3858–3866. [CrossRef]
15. Schwank, M.; Mätzler, C.; Guglielmetti, M.; Flühler, H. L-band radiometer measurements of soil water under growing clover grass. *IEEE Trans. Geosci. Remote Sens.* **2005**, *43*, 2225–2236. [CrossRef]
16. Schwank, M.; Wigneron, J.P.; López-Baeza, E.; Völksch, I.; Mätzler, C.; Kerr, Y.H. L-band radiative properties of vine vegetation at the MELBEX III SMOS cal/val site. *IEEE Trans. Geosci. Remote Sens.* **2012**, *50*, 1587–1601. [CrossRef]
17. Jackson, T.J.; Schmugge, T.J. Vegetation effects on the microwave emission of soils. *Remote Sens. Environ.* **1991**, *36*, 203–212. [CrossRef]
18. Mo, T.; Choudhury, B.J.; Schmugge, T.J.; Wang, J.R.; Jackson, T.J. A model for microwave emission from vegetation-covered fields. *J. Geophys. Res.* **1982**, *87*, 11229. [CrossRef]
19. Wigneron, J.P.; Chanzy, A.; Calvet, J.C.; Bruguier, N. A simple algorithm to retrieve soil moisture and vegetation biomass using passive microwave measurements over crop fields. *Remote Sens. Environ.* **1995**, *51*, 331–341. [CrossRef]
20. Grant, J.P.; Wigneron, J.P.; Drusch, M.; Williams, M.; Law, B.E.; Novello, N.; Kerr, Y. Investigating temporal variations in vegetation water content derived from SMOS optical depth. In Proceedings of the 2012 IEEE International Geoscience and Remote Sensing Symposium (IGARSS), Munich, Germany, 22–27 July 2012.
21. Schneebeli, M.; Wolf, S.; Kunert, N.; Eugster, W.; Mätzler, C. Relating the X-band opacity of a tropical tree canopy to sapflow, rain interception and dew formation. *Remote Sens. Environ.* **2011**, *115*, 2116–2125. [CrossRef]

22. Guglielmetti, M.; Schwank, M.; Mätzler, C.; Oberdörster, C.; Vanderborght, J.; Flühler, H. FOSMEX: Forest soil moisture experiments with microwave radiometry. *IEEE Trans. Geosci. Remote Sens.* **2008**, *46*, 727–735. [CrossRef]
23. Patton, J.; Member, S.; Hornbuckle, B. Initial validation of smos vegetation optical thickness in Iowa. *IEEE Geosci. Remote Sens. Lett.* **2013**, *10*, 647–651. [CrossRef]
24. Wigneron, J.P.; Kerr, Y.; Waldteufel, P.; Saleh, K.; Escorihuela, M.J.; Richaume, P.; Ferrazzoli, P.; de Rosnay, P.; Gurney, R.; Calvet, J.C.; et al. L-band microwave emission of the biosphere (L-MEB) model: Description and calibration against experimental data sets over crop fields. *Remote Sens. Environ.* **2007**, *107*, 639–655. [CrossRef]
25. Grant, J.P.; Wigneron, J.P.; De Jeu, R.A.M.; Lawrence, H.; Mialon, A.; Richaume, P.; Al Bitar, A.; Drusch, M.; van Marle, M.J.E.; Kerr, Y.; et al. Comparison of SMOS and AMSR-E vegetation optical depth to four MODIS-based vegetation indices. *Remote Sens. Environ.* **2016**, *172*, 87–100. [CrossRef]
26. Fernandez-Moran, R.; Wigneron, J.-P.; Lopez-Baeza, E.; Al-Yaari, A.; Bircher, S.; Coll-Pajaron, A.; Mahmoodi, A.; Parrens, M.; Richaume, P.; Kerr, Y. Analyzing the impact of using the SRP (Simplified roughness parameterization) method on soil moisture retrieval over different regions of the globe. In Proceedings of the 2015 IEEE International Geoscience and Remote Sensing Symposium (IGARSS), Milan, Italy, 26–31 July 2015.
27. Parrens, M.; Wigneron, J.-P.; Richaume, P.; Al Bitar, A.; Mialon, A.; Fernandez-Moran, R.; Al-Yaari, A.; O'Neill, P.; Kerr, Y. Considering combined or separated roughness and vegetation effects in soil moisture retrievals. *Int. J. Appl. Earth Obs. Geoinf.* **2017**, *55*, 73–86. [CrossRef]
28. Wigneron, J.P.; Chanzy, A.; Kerr, Y.H.; Lawrence, H.; Shi, J.; Escorihuela, M.J.; Mironov, V.; Mialon, A.; Demontoux, F.; De Rosnay, P.; et al. Evaluating an improved parameterization of the soil emission in L-MEB. *IEEE Trans. Geosci. Remote Sens.* **2011**, *49*, 1177–1189. [CrossRef]
29. Wigneron, J.P.; Schwank, M.; Baeza, E.L.; Kerr, Y.; Novello, N.; Millan, C.; Moisy, C.; Richaume, P.; Mialon, A.; Al Bitar, A.; et al. First evaluation of the simultaneous SMOS and ELBARA-II observations in the Mediterranean region. *Remote Sens. Environ.* **2012**, *124*, 26–37. [CrossRef]
30. Kaufman, Y.J.; Justice, C.O.; Flynn, L.P.; Kendall, J.D.; Prins, E.M.; Giglio, L.; Ward, D.E.; Menzel, W.P.; Setzer, A.W. Potential global fire monitoring from EOS-MODIS. *J. Geophys. Res.* **1998**, *103*, 32215–32238. [CrossRef]
31. Fernandez-Moran, R.; Wigneron, J.-P.; De Lannoy, G.; Lopez-Baeza, E.; Mialon, A.; Mahmoodi, A.; Parrens, M.; Al Bitar, A.; Richaume, P.; Kerr, Y. Calibrating the effective scattering albedo in the SMOS algorithm: Some first results. In Proceedings of the 2016 IEEE International Geoscience and Remote Sensing Symposium (IGARSS), Beijing, China, 10–16 July 2016.
32. Parrens, M.; Wigneron, J.P.; Richaume, P.; Mialon, A.; Al Bitar, A.; Fernandez-Moran, R.; Al-Yaari, A.; Kerr, Y.H. Global-scale surface roughness effects at L-band as estimated from SMOS observations. *Remote Sens. Environ.* **2016**, *181*, 122–136. [CrossRef]
33. Rouse, J.W.; Haas, R.H.; Schell, J.A. *Monitoring the Vernal Advancement and Retrogradation (Greenwave Effect) of Natural Vegetation*; NASA Goddard Space Flight Center: Texas, TX, USA, 1974; pp. 1–8.
34. Guglielmetti, M.; Schwank, M.; Mätzler, C.; Oberdörster, C.; Vanderborght, J.; Flühler, H. Measured microwave radiative transfer properties of a deciduous forest canopy. *Remote Sens. Environ.* **2007**, *109*, 523–532. [CrossRef]
35. Santi, E.; Paloscia, S.; Pampaloni, P.; Pettinato, S. Ground-based microwave investigations of forest plots in Italy. *IEEE Trans. Geosci. Remote Sens.* **2009**, *47*, 3016–3025. [CrossRef]
36. Qi, J.; Chehbouni, A.; Huete, A.R.; Kerr, Y.H.; Sorooshian, S. A modified soil adjusted vegetation index. *Remote Sens. Environ.* **1994**, *48*, 119–126. [CrossRef]
37. O'Neill, P.; Chan, S.; Njoku, E.; Jackson, T.; Bindlish, R. *Soil Moisture Active Passive (SMAP) Algorithm Theoretical Basis Document (ATBD). SMAP Level 2 & 3 Soil Moisture (Passive), (L2_SM_P, L3_SM_P)*; JPL: Pasadena, CA, USA, 2012.
38. Corbella, I.; Torres, F.; Duffo, N.; González-Gambau, V.; Pablos, M.; Duran, I.; Martín-Neira, M. MIRAS calibration and performance: Results from the SMOS in-orbit commissioning phase. *IEEE Trans. Geosci. Remote Sens.* **2011**, *49*, 3147–3155. [CrossRef]
39. Armstrong, R.; Brodzik, M.J.; Varani, A. The NSIDC EASE-Grid: Addressing the need for a common, flexible, mapping and gridding scheme. *Earth Syst. Monit.* **1997**, *7*, 6–7.

40. A Versatile Set of Equal-Area Projections and Grids. Available online: http://www.ncgia.ucsb.edu/globalgrids-book/ease_grid/ (accessed on 5 May 2017).
41. Kerr, Y.; Jacquette, E.; Al Bitar, A.; Cabot, F.; Mialon, A.; Richaume, P.; Quesney, A.; Berthon, L. *CATDS SMOS L3 Soil Moisture Retrieval Processor Algorithm Theoretical Baseline Document (ATBD)*; CESBIO: Toulouse, France, 2013.
42. Jacquette, E.; Al Bitar, A.; Mialon, A.; Kerr, Y.; Quesney, A.; Cabot, F.; Richaume, P. SMOS CATDS level 3 global products over land. *Proc. SPIE* **2016**. [CrossRef]
43. Oliva, R.; Daganzo-Eusebio, E.; Kerr, Y.H.; Mecklenburg, S.; Nieto, S.; Richaume, P.; Gruhier, C. SMOS radio frequency interference scenario: Status and actions taken to improve the RFI environment in the 1400–1427-MHZ passive band. *IEEE Trans. Geosci. Remote Sens.* **2012**, *50*, 1427–1439. [CrossRef]
44. Khazaal, A.; Anterrieu, E.; Cabot, F.; Kerr, Y.H. Impact of Direct Solar Radiations Seen by the Back-Lobes Antenna Patterns of SMOS on the Retrieved Images. *IEEE J. Sel. Top. Appl. Earth Obs. Remote Sens.* **2016**, *PP*, 1–8. [CrossRef]
45. Wang, J.R.; Choudhury, B.J. Remote sensing of soil moisture content, over bare field at 1.4 GHz frequency. *J. Geophys. Res.* **1981**, *86*, 5277–5282. [CrossRef]
46. Escorihuela, M.J.; Kerr, Y.H.; De Rosnay, P.; Wigneron, J.P.; Calvet, J.C.; Lemaître, F. A simple model of the bare soil microwave emission at L-band. *IEEE Trans. Geosci. Remote Sens.* **2007**, *45*, 1978–1987. [CrossRef]
47. Lawrence, H.; Wigneron, J.-P.; Demontoux, F.; Mialon, A.; Kerr, Y.H. Evaluating the Semiempirical H-Q Model Used to Calculate the L-Band Emissivity of a Rough Bare Soil. *IEEE Trans. Geosci. Remote Sens.* **2013**, *51*, 4075–4084. [CrossRef]
48. Ulaby, F.T.; Moore, R.K.; Fung, A.K. *Microwave Remote Sensing Active and Passive Volume II: Radar Remote Sensing and Surface Scattering and Emission Theory*; Addison Wesley: New York, NY, USA, 1982; Volume 2.
49. Mironov, V.; Kerr, Y.; Member, S.; Wigneron, J.; Member, S. Temperature- and Texture-Dependent Dielectric Model for Moist Soils at 1.4 GHz. *IEEE Geosci. Remote Sens. Lett.* **2012**, *10*, 1–5. [CrossRef]
50. Fernandez-Moran, R.; Wigneron, J.P.; Lopez-Baeza, E.; Al-Yaari, A.; Coll-Pajaron, A.; Mialon, A.; Miernecki, M.; Parrens, M.; Salgado-Hernanz, P.M.; Schwank, M.; et al. Roughness and vegetation parameterizations at L-band for soil moisture retrievals over a vineyard field. *Remote Sens. Environ.* **2015**, *170*, 269–279. [CrossRef]
51. Masson, V.; Champeaux, J.L.; Chauvin, F.; Meriguet, C.; Lacaze, R. A global database of land surface parameters at 1-km resolution in meteorological and climate models. *J. Clim.* **2003**, *16*, 1261–1282. [CrossRef]
52. FAO; UNESCO. *Soil Map of the World, Revised Legend*; Food and Agriculture Organization of the United Nations: Rome, Italy, 1988.
53. Berrisford, P.; Kållberg, P.; Kobayashi, S.; Dee, D.; Uppala, S.; Simmons, A.J.; Poli, P.; Sato, H. Atmospheric conservation properties in ERA-Interim. *Q. J. R. Meteorol. Soc.* **2011**, *137*, 1381–1399. [CrossRef]
54. Wigneron, J.-P.; Laguerre, L.; Kerr, Y.H. A simple parameterization of the L-band microwave emission from rough agricultural soils. *IEEE Trans. Geosci. Remote Sens.* **2001**, *39*, 1697–1707. [CrossRef]
55. Al-Yaari, A.; Wigneron, J.P.; Ducharne, A.; Kerr, Y.; de Rosnay, P.; de Jeu, R.; Govind, A.; Al Bitar, A.; Albergel, C.; Muñoz-Sabater, J.; et al. Global-scale evaluation of two satellite-based passive microwave soil moisture datasets (SMOS and AMSR-E) with respect to Land Data Assimilation System estimates. *Remote Sens. Environ.* **2014**, *149*, 181–195. [CrossRef]
56. Albergel, C.; Dorigo, W.; Balsamo, G.; Muñoz-Sabater, J.; de Rosnay, P.; Isaksen, L.; Brocca, L.; de Jeu, R.; Wagner, W. Monitoring multi-decadal satellite earth observation of soil moisture products through land surface reanalyses. *Remote Sens. Environ.* **2013**, *138*, 77–89. [CrossRef]
57. Leroux, D.J.; Kerr, Y.H.; Al Bitar, A.; Bindlish, R.; Member, S.; Jackson, T.J.; Berthelot, B.; Portet, G. Comparison Between SMOS, VUA, ASCAT, and ECMWF soil moisture products over four watersheds in US. *IEEE Trans. Geos. Remote Sens.* **2014**, *52*, 1562–1571. [CrossRef]
58. Albergel, C.; de Rosnay, P.; Gruhier, C.; Muñoz-Sabater, J.; Hasenauer, S.; Isaksen, L.; Kerr, Y.; Wagner, W. Evaluation of remotely sensed and modelled soil moisture products using global ground-based in situ observations. *Remote Sens. Environ.* **2012**, *118*, 215–226. [CrossRef]
59. Louvet, S.; Pellarin, T.; Al Bitar, A.; Cappelaere, B.; Galle, S.; Grippa, M.; Gruhier, C.; Kerr, Y.; Lebel, T.; Mialon, A.; et al. SMOS soil moisture product evaluation over West-Africa from local to regional scale. *Remote Sens. Environ.* **2015**, *156*, 383–394. [CrossRef]

60. De Jeu, R.A.M.; Owe, M. Further validation of a new methodology for surface moisture and vegetation optical depth retrieval. *Int. J. Remote Sens.* **2003**, *24*, 4559–4578. [CrossRef]
61. Andela, N.; Liu, Y.Y.; Van Dijk, A.I.J.M.; De Jeu, R.A.M.; McVicar, T.R. Global changes in dryland vegetation dynamics (1988-2008) assessed by satellite remote sensing: Comparing a new passive microwave vegetation density record with reflective greenness data. *Biogeosciences* **2013**, *10*, 6657–6676. [CrossRef]
62. Tian, F.; Brandt, M.; Liu, Y.Y.; Rasmussen, K.; Fensholt, R. Mapping gains and losses in woody vegetation across global tropical drylands. *Glob. Chang. Biol.* **2016**, *23*, 1748–1760. [CrossRef] [PubMed]
63. Tian, F.; Brandt, M.; Liu, Y.Y.; Verger, A.; Tagesson, T.; Diouf, A.A.; Rasmussen, K.; Mbow, C.; Wang, Y.; Fensholt, R. Remote sensing of vegetation dynamics in drylands: Evaluating vegetation optical depth (VOD) using AVHRR NDVI and in situ green biomass data over West African Sahel. *Remote Sens. Environ.* **2016**, *177*, 265–276. [CrossRef]
64. Dorigo, W.A.; Xaver, A.; Vreugdenhil, M.; Gruber, A.; Hegyiová, A.; Sanchis-Dufau, A.D.; Zamojski, D.; Cordes, C.; Wagner, W.; Drusch, M. Global Automated Quality Control of In Situ Soil Moisture Data from the International Soil Moisture Network. *Vadose Zone J.* **2013**. [CrossRef]
65. Albergel, C.; de Rosnay, P.; Balsamo, G.; Isaksen, L.; Muñoz-Sabater, J. Soil moisture analyses at ECMWF: evaluation using global ground-based in situ observations. *J. Hydrometeorol.* **2012**, *13*, 1442–1460. [CrossRef]
66. Koster, R.D.; Guo, Z.C.; Yang, R.Q.; Dirmeyer, P.A.; Mitchell, K.; Puma, M.J. On the Nature of Soil Moisture in Land Surface Models. *J. Clim.* **2009**, *22*, 4322–4335. [CrossRef]
67. Escorihuela, M.J.; Chanzy, A.; Wigneron, J.P.; Kerr, Y.H. Effective soil moisture sampling depth of L-band radiometry: A case study. *Remote Sens. Environ.* **2010**, *114*, 995–1001. [CrossRef]
68. Njoku, E.G.; Kong, J.-A. Theory for passive microwave remote sensing of near-surface soil moisture. *J. Geophys. Res.* **1977**, *82*, 3108–3118. [CrossRef]
69. Sheffield, J.; Goteti, G.; Wen, F.; Wood, E.F. A simulated soil moisture based drought analysis for the United States. *J. Geophys. Res. D Atmos.* **2004**, *109*, 1–19. [CrossRef]
70. Fan, Y.; van den Dool, H. Climate prediction center global monthly soil moisture data set at 0.5° resolution for 1948 to present. *J. Geophys. Res. D Atmos.* **2004**, *109*, D10102. [CrossRef]
71. Mahmoodi, A.; Richaume, P.; Kerr, Y.; Mialon, A.; Bircher, S.; Leroux, D. Evaluation of MODIS IGBP land cover data on the SMOS Level 2 soil soisture retrievals. In Proceedings of the 2nd SMOS Science Conference, Madrid, Spain, 25–29 May 2015.
72. Saleh, K.; Wigneron, J.P.; De Rosnay, P.; Calvet, J.C.; Kerr, Y. Semi-empirical regressions at L-band applied to surface soil moisture retrievals over grass. *Remote Sens. Environ.* **2006**, *101*, 415–426. [CrossRef]
73. Ferrazzoli, P.; Guerriero, L.; Wigneron, J.P. Simulating L-band emission of forests in view of future satellite applications. *IEEE Trans. Geosci. Remote Sens.* **2002**, *40*, 2700–2708. [CrossRef]
74. Grant, J.P.; Saleh-Contell, K.; Wigneron, J.-P.; Guglielmetti, M.; Kerr, Y.H.; Schwank, M.; Skou, N.; Van de Griend, A. Calibration of the L-MEB model over a conniferous and a deciduous forest. *IEEE Trans. Geosci. Remote Sens.* **2008**, *46*, 808–818. [CrossRef]
75. Reichle, R.H.; Koster, R.D.; De Lannoy, G.J.M.; Forman, B.A.; Liu, Q.; Mahanama, S.P.P.; Toure, A. Assessment and enhancement of MERRA land surface hydrology estimates. *J. Clim.* **2011**, *24*, 6322–6338. [CrossRef]
76. Lawrence, H.; Wigneron, J.P.; Richaume, P.; Novello, N.; Grant, J.; Mialon, A.; Al Bitar, A.; Merlin, O.; Guyon, D.; Leroux, D.; et al. Comparison between SMOS Vegetation Optical Depth products and MODIS vegetation indices over crop zones of the USA. *Remote Sens. Environ.* **2014**, *140*, 396–406. [CrossRef]